Graduate School ETD Form 9
(Revised 12/07)

PURDUE UNIVERSITY
GRADUATE SCHOOL
Thesis/Dissertation Acceptance

This is to certify that the thesis/dissertation prepared

By Andrey A. Dovzhenok

Entitled
Mathematical Models of Basal Ganglia Dynamics

For the degree of Doctor of Philosophy

Is approved by the final examining committee:

Leonid Rubchinsky
Chair

Gregery Buzzard

Alexey Kuznetsov

Alexander Its

Robert Worth

To the best of my knowledge and as understood by the student in the *Research Integrity and Copyright Disclaimer (Graduate School Form 20)*, this thesis/dissertation adheres to the provisions of Purdue University's "Policy on Integrity in Research" and the use of copyrighted material.

Approved by Major Professor(s): Leonid Rubchinsky

Approved by: Evgeny Mukhin 04/13/2012
Head of the Graduate Program Date

Graduate School Form 20
(Revised 9/10)

PURDUE UNIVERSITY
GRADUATE SCHOOL

Research Integrity and Copyright Disclaimer

Title of Thesis/Dissertation:

Mathematical Models of Basal Ganglia Dynamics

For the degree of Doctor of Philosophy

I certify that in the preparation of this thesis, I have observed the provisions of *Purdue University Executive Memorandum No. C-22,* September 6, 1991, *Policy on Integrity in Research.**

Further, I certify that this work is free of plagiarism and all materials appearing in this thesis/dissertation have been properly quoted and attributed.

I certify that all copyrighted material incorporated into this thesis/dissertation is in compliance with the United States' copyright law and that I have received written permission from the copyright owners for my use of their work, which is beyond the scope of the law. I agree to indemnify and save harmless Purdue University from any and all claims that may be asserted or that may arise from any copyright violation.

Andrey A. Dovzhenok

Printed Name and Signature of Candidate

04/13/2012

Date (month/day/year)

*Located at http://www.purdue.edu/policies/pages/teach_res_outreach/c_22.html

MATHEMATICAL MODELS OF BASAL GANGLIA DYNAMICS

A Dissertation

Submitted to the Faculty

of

Purdue University

by

Andrey A. Dovzhenok

In Partial Fulfillment of the

Requirements for the Degree

of

Doctor of Philosophy

May 2012

Purdue University

Indianapolis, Indiana

For my wife and parents.

ACKNOWLEDGMENTS

First, I am extremely grateful to my advisor Dr. Leonid L. Rubchinsky for his restless guidance and mentoring throughout my PhD study. I would also like to thank my co-advisor Dr. Alexey S. Kuznetsov for his advice and support during the last six years.

I thank Choongseok Park for providing me the model code and help with Matlab programming. I also thank Joon Ha and Sungwoo Ahn for their help with various modeling issues and valuable career advice.

I am indebted to my wife, Anna Muraveva, who encouraged and supported me on this challenging journey.

Finally, I thank my parents for giving me the opportunity to study in the US and for their support throughout my studies.

TABLE OF CONTENTS

Page

Page

Page

LIST OF TABLES

LIST OF FIGURES

Figure Page

ABSTRACT

Dovzhenok, Andrey A. Ph.D., Purdue University, May 2012. Mathematical Models of Basal Ganglia Dynamics. Major Professor: Leonid Rubchinsky.

Physical and biological phenomena that involve oscillations on multiple time scales attract attention of mathematicians because resulting equations include a small parameter that allows for decomposing a three- or higher-dimensional dynamical system into fast/slow subsystems of lower dimensionality and analyzing them independently using geometric singular perturbation theory and other techniques. However, in most life sciences applications observed dynamics is extremely complex, no small parameter exists and this approach fails. Nevertheless, it is still desirable to gain insight into behavior of these mathematical models using the only viable alternative – ad hoc computational analysis. Current dissertation is devoted to this latter approach.

Neural networks in the region of the brain called basal ganglia (BG) are capable of producing rich activity patterns. For example, burst firing, i.e. a train of action potentials followed by a period of quiescence in neurons of the subthalamic nucleus (STN) in BG was shown to be related to involuntary shaking of limbs in Parkinson's disease called tremor. The origin of tremor remains unknown; however, a few hypotheses of tremor-generation were proposed recently. The first project of this dissertation examines the BG-thalamo-cortical loop hypothesis for tremor generation by building

physiologically-relevant mathematical model of tremor-related circuits with negative delayed feedback. The dynamics of the model is explored under variation of connection strength and delay parameters in the feedback loop using computational methods and data analysis techniques. The model is shown to qualitatively reproduce the transition from irregular physiological activity to pathological synchronous dynamics with varying parameters that are affected in Parkinson's disease. Thus, the proposed model provides an explanation for the basal ganglia-thalamo-cortical loop mechanism of tremor generation.

Besides tremor-related bursting activity BG structures in Parkinson's disease also show increased synchronized activity in the beta-band (10-30Hz) that ultimately causes other parkinsonian symptoms like slowness of movement, rigidity etc. Suppression of excessively synchronous beta-band oscillatory activity is believed to suppress hypokinetic motor symptoms in Parkinson's disease. Recently, a lot of interest has been devoted to desynchronizing delayed feedback deep brain stimulation (DBS). This type of synchrony control was shown to destabilize synchronized state in networks of simple model oscillators as well as in networks of coupled model neurons. However, the dynamics of the neural activity in Parkinson's disease exhibits complex intermittent synchronous patterns, far from the idealized synchronized dynamics used to study the delayed feedback stimulation. The second project of this dissertation explores the action of delayed feedback stimulation on partially synchronous oscillatory dynamics, similar to what one observes experimentally in parkinsonian patients. We employ a computational model of the basal ganglia networks which reproduces the fine temporal structure of the synchronous dynamics observed experimentally. Modeling results suggest that delayed

feedback DBS in Parkinson's disease may boost rather than suppresses synchronization and is therefore unlikely to be clinically successful.

Single neuron dynamics may also have important physiological meaning. For instance, bistability – coexistence of two stable solutions observed experimentally in many neurons is thought to be involved in some short-term memory tasks. Bistability that occurs at the depolarization block, i.e. a silent depolarized state a neuron enters with excessive excitatory input was proposed to play a role in improving robustness of oscillations in pacemaker-type neurons. The third project of this dissertation studies what parameters control bistability at the depolarization block in the three-dimensional conductance-based neuronal model by comparing the reduced dopaminergic neuron model to the Hodgkin-Huxley model of the squid giant axon. Bifurcation analysis and parameter variations revealed that bistability is mainly characterized by the inactivation of the Na^+ current, while the activation characteristics of the Na^+ and the delayed rectifier K^+ currents do not account for the difference in bistability in the two models.

1. INTRODUCTION

Brain neural elements generate complex electrical activity that is necessary to execute various cognitive and behavioral tasks. When these processes occur on different time scales, the resulting dynamical system may be separated into lower-dimensional subsystems by means of fast/slow decomposition. Analytical results are straightforwardly obtained for systems that can be decomposed into subsystems of dimension 1 or 2. The long-term behavior of such dynamical systems can only include limit cycles and/or equilibrium points as follows from Poincare-Bendixson theorem in dimension 2 and from a simple argument in dimension 1. Hence, standard methods of geometric singular perturbation theory can be used in dimensions 1 and 2 to analyze each subsystem independently. Then, the dynamics of the full higher-dimensional system can be faithfully reconstructed by gluing the obtained solutions together.

However, in many life sciences' problems like modeling tremor and deep brain stimulation in Parkinson's disease oscillations occur on some intermediate time scale and may even include delayed feedback (Glass and Mackey, 1988). In these cases, the fast/slow decomposition is not applicable. Moreover, the behavior of the dynamical system in dimension 3 and higher may be extremely complex and even include chaos, but virtually no other standard methods for analysis exist. In this case, numerical simulations are the only way to obtain valuable information about the system's behavior, but more

importantly computational analysis is indispensable because it can give the intuition to develop novel analytical tools and theories to study those mathematical models.

Similar obstacles arise in the analysis of synchronization in networks of neural oscillators. Synchronization in ensembles of interacting elements is a rapidly developing field of study with possible applications in physics, chemistry and life sciences, in particular, to Parkinson's disease and epilepsy (Pikovsky et al., 2001). Most of the synchronization analysis methods characterize a system close to the synchronized state (that is also called synchronization manifold) or near bifurcation points. For example, time series analysis allows measuring the degree of correlation between two signals, i.e. how far the system is from the synchronized state. Then, Lyapunov exponents may be used to estimate its stability.

These universal methods are well-suited for physical or engineering systems where synchronization is relatively strong and the system spends most of the time near the synchronization manifold. However, in biological systems (neuronal populations, for example) phase synchronization is frequently very weak. In this case, the system spends relatively little time close to the synchronized state and the above methods may not be very informative of the overall dynamics of the system. Thus, one must retreat to either numerical analysis or devise alternative ad hoc computational methods to study synchronization dynamics.

Another important area of application of numerical simulation and analysis arises when experimenters are limited in their ability to test a hypothesis due to limitations on human testing or when the experiment is not feasible to implement. The former is true in the context of developing novel stimulation techniques that may be used in the treatment

of Parkinson's disease symptoms where it is not desirable to involve human subjects during the early stages of the project. The latter is the case in testing the basal ganglia-thalamocortical loop hypothesis for tremor that is studied in Chapter 2. Mathematical modeling and simulations may be the only available option that can provide deeper insight and valuable information in this case. That is why mathematical and computational neuroscience has become an important tool for studying various neurological disorders from schizophrenia and epilepsy to Parkinson's disease (Ermentrout and Terman, 2010; Izhikevich, 2007).

Bibliography

Ermentrout, G. B., & Terman, D. H. (2010). *Mathematical foundations of neuroscience.* Springer.

Glass, L., & Mackey, M. C. (1988). *From clocks to chaos: the rhythms of life*. Princeton: University Press.

Izhikevich, E. (2007). *Dynamical systems in neuroscience*. Cambridge, MA: The MIT Press.

Pikovsky, A., Rosenblum, M., & Kurths, J. (2001). *Synchronization: a universal concept in nonlinear science*. Cambridge Univ. Press, Cambridge, UK.

2. ON THE ORIGIN OF TREMOR IN PARKINSON'S DISEASE

2.1 Introduction

Tremor is one of the cardinal symptoms of Parkinson's disease. Some studies report it to be present in up to 80% of patients with autopsy-proven Parkinson's disease (Gelb et al., 1999). It is a well-recognized feature of Parkinson's disease and is a disabling symptom. Parkinsonian tremor is primarily a rest tremor with the frequency in 3-7 Hz range, it is episodic in time, can be modulated (suppressed or enhanced) by motor or cognitive activity; cortical and subcortical motor areas during episodes of Parkinsonian tremor exhibit bursty neuronal firing correlated with tremor EMG (Lenz et al., 1994; Elble and Koller, 1990; Deuschl et al., 2000; Rubchinsky et al., 2007). Tremor is believed to be different from akineto-rigid symptoms of the disease both in the patterns of degeneration of dopaminergic neurons (Jellinger, 1999) and in the spatial location and spectral content of the neuronal activity in the basal ganglia circuits (Rivlin-Etzion et al., 2006; Moran et al., 2008; Weinberger et al., 2009).

While the occurrence of parkinsonian tremor is naturally related to dopaminergic degeneration (or, potentially, some other degeneration in Parkinson's disease), the network, cellular and synaptic mechanisms of parkinsonian tremor are not clear. It is commonly acknowledged that parkinsonian tremor has a central origin, but the localization of this central oscillator (oscillators) is still debatable. A few hypotheses of

tremor generation have been proposed previously (reviewed in (Deuschl et al., 2000)). Some of them place an emphasis on the thalamus, suggesting that it either generates tremor because of the rebound activity of thalamic cells when they are released from excessive pallidal inhibition (Llinas, 1984), or that it filters (or otherwise promotes, Guehl et al., 2003) low-frequency oscillations out of a broader band (Pare et al., 1990). Another suggests that the basal ganglia circuits may be the tremor-generating oscillator on its own (Wichmann and DeLong, 1999). However, the increase in interspike interval within the burst characteristic of the thalamic rebound bursting is not observed in thalamic bursts seen in parkinsonian tremor (Zirh et al., 1998). Neither is the thalamic filter hypothesis supported by data analysis (Raethjen et al., 2009) nor does it explain the origin of 10-15Hz oscillations. The tremor-suppressing effect of lesions outside the basal ganglia (such as lesions in the thalamus (Zirh et al., 1998; Lenz et al., 1994) and cortex (Volkmann et al., 1996)) suggests that the tremor generator may extend beyond the basal ganglia networks. Cerebellar circuits are involved in the tremulous movement, but appear to be not directly connected with the tremor movement (Timmermann et al., 2003) and are thus unlikely to be its generator (reviewed in (Deuschl et al., 2000)).

A very plausible view is that the tremor oscillator is localized in the basal ganglia-thalamo-cortical circuits (Fig. 2.1a) (reviewed in (Deuschl et al., 2000)). The basal ganglia cells are known to possess rich membrane properties, which support pacemaking (Surmeier et al., 2005; Bevan et al., 2006), but do not produce tremor oscillations in healthy basal ganglia circuits. In contrast, in parkinsonian circuits tremor-related activity (i.e. neural activity in the tremor frequency band, correlated with the tremor movement or tremor EMG) was observed in the basal ganglia (in the subthalamic nucleus, STN (Levy

et al., 2000) and in pallidum (Hutchison et al., 1997)), in the thalamus (Zirh et al., 1998; Lenz et al., 1994), and in cortex (Timmermann et al., 2003; Volkmann et al., 1996). Surgical lesions in different parts of the basal ganglia-thalamo-cortical loop (in the STN (Alvarez et al., 2005), in cortex (reviewed in (Deuschl et al., 2000)), in pallidum and the thalamus (Tarsy et al., 2003)) suppress tremor. The fact that breaking the loop at multiple sites leads to the same effect – tremor suppression – suggests that the loop itself, more than any of its parts, is a tremor generator. However, this evidence is indirect and does not tell how tremor is generated.

The present study explores the possibility of the basal ganglia-thalamo-cortical loop theory. We use computational neuroscience techniques to study the dynamics of this loop. While the physiology of the cortico-basal ganglia loops has been the subject of earlier computational studies (e.g., Beiser and Houk, 1998), including studies (Humphries et al., 2006; Leblois et al., 2006), which provided further confirmation for the role of dopamine depletion in promoting oscillatory activity in various frequency bands (usually beta-band), these studies were mostly concerned with the action selection in basal ganglia and did not consider tremor oscillations. We show that the membrane properties of basal ganglia neurons together with anatomy of the basal ganglia circuits (Fig. 2.1a) and the gross feedback-like structure of the basal ganglia-thalamo-cortical loop may generate tremor-like oscillations if the synaptic projections change their strength (as is expected to be the case in Parkinson's disease due to dopaminergic degeneration, discussed in more details in Section 2.2.3). These tremor-like oscillations in the model are suppressed by breaking the loop in various locations. Deeper understanding of the tremor mechanisms

a)

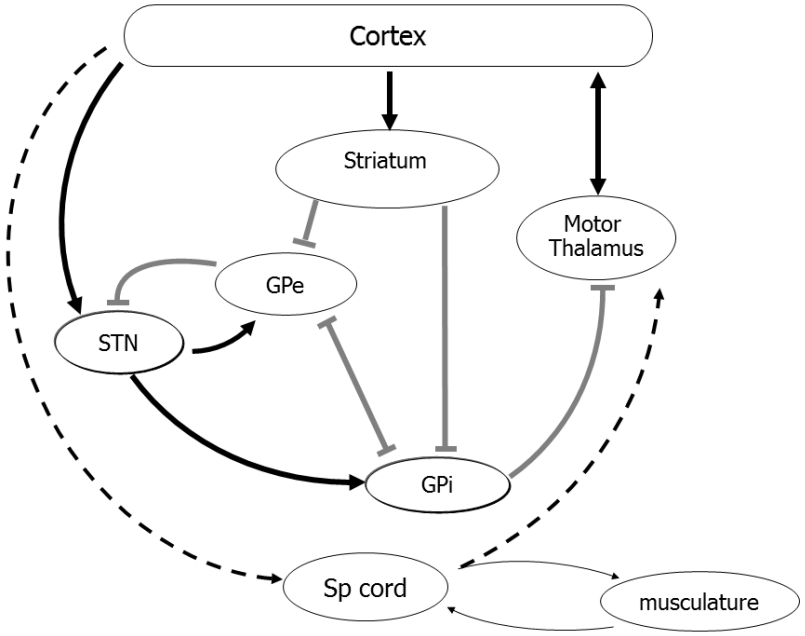

b)

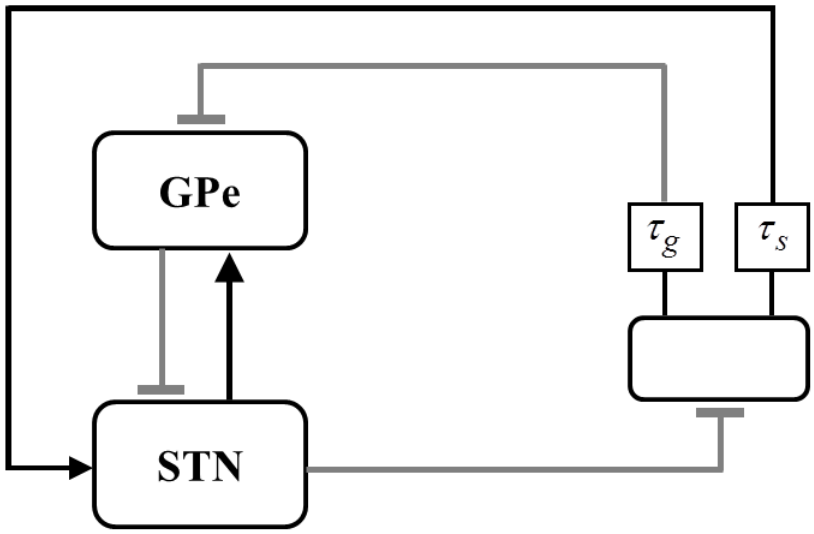

Figure 2.1. Basal ganglia-thalamo-cortical circuit. a) is the schematics of the anatomy. b) is the model circuit. The model circuit consists of one GPe neuron, one STN neuron and a feedback neuron, represented by a feedback box. Arrows indicate excitatory synapses and bars indicate inhibitory synapses. Squares indicate the delay units with the delays τ_s and τ_g.

will allow for improved treatment of parkinsonian tremor and will enhance our understanding of basal ganglia physiology.

2.2 Methods

2.2.1 Model Circuit Development

In vitro studies (Plenz and Kitai, 1999) demonstrated how a cultured network of GPe and STN neurons can generate low-frequency oscillations. The bursting they observed is not necessarily the same as tremor oscillations. However, this experimental result indicates that pallido-subthalamic networks have the necessary cellular and synaptic properties to produce low-frequency oscillatory dynamics. Nevertheless, in healthy humans *in vivo*, subthalamo-pallidal networks do not generate tremor oscillations. Various studies (see Section 2.2.3) have provided evidence for how the basal ganglia-thalamo-cortical loop may become more strongly connected in Parkinson's disease. Lesions in different parts of the basal ganglia-thalamo-cortical loop in Parkinson's disease suppress tremor (see references in Section 2.1). This suggests an intriguing possibility that subthalamo-pallidal circuits embedded in a pathologically connected basal ganglia-thalamo-cortical loop may be the generator of tremor oscillations. Thus, the strength of the loop (defined by the underlying synaptic projections) becomes stronger in Parkinson's disease giving rise to tremor, while dopaminergic medication or surgical lesions would decrease the strength of or partially break the loop, suppressing tremor.

This reasoning suggests the following organization of the model network: a network of connected subthalamic and pallidal cells, embedded in a larger feedback loop

(provided by basal ganglia, thalamic, cortical, and possibly other circuitry). To study the basic properties of the tremor oscillations in this loop, we consider a model, which retains some anatomical, synaptic and cellular properties of the underlying circuits, but simplifies others, especially those, which are not well-known. Thus, we suggest considering the circuit presented in Fig. 2.1b. We retain the cellular properties of subthalamic and pallidal cells and circuits (which have some pacemaking properties (Plenz and Kitai, 1999)) by utilizing the detailed models of STN and GPe neurons developed by (Terman et al., 2002), but simplify the rest of the complex basal ganglia-thalamo-cortical network, which is represented in this study by a single neuron model and two delay units to incorporate the delays in the polysynaptic pathways the signals will travel through. This model network is in agreement with the known organization of the basal ganglia and related circuits (Wilson, 2004), but obviously does not consider the detailed properties and parameters of the loop (which would be hard to estimate from experiments anyway). Thus, the results of the study will be sensitive to only general properties of the loop – essentially its presence or absence and overall connection strength.

The inhibitory input to the pallidal segment in the model represents thalamo-cortico-striatal and, possibly, thalamo-striatal (Smith et al., 2004) pathways. Excitatory input to STN represents the thalamo-cortico-STN pathway. GPi is not explicitly present in the model. Hence, the model architecture assumes GPi to be enslaved to STN input. While GPi intrinsic dynamics and non-STN inputs to GPi may affect the dynamics in the loop, the exclusion of GPi provides us with a model, which considers GPe-STN

interaction with the feedback loop. GPi projection to thalamus is inhibitory, which is reflected by inhibitory output of the model STN (in reality the latter sends excitatory projections to GPi).

2.2.2 Model Neurons

Each module in the model circuit (Fig. 2.1b) is represented by a single neuron modeled as a one-compartment conductance-based model. Since the properties of the subthalamic and pallidal cells are likely to contribute to the birth of oscillations (see Section 2.2.1), we use conductance-based model of GPe and STN neurons developed in (Terman et al., 2002) and further utilized in an array of studies (e.g., Rubchinsky et al., 2003; Rubin and Terman, 2004; Best et al., 2007). On the contrary, the basal ganglia-thalamo-cortical feedback is represented by delay units and a very simple neuronal model. This generic model serves the mere purpose of the feedback signal propagation in the model circuit and does not include any further details of the loop architecture (see the reasoning in Section 2.2.1).

The models for GPe and STN neuronal modules (Fig. 2.1b) include a leak current, fast spike-producing potassium and sodium currents, low threshold T-type and high-threshold Ca^{2+}-currents, and a Ca^{2+}-activated voltage-independent afterhyperpolarization K^{+}-current (AHP), so that the equation governing the transmembrane potential takes the form

$$C\frac{dV}{dt} = -I_L - I_K - I_{Na} - I_T - I_{Ca} - I_{AHP} - I_{syn} + I_{app}$$

with the membrane currents given as

$$I_L = g_L(V - V_L),$$

$$I_K = g_K n^4 (V - V_K),$$

$$I_{Na} = g_{Na} m_\infty^3(V) h (V - V_{Na}),$$

$$I_T = g_T a_\infty^3(V) b_\infty^2(r)(V - V_{Ca}),$$

$$I_{Ca} = g_{Ca} s_\infty^2(V)(V - V_{Ca}),$$

$$I_{AHP} = g_{AHP}([Ca]/([Ca] + k_1))(V - V_K).$$

The intracellular calcium balance is described by the equation

$$d[Ca]/dt = \varepsilon(-I_{Ca} - I_T - k_{Ca}[Ca]).$$

The gating variables are described by the 1st order kinetic equation in the form:

$$dx/dt = (x_\infty(V) - x)/\tau(V),$$

where x can be n, h and r .

The inactivation function $b_\infty(r)$ for the T current was modeled as in (Terman et al., 2002). Voltage-dependent gating variables $m_\infty(V)$, $a_\infty(V)$ and $s_\infty(V)$ are assumed to be instantaneous. GPe and STN neurons differ in parameter values, which were taken from (Terman et al., 2002), except for the parameter changes that follow (Rubin and Terman 2004) with applied current to STN further increased to I_{app}=32 pA/μm^2 to produce more realistic firing rates.

The conductance-based model of the feedback neuronal module (Fig. 2.1b) includes equation for the membrane potential

$$C\frac{dV}{dt} = -I_L - I_K - I_{Na,p} - I_{syn} + I_{app}$$

with persistent potassium, instantaneously activating persistent (non-inactivating) sodium and leak currents given by

$$I_K = g_K n(V - V_K),$$

$$I_{Na,p} = g_{Na} m_\infty(V)(V - V_{Na}),$$

$$I_L = g_L(V - V_L).$$

The gating variable *n* has first-order dynamics

$$\frac{dn}{dt} = (n_\infty - n)/\tau_n(v)$$

with

$$n_\infty = 1/\left(1 + \exp((\theta_n - v)/k\right)$$

while instantaneous activation of Na^+ current is given by

$$m_\infty = 1/\left(1 + \exp((\theta_m - v)/k\right)$$

Mathematically, this model is similar to Morris-Lecar model. This neuron is tonically active (Fig. 2.2c). The model, $I_{Na,p} + I_K$-model, and parameters were taken from (Izhikevich, 2007). Two delay units were chosen to approximate the time it takes for the neuronal activity to travel through (potentially multiple) basal ganglia-thalamo-cortical loops before reaching STN and GPe regions. We use delay times τ_s=30 ms and τ_g=50 ms for the modeling reported below which appear to be physiologically plausible (Romo and Schultz, 2002), however, eventually we explore a wide range of the delays.

All connections in the model circuit are excitatory glutamatergic and inhibitory GABAergic synapses modeled by the 1st-order kinetic equations describing the fraction of activated channels

$$\frac{ds}{dt} = \alpha H_{\infty}(V_{presyn} - \theta_g)(1-s) - \beta s,$$

where the sigmoidal function $H_{\infty} = 1/(1+\exp[-(V-\Theta_g^H)/\sigma_g^H])$ and the values of all synaptic parameters are taken from (Terman et al., 2002). The maximal synaptic conductance from neuron X to neuron Y is denoted $g_{X\to Y}$, with X, Y taking values S, G and F for STN, GPe and feedback neurons, respectively. The values of synaptic strengths in the "normal" state (high dopamine level) are $g_{F\to G}$= 0.18, $g_{G\to S}$= 0.695, $g_{S\to F}$= 0.25, $g_{F\to S}$= 0.215, $g_{S\to G}$= 0.051, and the maximal conductance of the AHP current in STN neuron was set to g_{AHP} = 4.23 nS/μm^2. The values of synaptic strengths corresponding to the parkinsonian (low dopamine level) state are $g_{F\to G}$ = 0.36, $g_{G\to S}$ = 1.39, $g_{S\to F}$ = 0.5, $g_{F\to S}$ = 0.43, $g_{S\to G}$ = 0.103, with STN cell's AHP conductance set to g_{AHP} = 8.46 nS/μm^2. Parameters for the parkinsonian state were found by varying synaptic strengths in physiologically relevant ranges to obtain distinct tremor-like activity in the model. Then, the normal state parameters were assumed to be 50% of their strength in the parkinsonian state. Further clarification of what a normal and a parkinsonian states are from the activity pattern standpoint are given in Section 2.3 and Fig. 2.2. Ultimately, we considered a large range of values for the synaptic strengths as we discuss below.

The model circuit equations were simulated with XPP software (Bard Ermentrout, University of Pittsburg, http://www.math.pitt.edu/~bard/xpp/xpp.html).

2.2.3 Dopamine-Dependent Parameters

Because of the well-established dopaminergic degeneration in Parkinson's disease, the positive effect of L-DOPA on the symptoms (at least at the initial phase of

treatment) and the tremor reduction produced by dopamine agonists (Elble, 2002), we study how the dynamics of the model system depends on parameters, which, in turn, are affected by the action of nigral dopamine.

Since nigral dopamine may modulate many types of synapses and cells in the basal ganglia, we consider two dopaminergic parameters, s_1 and s_2, which take into account several known dopaminergic actions. The first one, s_1, considers dopaminergic modulation of striato-pallidal and pallido-subthalamic synapses, and s_2 describes the modulation of cortico-subthalamic and subthalamo-pallidal synapses and of Ca^{2+}-activated K^+ current in STN. Dopamine is known to act on presynaptic receptors at striato-pallidal synapses reducing GABA release in GPe (Cooper and Stanford, 2001; see also Ogura and Kita, 2000). In perhaps a similar manner, dopaminergic action in STN inhibits GABA release, in particular, from synapses from GPe (Shen et al., 2003; Floran et al., 2004; Cragg et al., 2004; Shen and Johnson, 2005; Baufreton and Bevan, 2008). These experiments also suggest that dopamine is able to suppress excitatory transmission to STN from cortex (Shen and Johnson, 2000), while excitatory projections from STN to GPe are also suppressed by dopaminergic action (Hernandez et al., 2006). Dopamine also has a tendency to depolarize STN cells by multiple mechanisms, in particular, including modulation of Ca^{2+}-activated K^+-current (Baufreton et al., 2005; Ramanathan et al., 2008). Overall, dopamine depletion seems to make the elements of the basal ganglia circuitry more functionally connected (e.g., Bevan et al., 2006).

Thus, we set up two dopaminergic parameters s_1 and s_2 to modulate synaptic or membrane conductance to make them weaker or stronger, as one expects them to be in the presence or absence of dopamine. A dopamine-modulated conductance

$g = (2 - s_i)g_0, i = 1,2$, where g_0 for s_1 involves $g_{F\to G}$ and $g_{G\to S}$, and g_0 for s_2 involves $g_{F\to S}$, $g_{S\to G}$, and g_{AHP}. We usually vary s_1 and s_2 in the [1, 2] range, so that lower values of s_1 and s_2 correspond to lower dopamine levels and stronger conductances. As dopaminergic parameters $s_{1,2}$ are decreased from 2 to 1, conductance g increases from 0 to some maximal value g_0 which would correspond to the transition from high to low dopamine level (with transition from normal to parkinsonian state presumably being somewhere within these bounds). Obviously, the real modulation by the dopamine may not necessarily scale in the same way for all of its targets and is unlikely to go all the way to 0. Above division of parameters affected by dopamine into two groups is somewhat arbitrary. But our approach allows us to explore the parameter space in the model when s_1 and s_2 are changing in a particular direction (of increasing or decreasing dopamine level) over a large range. Exploration of the two-parametric space is a compromise, which allows us to avoid exploration of a high-dimensional parametric space (which may be hard to interpret anyway), yet, lets us study what happens with the network dynamics, when more than just one dopamine-sensitive parameter is being modulated.

2.2.4 Time-Series Analysis

To quantify the presence of tremor-like oscillations in the modeling circuit we used a modified version of the signal to noise ratio (SNR) criterion adopted in (Hurtado et al., 2004, 2005) to study the dynamics of tremor in parkinsonian patients:

$$SNR1 = \frac{\max\limits_{\omega_a \le \omega \le \omega_b} \{P(\omega)\}}{\operatorname{avg}\limits_{\omega_{\min} \le \omega \le \omega_{\max}} \{P(\omega)\}}$$

where $P(\omega)$ is the power spectrum. This SNR criterion is used here to measure the degree of bursting activity in the tremor frequency range in the STN model neuron. The parameter setting of this criterion are ω_a = 4 Hz, ω_b = 8 Hz for the tremor band [ω_a , ω_b] and $\omega_{\min}$ = 3 Hz, $\omega_{\max}$ = 30 Hz for the wider band [$\omega_{\min}$, $\omega_{\max}$]. While the real parkinsonian tremor may present with frequencies slightly lower than 4 Hz, the 4-8 Hz range in the model appears to be sufficient to study the bursting in the system. Moreover, proprioceptive feedback tends to lower parkinsonian tremor frequency (Pollock and Davis, 1930; Rack and Ross, 1986). This sensory feedback is not a part of the central mechanisms represented by the model.

To avoid analyzing transients, we ran simulations for 3 s first and used the next 8.2 s for time-series analysis. The time-series analysis steps were similar to those in (Hurtado et al., 2004). The time-series of STN voltage was cut into non-overlapping intervals of equal length of around 0.8 s, multiplied with a Hanning tapering window and processed with fast Fourier transform (FFT) for each interval in the data sample. Obtained values were normalized by the interval size. Finally, SNR was calculated as a mean of values for each time interval. Only time-averaged SNR was considered in the current paper.

To show the robustness of tremor detection we introduced three more variations in SNR criteria. The second SNR criterion identified the position ω_{m} of the peak of the power spectrum in 3-8 Hz range to create a $\Delta\omega$ frequency band centered around this peak: $[\omega_m - \Delta\omega/2, \omega_m + \Delta\omega/2]$ and then computed

$$SNR2 = \frac{\max\limits_{\omega_m - \Delta\omega/2 \le \omega \le \omega_m + \Delta\omega/2} \{P(\omega)\}}{\operatorname{avg}\limits_{\omega_{\min} \le \omega \le \omega_{\max}} \{P(\omega)\}}$$

with $\Delta\omega = 4Hz$. Therefore, SNR2 was supposed to identify oscillations in a band of the same width, but different center frequency than SNR1 (such as 3-7 Hz, 5-9 Hz, etc.), detecting oscillations in part of the spectrum slightly wider than usual parkinsonian frequencies.

The other two criteria used average power in the fixed 4-8 Hz tremor band or average power in the floating band around the peak $[\omega_m - \Delta\omega/2, \omega_m + \Delta\omega/2]$, instead of the maximal values, i.e.

$$SNR3 = \frac{\operatorname{avg}\limits_{\omega_a \le \omega \le \omega_b} \{P(\omega)\}}{\operatorname{avg}\limits_{\omega_{\min} \le \omega \le \omega_{\max}} \{P(\omega)\}}$$

and

$$SNR4 = \frac{\operatorname{avg}\limits_{\omega_m - \Delta\omega/2 \le \omega \le \omega_m + \Delta\omega/2} \{P(\omega)\}}{\operatorname{avg}\limits_{\omega_{\min} \le \omega \le \omega_{\max}} \{P(\omega)\}}$$

While not completely equivalent, these criteria are similar, as intended, since they all are aimed at identification of oscillations. All time-series analysis was performed in MATLAB (MathWorks, Natick, MA).

2.3 Results

2.3.1 Tremor Oscillations in the Model of Basal Ganglia-Thalamo-Cortical Loop

Although pallidal and subthalamic cells and their computational models used here are known to possess burst properties (see Section 2.1) under certain conditions, the modeling network (see Fig. 2.1b) exhibits tonic spiking activity under moderate values of the coupling strength ($s_1 = 1.5$, $s_2 = 1.5$) (Fig. 2.2a). We consider these dynamics as the normal (healthy) state, as no tremor-like oscillations are present in the modeling circuits.

As the coupling increases ($s_1 = 1$, $s_2 = 1$), STN and GPe neurons in the model network exhibit bursting activity (Fig. 2.2b) with a frequency around 6 Hz. This kind of dynamics, with bursting in the STN neuron at the tremor range is considered here as a parkinsonian state, because it exhibits tremor-like oscillations.

To further explore the relevance of these model oscillations to the real tremor we will study the dynamics of the model in response to the modifications of the network, representing dopaminergic treatment (see Section 2.3.2) and therapeutic lesions used to suppress tremor. There is no explicit representation of GPi in the model network, so that pallidotomy may be represented in the model by removing the projection from STN to the thalamo-cortical circuits. When this projection is removed from the model in the parkinsonian state ($s_1 = 1$, $s_2 = 1$) the STN activity is almost tonic (this will be quantified in Section 2.3.2 with the SNR criteria, as described in Section 2.2.4). Even though GPe is silent here (presumably due to stronger inhibition from the feedback neuron in the absence of subthalamic inhibitory input), the tonic nature of STN discharge (Fig. 2.2c) confirms that the system returns in a normal state.

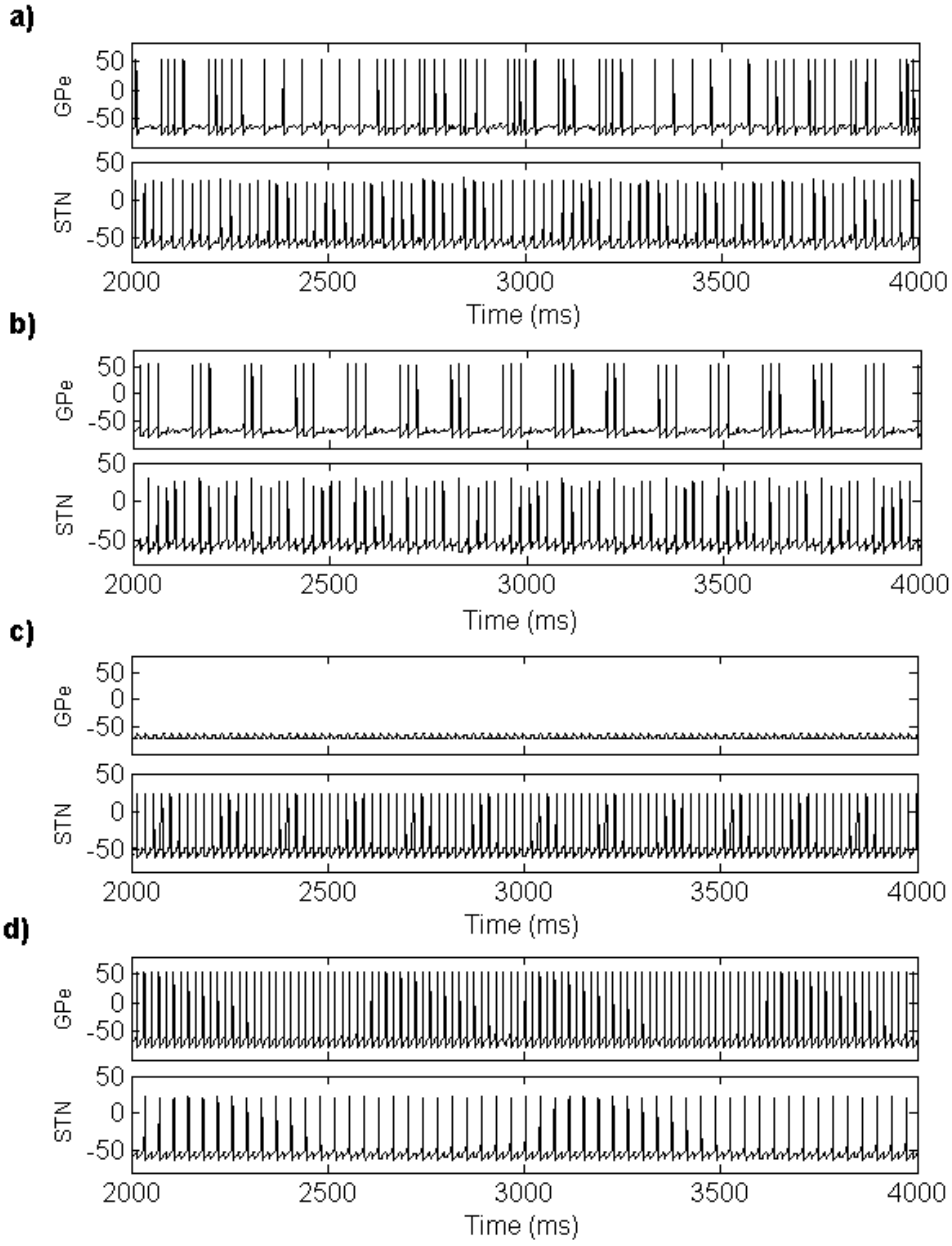

Figure 2.2. Membrane potential (in millivolts) in GPe and STN cells in the model circuit shows activity patterns in different states and after lesions. a) "Normal" state, the activity pattern in GPe, STN and feedback neurons is tonic spiking. b) "Parkinsonian" state in the circuit with stronger feedback; STN and GPe neurons exhibit bursting discharge. c) the result of a lesion at the level of STN output, and d) the result of a lesion at the level of inputs to GPe and STN. While GPe is silent in c), STN firing is essentially tonic after both lesions, thus, the model basal ganglia circuit may generate tonic (and presumably more healthy) output. Parameter values in a) are: $s_1 = 1.5$, $s_2 = 1.5$. Parameters in b, c and d) are: $s_1 = 1$, $s_2 = 1$.

The other kind of lesion reproduced in the model is at the level of cortex or thalamus. In the model that would correspond to a lesion of inputs to the GPe and STN segments (or, in other words, removal of the feedback neuron). In this case, the activity patterns of both GPe and STN are switched to tonic firing (Fig. 2.2d). Note that in the case of this lesion at the level of basal ganglia input the feedback neuron shows somewhat bursty output. However, this bursting activity is at a much higher frequency and, therefore, cannot lead to tremulous movement of limbs. The characteristic feature of GPe neuron is its tonic activity and high firing rate.

While the interpretation of the model lesions is not unique (and is left for Discussion), in both lesion cases the feedback is removed in one way or another and in the "normal" case the feedback is weakened. Section 2.3.2 provides a systematic study of the circuit behavior for varying feedback.

2.3.2 The Effect of Dopaminergic Modulation

To study the effects of dopaminergic modulation we varied dopaminergic parameters s_1 and s_2 as proxy for the presence of dopaminergic modulation (see Section 2.2.3). The results of Section 2.3.1 suggest that the strength of the feedback is essential for the occurrence of bursting, so we varied the dopaminergic parameters in a broad range to see how bursty the discharge is (as quantified by SNR criterion, see Section 2.2.4).

As an example, we consider the SNR1 as we vary the dopaminergic parameter s_1 in the interval [1, 2] (Fig. 2.3). As the dopaminergic parameter increases, SNR1, which indicates the presence of the tremor-related bursting (the presence of oscillations in the

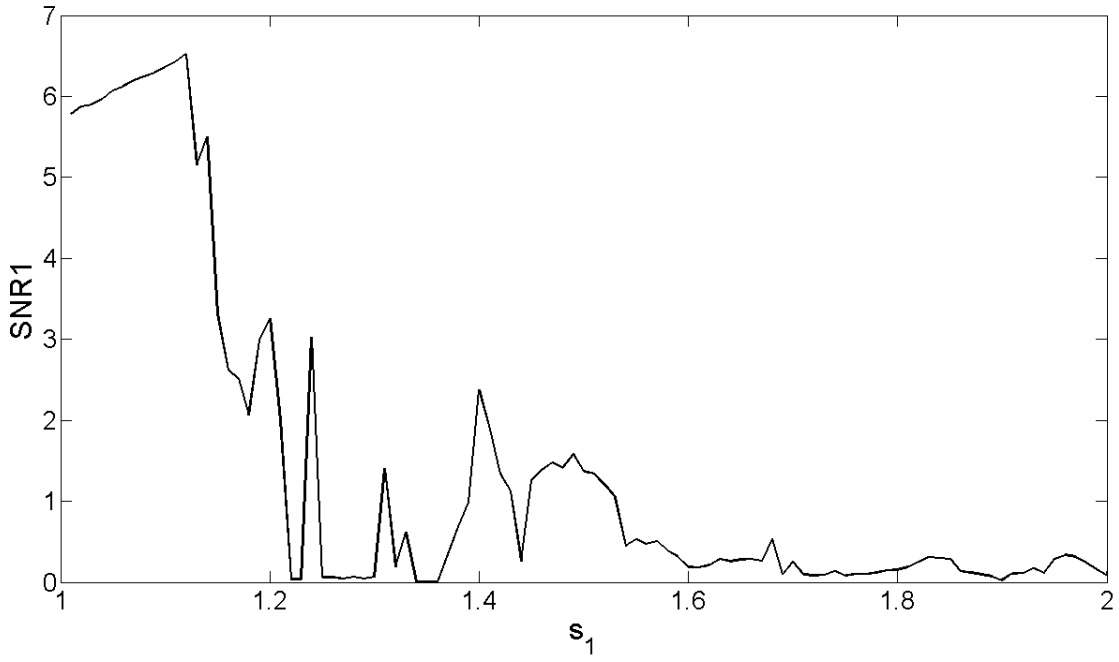

Figure 2.3. The presence of tremor frequency band activity in the STN neuron as measured by the value of SNR1 in dependence on the dopaminergic parameter s_1. The dopaminergic parameter $s_2 = 1.1$.

tremor frequency band), decreases, first moderately, then sharply to less than 1 (the lack of activity in the tremor frequency range). Thus, Fig. 2.3 illustrates the transition between tremulous and non-tremulous case, as the dopaminergic action changes. Of note is a relatively sharp onset of tremor oscillations in the model and jagged profile of SNR. We think this is most likely due to the simplicity of the model. While gross structure (strong coupling – oscillations; weak coupling – no oscillations) is captured by the model, the exact details of oscillatory/nonoscillatory transition in the model depend on a particular set of bifurcations the model experiences as the parameters are varied. This bifurcation cascade is likely to be model-specific. Moreover, if dopamine-dependent parameters are varied in different ways, the SNR profile may be different.

While the example above may be illustrative of the role of the dopamine-modulated thalamo-cortical feedback loop, the results of dopamine action on different synapses and cells in the system may be different. As we explain in the Methods, we study the effect of independent modulation of different properties of the network employing two dopaminergic parameters s_1 and s_2. How exactly dopamine will affect different synaptic and cellular parameters is not known, but the independent variation of two dopaminergic parameters (which, in turn, corresponds to variation of several synaptic and cellular parameters, see Section 2.2.3) should give some general knowledge about the effect of the basal ganglia-thalamo-cortical feedback loop on the tremor-like bursting in the basal ganglia circuits.

We varied both s_1 and s_2 in the range from 1 to 1.9, which corresponds to the variation of the underlying network parameters from some maximal values to almost zero. The presence of tremor-like activity in STN (the output node of our simplified basal

ganglia network) was assessed with SNR criteria. Figure 2.4 presents the result of this numerical experiment. Four different sub-plots were generated with the different SNR criteria (SNR1-4). Lighter shade of grey indicates stronger tremor activity. It is hard to define the exact level of SNR above which the activity can be called tremulous. However, the present SNR criteria are based on an earlier experimental study of tremor in parkinsonian patients (Hurtado et al., 2004), which uses 3.7 as a critical value for SNR1. The four SNR criteria employed here are slightly different one from another and the resulting subplots in Fig. 2.4 are also slightly different. In particular, maximal SNR tends to yield larger values than those of averaged SNR, which may be attributed to the large height and small width of the spectral peaks. However, overall, tremor-like activity is present in the same regions, regardless of the criteria used. The smallness of the differences between the subplots points to the generic character of the observed phenomena.

Figure 2.4 shows that the low values of dopaminergic parameters, i.e. low s_1 and s_2, tend to promote bursting in the tremor frequency range. This indicates that the strength of the coupling in the basal ganglia-thalamo-cortical feedback loop is responsible for the tremor oscillations. However, the dependence of SNR on the dopaminergic parameters is not monotonic. The areas of high SNR are interspersed with the areas of low SNR. The relative contribution of s_1 and s_2 is also different. Nevertheless, the general pattern (low dopaminergic parameter values – more tremulous activity, high values – less tremulous activity) is persistent.

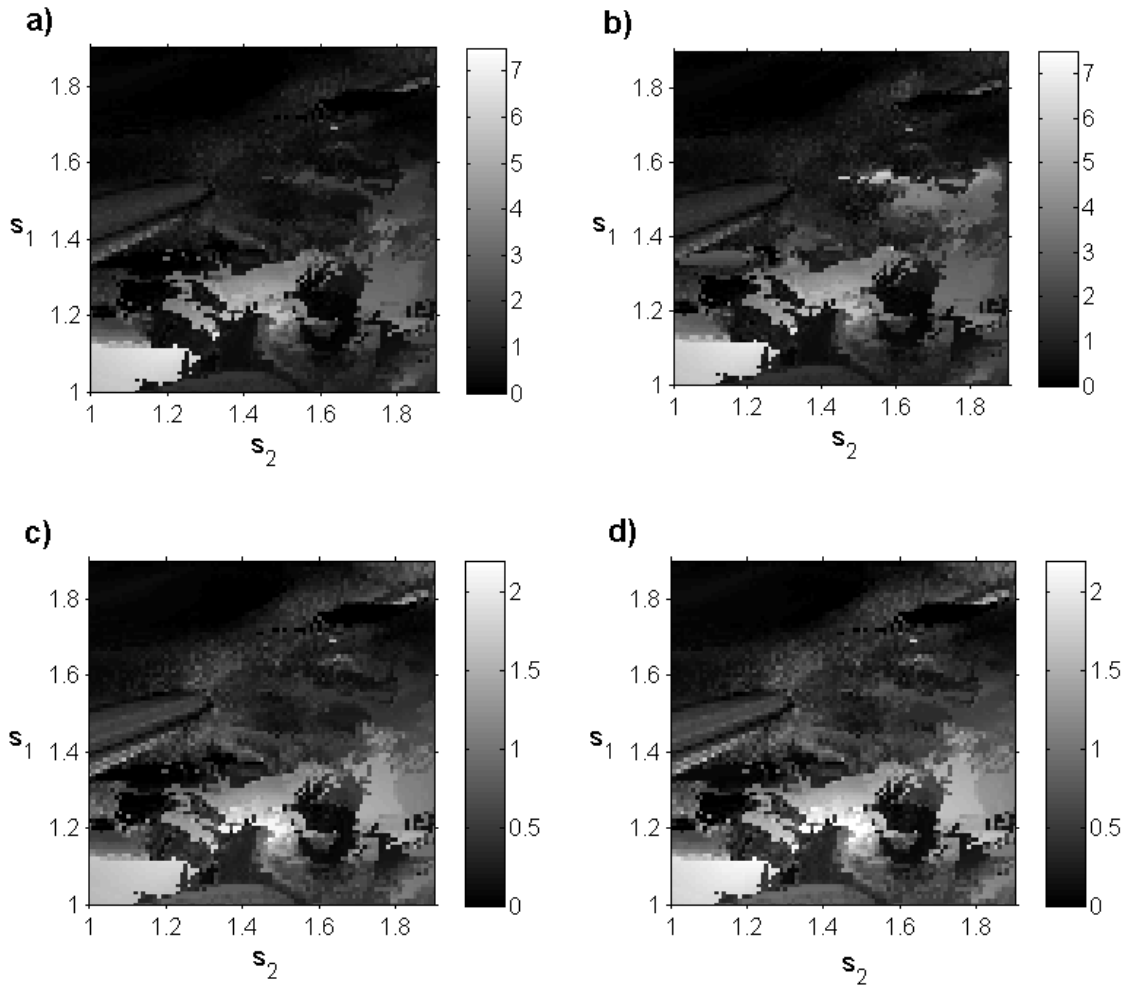

Figure 2.4. Tremulous activity with variation of dopaminergic parameters. The parameters s_1 and s_2 run along vertical and horizontal axis respectively, the grey shade codes for the value of SNR. The point (1, 1) corresponds to the bursting mode shown in Figure 2.2b. a), b), c), and d) represent SNR1,2,3, and 4 respectively. Parameters s_1 and s_2 are proxies of dopaminergic status and their higher values correspond to stronger dopamine influence. Thus upper right corner corresponds to a "normal" state of the network, while lower left corner corresponds to a "parkinsonian" state. Black color indicates the absence of tremor-band oscillations, grey and white areas indicate prominent oscillations.

2.3.3 The Effect of Calcium, AHP and T-type Currents

We also study the effect of individual currents on the tremor-like oscillations in the loop. Fig. 2.5a shows how the dopaminergic action parameter s_1 and the conductance of the AHP current in STN neuron g_{AHP} affect SNR of tremor frequency oscillations. Tremor-like oscillations exist in a region of relatively strong values of the AHP current conductance and the parameter s_1 around the parkinsonian state of Fig. 2.2b (s_1=1, g_{AHP}=1). Unlike Fig. 2.4, dependence of SNR on the dopaminergic parameter s_1 and the AHP current conductance alone is monotonic: SNR abruptly decreases and remains low indicating disappearance of bursting activity in the tremor band as the value of g_{AHP} decreases. Hence, the tremor-like oscillations in the loop substantially depend on the AHP current.

Similar results are obtained when we varied the Ca^{2+} current conductance together with the dopaminergic parameter s_1 as shown in Fig. 2.5b. Again, the dependence of SNR on the parameters is monotonic: tremor-like oscillations in the model exist in a single region around (s_1 = 1, g_{AHP} = 1) and disappear when the value of the Ca^{2+} current conductance is lowered. This similarity may be due to the fact that the decrease in the Ca^{2+} current lowers the intracellular Ca^{2+} concentration and therefore leads to reduction in the calcium-dependent AHP current in STN neuron.

Interestingly, our study revealed no substantial dependence of oscillations on the T-type current (not shown). In the model circuit STN neuron's T-type current is almost inactivated and cannot deinactivate due to relatively small inhibition from the GPe neuron. Hence, these results may indicate that the T current is not strongly involved in generation of tremor-like activity.

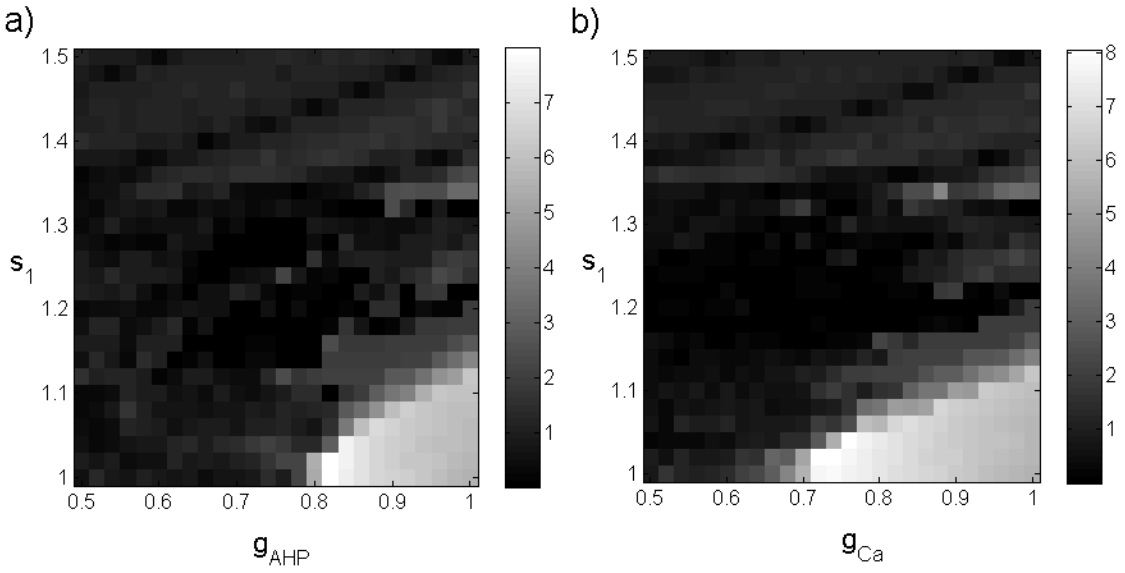

Figure 2.5. Tremulous activity with variation of current conductances. The shades of gray code for the value of SNR1 so that lighter areas exhibit stronger tremor oscillations. (a) Bursting activity with variation of the dopaminergic parameter s_1 and the AHP current conductance g_{AHP}. (b) Bursting activity with variation of the dopaminergic parameter s_1 and the Ca^{2+} current conductance g_{Ca}. Parameters are the same as in Fig. 2.2b. g_{AHP} and g_{Ca} are in units of the AHP current and the Ca^{2+} current conductances in Parkinsonian state respectively (g_{AHP}=8.46, g_{Ca}=0.5). Lower values of AHP and Ca^{+} currents conductances lead to disappearance of tremor.

2.3.4 The Influence of Delays in the Basal Ganglia-Thalamo-Cortical Loop

The model circuit (Fig. 2.1b) incorporates two delay units, which represent synaptic and conductance delays in polysynaptic pathways from STN to GPi to thalamus to cortico-striatal system. While these delays are likely to be fixed for each individual subject, we do not know their exact values. Therefore we study the impact of the delays on the tremor-like activity in the model network. Both delays, τ_s and τ_g, were varied independently in a relatively large range. This range may include biologically unrealistic delay values but the objective is to ensure that the real delays are in the domain studied. Figure 2.6 describes how delays affect SNR of tremor frequency oscillations. The regions of tremulous activity in the plane of delays are in the form of relatively narrow stripes; the slope of these stripes does not vary much and is close to 1. This suggests that the difference between delays may be more important than the values of the delays. Figure 2.6 also indicates that the oscillations are robust with respect to variation in delay values and tremor-like bursting exists for multiple values of the delays. Thus even though the exact values of the delays in the loop are not known, there are likely to be some fitting with those at the domains of tremor existence.

2.3.5 The Influence of the Feedback Neuron Model on the Dynamics of the Network

Finally, we substitute the Morris-Lecar-type feedback neuron considered so far in this paper with a more physiologically realistic thalamocortical relay cell model in the form used in (Rubin and Terman, 2004), which includes sodium , potassium and leak currents, as well as low-threshold calcium current. Figure 2.7 shows how SNR depends on the dopaminergic parameters $s_{1,2}$ in the case of this modified model circuit. Similarly

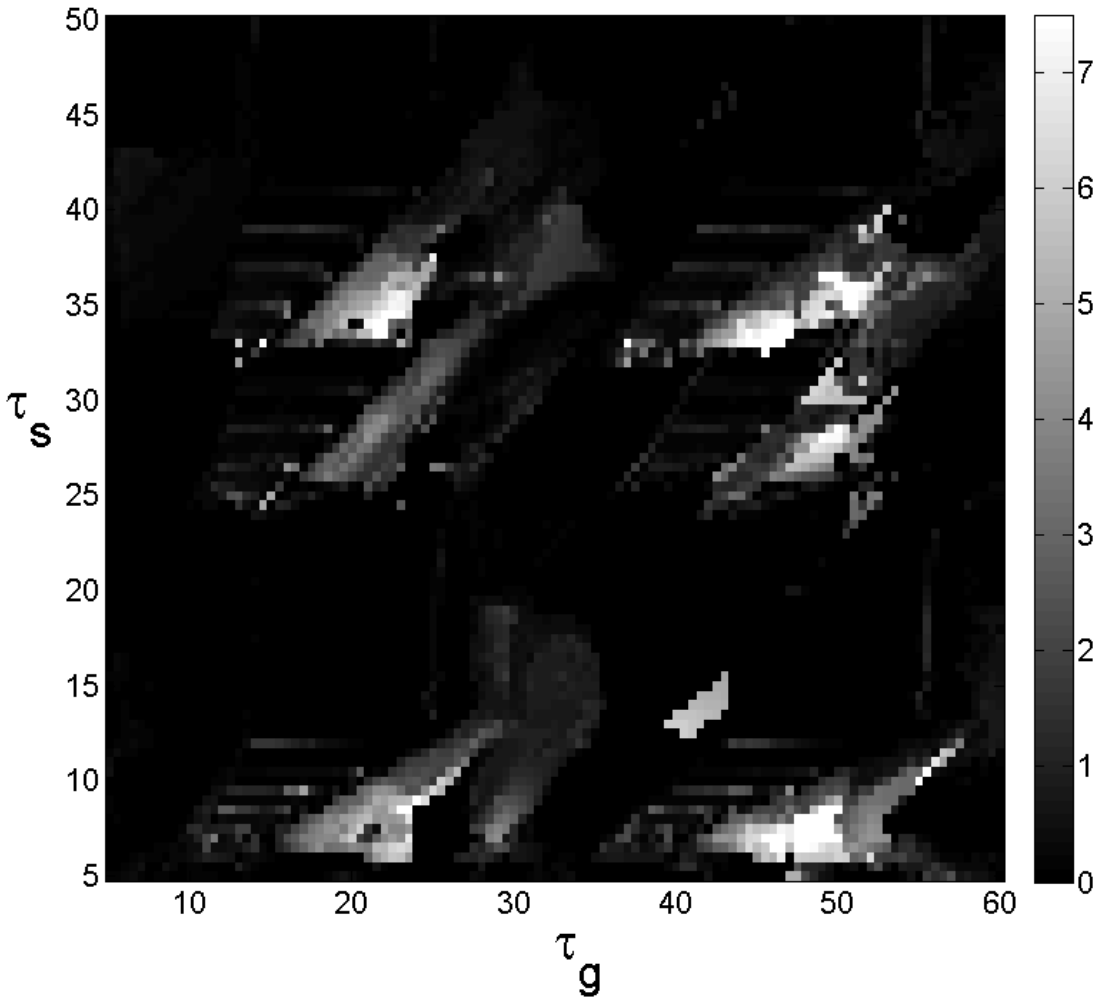

Figure 2.6. Tremulous activity with variation in delays. The parameters are the same as in Fig. 2.2b. The shades of gray code for the value of SNR1 so that lighter areas exhibit stronger tremor oscillations (gray and white areas are tremulous dynamics)

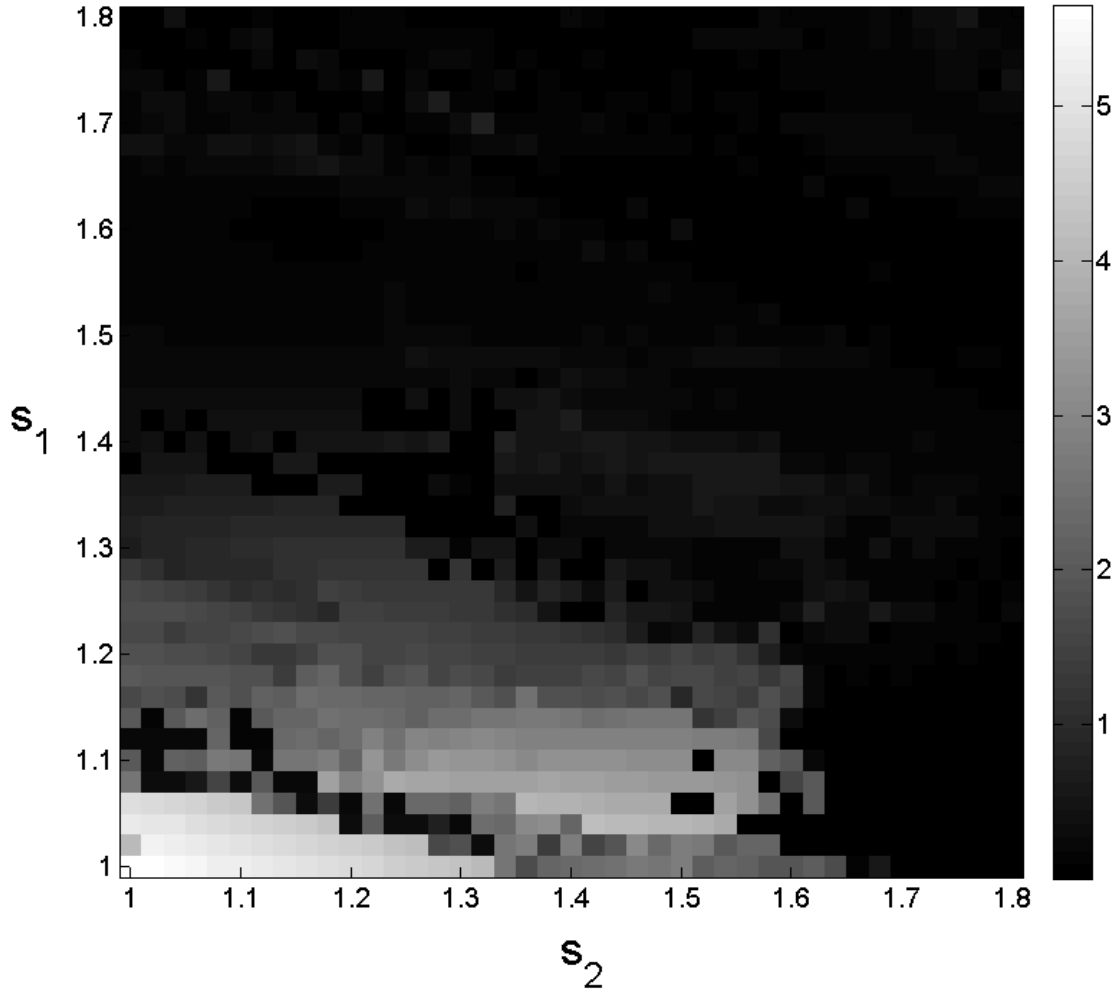

Figure 2.7. Tremulous activity with a thalamocortical relay cell instead of a feedback neuron in the thalamocortical feedback loop. The point (1, 1) corresponds to parameter values as in Figure 2.2b, except $g_{\mathrm{STN}\rightarrow\mathrm{Th}}$=0.46. Thalamocortical neuron parameters are taken from (Rubin and Terman, 2004) with I_{appth}=0.85. The parameters s_1 and s_2 run along vertical and horizontal axis respectively, the shades of gray code for the value of SNR1.

to the simple feedback model (Fig. 2.4), STN oscillations in tremor frequency-band exist in the model network in parkinsonian state and cease when the dopaminergic parameter s_1 increases to indicate higher dopamine level and presumably normal state. This suggests that the observed dynamics are robust with respect to different types of the feedback neuron in the model network. In turn, this suggests that the delayed feedback loop itself is likely to be essential for tremor-like oscillations in the model together with the cellular properties of STN and GPe neurons.

2.4 Discussion

2.4.1 Summary of the Modeling Results

The modeling shows that anatomical and membrane properties of subthalamo-pallidal circuits are prone to generation of tremor-like bursting in the presence of relatively strong basal ganglia-thalamo-cortical feedback. As we strengthen synaptic projections in the network (the expected outcome from the lack of dopaminergic modulation in Parkinson's disease), the tremor-like oscillations become more prominent. The destruction of the feedback leads to the suppression of the tremor-like oscillations (as one would expect from the outcomes of surgical lesions in parkinsonian patients).

The dependence of the strength of tremor-like oscillations on the strength of dopamine-dependent synaptic projections is not monotonic. Based on the simple model setup, one can hardly specify which range of synaptic parameters corresponds to the actual range of variation of the synaptic strength experienced in Parkinson's disease. Moreover, the effects of adding in dopamine agonist (which guided the choice of

parameters modulated by dopamine) are not necessarily opposite to the effects of dopamine depletion taking place in Parkinson's disease. However, the model study demonstrates the general pattern of the change: as the basal ganglia-thalamo-cortical feedback loop becomes stronger, oscillations are likely to occur. The phenomenon is robust with respect to different kinds of modulation of the dopamine-dependent parameters. The phenomenon is also robust with respect to different values of delays in the feedback loop. While the actual delays are not likely to change in Parkinson's disease, they are not well-known. But the studied phenomenon persists for different values of delays.

Interestingly, recent studies suggest that the dopamine depletion negatively impacts autonomous activity in GPe (Chan et al., 2011). Such a decline in GPe pacemaking may be seen at least to some extent similar to the increase in synaptic coupling, since in both cases the degree to which intrinsic dynamics influences the overall activity of a neuron is diminished in comparison with synaptic influence.

Finally we would like to note that the model effectively utilizes a negative delayed feedback (just follow the signs of synaptic connections in the loop for the STN unit, Fig. 2.1b), which is known to be able to give rise to oscillations (Mackey and Glass, 1977). A generic model for parkinsonian tremor with delayed negative feedback was studied by (Beuter and Vasilakos, 1995). Their model, however, was concerned with delayed proprioceptive feedback which had long been shown not to be significantly involved in the origin of parkinsonian tremor (Pollock and Davis, 1930; Hassler, 1970; Rack and Ross, 1986; Burne et al., 1987). It also did not represent the cortico-subcortical circuitry and membrane properties of the involved cells. In that respect it was a more

generic study of how the feedback may influence oscillations. In the current study we consider the cellular models with appropriate membrane properties, realistic network anatomy, the modulation of the network due to the lack of dopamine, and the results of known surgical interventions in Parkinson's disease and how they affect tremulous activity. Thus the feedback mechanism is considered in Parkinsonian context, which allows us to suggest that this is the dopamine-mediated strength of cortico-subcortical loop, which facilitates the birth of tremulous oscillations.

The very general nature of the feedback in the model and the robustness of the studied phenomenon indicate that the details of the feedback are unlikely to produce a substantial qualitative change in the modeling results.

2.4.2 Limitations of the Model

The model considered clearly has some limitations. The simplicity of the model basal ganglia-thalamo-cortical feedback is both its advantage (as it provides a way to study the generic effects of the feedback) and disadvantage (as it limits the model in many ways). Several limitations are discussed below.

The model network includes only single STN and GPe neurons necessary in the framework of minimalistic approach to modeling. We do not believe that results would change much qualitatively with the addition of more neurons in the model; however, the complexity of the real network and the number of possible (and sometimes unknown) connection parameters in the loop is huge. The introduction of these elements into the model will substantially increase the number of unknown parameters. In particular, earlier modeling studies of Terman et al. (2002) considered oscillations within the basal

ganglia network (but not cortico-subcortical loops) and the effect of the intrapallidal connectivity on these oscillations. However, the oscillations considered in that framework (which are likely to correspond to the beta-band oscillations accompanying hypokinetic symptoms of Parkinson's disease) are not related to tremor oscillations and can be supported by networks without intrapallidal connectivity (Best et al., 2007; Park et al., 2011). While overall the model neurons exhibit reasonable patterns of neural activity, the case of the model lesions at the level of basal ganglia output may present some problem. When the STN firing does not exhibit tremulous activity, GPe is silent (Fig. 2.2c). Hence, our modeling predicts the reduction in GPe activity after GPi lesion. It is hard to know if this is what happens in parkinsonian patients after lesions in internal pallidum (we are not aware of recordings in GPe after lesion in ipsilateral GPi in patients with tremor). Moreover, some studies indicate that GP intrinsic oscillation capability may increase after STN lesion (Kita and Kita, 2011) which would break the feedback to the basal ganglia. However, STN lesion also removes direct STN input to GPe and thus is not equivalent to GPi lesion in our model. Thus we believe the numerical studies still indicate that a stronger basal ganglia-thalamo-cortical feedback promotes tremor oscillations and its destruction suppresses them. Even though the lack of activity is visible in GPe in the computational results, the output of the model basal ganglia lacks burstiness. Likewise, in the case of the model lesions at the level of basal ganglia input the feedback neuron shows bursty output. Nevertheless, this bursting activity is high-frequency and, therefore, cannot give rise to tremor. Given the minimalistic modeling approach, the model should not be expected to reproduce the results of all known cortical and subcortical lesions with

high fidelity. Similarly, minimalistic modeling approach may not necessarily reproduce the firing rates with high fidelity.

The traditional target for anti-tremor thalamotomy in Parkinson's disease is thalamic nucleus ventralis intermedius, Vim, although basal ganglia projections to thalamus target the nucleus ventro-oralis posterior, Vop (Jones, 2001). Vim is not directly represented in our model circuit. However, Vim is effective site for surgical treatment (whether lesion or deep brain stimulation) of many tremor types beyond Parkinson's disease (Deuschl and Bergman, 2002; Speelman et al., 2002). This does not necessarily indicate that Vim is the ultimate tremor-generator, rather it may be a downstream part of the circuitry between tremor generator and limbs. Thalamus may be a "bottleneck" for cortico-subcortical circuits involved in tremor generation and maintenance (Raethjen and Deuschl, 2009). As we discussed in the introduction, cerebellar networks, while involved with the parkinsonian tremor movement, are unlikely to generate it directly (Deuschl et al., 2000; Timmermann et al., 2003). Moreover, the basal ganglia (in particular, STN) have a disynaptic projection to the cerebellar cortex, which can be a way for basal ganglia dynamics to affect the activity in cerebellar circuits (Bostan et al., 2010).

We did not consider the effect of deep brain stimulation (DBS) on tremor in the model. DBS may have differential effects on various neuronal elements, which are not present in the model (e.g., Miocinovic et al., 2006). Nevertheless, the complicated network effect of DBS appears to perform "informational lesion". i.e. functionally disrupt the flow of pathological signals through the basal ganglia-thalamo-cortical loop (see, e.g., Lozano et al., 2002; Grill et al., 2004; McIntyre et al., 2004). Thus the effect of DBS in the context of the present minimal model may be equivalent to that of a lesion.

The dopaminergic system is not the only transmission and modulation system affected in Parkinson's disease. Cholinergic and serotonergic disruptions have been observed as well (discussed in e.g., Rivlin-Etzion et al., 2006). Tremor severity in Parkinson's disease is poorly correlated with the degree of dopaminergic denervation, at least in striatum. Nevertheless, even in cases of Parkinson's disease with tremor only, i.e. monosymptomatic rest tremor, a dopaminergic deficit is present (Antonini et al., 1998). Dissociation of parkinsonian tremor and hypokinetic symptoms may be due to the different patterns of nigral degeneration (Jellinger, 1999). Thus, the variations in the dopamine level are likely to act in the way in which they are considered in the model. Moreover, if the effect of cholinergic or other pathologies in Parkinson's disease is to increase effective coupling in the basal ganglia-thalamo-cortical circuitry, these pathologies are likely to induce tremor-like bursting. This is expected because our modeling indicates that the lack of dopamine promotes oscillations due to the increase in the coupling in the circuits.

Compensatory effects are not considered in our model although they have been conjectured to play a role in the tremor genesis (e.g., Rivlin-Etzion et al., 2006). Compensatory effects may slow down the increase of the feedback strength or may even eventually weaken it as a result of overcompensation (which may be one of the explanations for why the tremor severity may decrease in the advanced state of Parkinson's disease). However, the variation of feedback strength is not removed by these kinds of compensations, rather the timing of the processes and its magnitude are altered. Therefore the modeling conclusions are unlikely to be invalidated by the presence of compensation.

Finally, it is known, that the neural activity in tremor-supporting networks exhibits a complex spatio-temporal structure (Hurtado et al., 2005). These patterns are likely to be induced by the complex anatomical structure of the tremor-supporting networks and thus cannot be reproduced in our model.

2.4.3 Implications for the Tremor-Genesis and Tremor Therapies

Earlier indirect evidences (discussed in Introduction) suggested that parkinsonian tremor arises in the basal ganglia-thalamo-cortical loops, and that the presence of the thalamocortical feedback to basal ganglia is essential for tremor occurrence. However, there was no direct experimental study of this hypothesis. Such a study is clearly hard to implement. *In vitro* preparations will not be able to maintain the structure of the loop which spans multiple subcortical and cortical locations. *In vivo* studies would be limited by the difficulty of recording from multiple locations of the circuitry and with variation of multiple parameters. Available animal models of Parkinson's disease either do not exhibit tremor at all or exhibit tremor, which is not really similar to the human parkinsonian tremor (Bergman et al., 1998; Wilms et al., 1999). In these circumstances, the computational neuroscience approaches become especially valuable.

The minimalistic representation of the thalamo-cortical feedback in the present modeling study signifies a very general role of this feedback in the tremor genesis. This study suggests that just the presence of the relatively strong basal ganglia-thalamo-cortical feedback leads to the birth of tremor-like oscillations under rather general conditions. The study indicates that the parkinsonian tremor genesis has its origin in both the properties of local basal ganglia circuits and in the thalamo-cortical feedback to the

basal ganglia. This feedback loop is modulated by dopamine and as dopamine level decreases, the strength of the loop increases to generate tremor-like oscillations. While weakly-connected (presumably normal) cortico-subcortical loops through the basal ganglia and thalamus may be crucial for movement control and other functions, we show that malfunctioning of modulatory mechanisms of these loops can cause tremor.

The feedback-loop mediated origin of tremor suggests directions for its treatment. Since the weakening or destruction of the loop itself (rather than a particular node of the loop network) may suppress tremor, different sites in the loop network may be explored as anatomical targets for surgical or pharmacological intervention. Lesions or high-frequency stimulation beyond traditional pallidal or thalamic sites may turn out to be efficient. Similarly, pharmacological influences of different nature may prove to be effective as long as they appropriately decrease the strength of the basal ganglia-thalamo-cortical loop at any of its parts.

Bibliography

Alvarez, L., Macias, R., Lopez, G., Alvarez, E., Pavon, N., Rodriguez-Oroz, M. C., Juncos, J. L., Maragoto, C., Guridi, J., Litvan, I., Tolosa, E. S., Koller, W., Vitek, J., DeLong, M. R., & Obeso, J. A. (2005). Bilateral subthalamotomy in Parkinson's disease: initial and long-term response. *Brain* 128:570–583.

Antonini, A., Moeller, J. R., Nakamura, T., Spetsieris, P., Dhawan, V., & Eidelberg, D. (1998). The metabolic anatomy of tremor in Parkinson's disease. *Neurology* 51:803–810.

Baufreton, J., & Bevan, M. D. (2008). D2-like dopamine receptor-mediated modulation of activity-dependent plasticity at GABAergic synapses in the subthalamic nucleus. *J Physiol* 586:2121–2142.

Baufreton, J., Zhu, Z. T., Garret, M., Bioulac, B., Johnson, S. W., & Taupignon, A. I. (2005). Dopamine receptors set the pattern of activity generated in subthalamic neurons. *FASEB* J 19: 1771–1777.

Beiser, D. G., & Houk, J. C. (1998). Model of cortical-basal ganglionic processing: encoding the serial order of sensory events. *J Neurophysiol* 79:3168–3188.

Bergman, H., Raz, A., Feingold, A., Nini, A., Nelken, I., Hansel, D., Ben-Pazi, H., & Reches, A. (1998). Physiology of MPTP tremor. *Mov Disord* 13(Suppl 3):29–34.

Best, J., Park, C., Terman, D., & Wilson, C. (2007). Transitions between irregular and rhythmic firing patterns in excitatory-inhibitory neuronal networks. *J Comput Neurosci* 23:217–235.

Bevan, M. D., Atherton, J. F., & Baufreton, J. (2006). Cellular principles underlying normal and pathological activity in the subthalamic nucleus. *Curr Opin Neurobiol* 16:621–628.

Bostan, A. C., Dum, R. P., & Strick, P. L. (2010). The basal ganglia communicate with the cerebellum. *Proc Natl Acad Sci USA* 107:8452–8456.

Beuter, A., & Vasilakos, K. (1995). Tremor: Is Parkinson's disease a dynamical disease? *Chaos* 5:35–42.

Burne, J. A. (1987). Reflex origin of parkinsonian tremor. *Exp Neurol* 97:327–339.

Chan, C. S., Glajch, K. E., Gertler, T. S., Guzman, J. N., Mercer, J. N., Lewis, A. S., Goldberg, A. B., Tkatch, T., Shigemoto, R., Fleming, S. M., Chetkovich, D. M., Osten, P., Kita, H., & Surmeier, D. J. (2011). HCN channelopathy in external globus pallidus neurons in models of Parkinson's disease. *Nat Neurosci* 14:85–92.

Cooper, A. J., & Stanford, I. M. (2001). Dopamine D2 receptor mediated presynaptic inhibition of striatopallidal GABA(A) IPSCs in vitro. *Neuropharmacology* 41:62–71.

Cragg, S. J., Baufreton, J., Xue, Y., Bolam, J. P., & Bevan, M. D. (2004). Synaptic release of dopamine in the subthalamic nucleus. *Eur J Neurosci* 20:1788–1802.

Deuschl, G., & Bergman, H. (2002). Pathophysiology of nonparkinsonian tremors. *Mov Disord* 17 (Suppl 3):S41–S48.

Deuschl, G., Raethjen, J., Baron, R., Lindemann, M., Wilms, H., & Krack, P. (2000). The pathophysiology of parkinsonian tremor: a review. *J Neurol* 247 (Suppl 5):V33–V48.

Elble, R. J. (2002). Tremor and dopamine agonists. *Neurology* 58:S57–62.

Elble, R. J., & Koller, W. G. (1990). *Tremor*. Baltimore, MD: John Hopkins University Press.

Floran, B., Floran, L., Erlij, D., & Aceves, J. (2004). Dopamine D4 receptors inhibit depolarization-induced [3H]GABA release in the rat subthalamic nucleus. *Eur J Pharmacol* 498:97–102.

Gelb, D. J., Oliver, E., & Gilman, S. (1999). Diagnostic Criteria for Parkinson Disease. *Arch Neurol* 56:33–39.

Grill, W. M., Snyder, A. N., & Miocinovic, S. (2004). Deep brain stimulation creates an informational lesion of the stimulated nucleus. *Neuroreport* 15:1137–1140.

Guehl, D., Pessiglione, M., François, C., Yelnik, J., Hirsch, E. C., Féger, J., & Tremblay, L. (2003). Tremor-related activity of neurons in the 'motor' thalamus: changes in firing rate and pattern in the MPTP vervet model of parkinsonism. *Eur J Neurosci* 17:2388–2400.

Hassler, R., Mundinger, F., & Riechert, T. (1970). Pathophysiology of tremor at rest derived from the correlation of anatomical and clinical data. *Conf Neurol* 32:79–87.

Hernandez, A., Ibanez-Sandoval, O., Sierra, A., Valdiosera, R., Tapia, D., Anaya, V., Galarraga, E., Bargas, J., & Aceves, J. (2006). Control of the subthalamic innervation of the rat globus pallidus by D2/3 and D4 dopamine receptors. *J Neurophysiol* 96:2877–2888.

Humphries, M. D., Stewart, R. D., & Gurney, K. N. (2006). A physiologically plausible model of action selection and oscillatory activity in the basal ganglia. *J Neurosci* 26:12921–12942.

Hurtado, J. M., Rubchinsky, L. L., & Sigvardt, K. A. (2004). Statistical method for detection of phase locking episodes in neural oscillations. *J Neurophysiol* 91:1883–1898.

Hurtado, J. M., Rubchinsky, L. L., Sigvardt, K. A., Wheelock, V. L., & Pappas, C. T. E. (2005). Temporal evolution of oscillations and synchrony in GPi/muscle pairs in Parkinson's disease. *J Neurophysiol* 93:1569–1584.

Hutchison, W. D., Lozano, A. M., Tasker, R. R., Lang, A. E., & Dostrovsky, J. O. (2007). Identification and characterization of neurons with tremor-frequency activity in human globus pallidus. *Exp Brain Res* 113:557–563.

Izhikevich, E. M. (2007). *Dynamical Systems in Neuroscience: The Geometry of Excitability and Bursting.* Cambridge, MA: The MIT Press.

Jellinger, K. A. (1999). Post mortem studies in Parkinson's disease: is it possible to detect brain areas for specific symptoms? *J Neural Transm Suppl* 56:1–29.

Jones, E. G. (2001). Morphology, nomenclature and connections of the thalamus and basal ganglia. In J. K. Krauss, J. Jankovic, & R. G. Grossman (Ed.), *Surgery for Parkinson's Disease and Movement Disorders* (pp. 24–47). Philadelphia: Lippincott, Williams and Wilkins.

Kita, H., & Kita, T. (2011) Role of striatum in the Pause and Burst Generation in the Globus Pallidus of 6-OHDA-Treated Rats. *Front Syst Neurosci* 5:42.

Leblois, A., Boraud, T., Meissner, W., Bergman, H., & Hansel, D. (2006). Competition between feedback loops underlies normal and pathological dynamics in the basal ganglia. *J Neurosci* 26:3567–3583.

Lenz, F., Kwan, H., Martin, R., Tasker, R. R., Dostrovsky, J. O., & Lenz, Y. E. (1994). Single unit analysis of the human ventral thalamic nuclear group. Tremor-related activity in functionally identified cells. *Brain* 117:531–543.

Levy, R., Hutchison, W. D., Lozano, A. M., & Dostrovsky, J. O. (2000). High-frequency synchronization of neuronal activity in the subthalamic nucleus of parkinsonian patients with limb tremor. *J Neurosci* 20:7766–7775.

Llinas, R. (1984). Rebound excitation as the physiological basis for tremor: a biophysical study of the oscillatory properties of mammalian central neurons in vitro. In L. J. Finley, & R. Capildeo (Ed.), *Movement Disorders, Tremor* (pp. 339–351). Macmillan, London.

Lozano, A. M., Dostrovsky, J., Chen, R., & Ashby, P. (2002). Deep brain stimulation for Parkinson's disease: disrupting the disruption. *Lancet Neurol* 1:225–231.

Mackey, M. C., & Glass, L. (1977). Oscillations and chaos in physiological control system. *Science* 197:287–289.

McIntyre, C. C., Mori, S., Sherman, D. L., Thakor, N. V., & Vitek, J. L. (2004). Electric field and stimulating influence generated by deep brain stimulation of the subthalamic nucleus. *Clin Neurophysiol* 115:589–595.

Miocinovic, S., Parent, M., Butson, C. R., Hahn, P. J., Russo, G. S., Vitek, J. L., & McIntyre, C. C. (2006). Computational analysis of subthalamic nucleus and lenticular fasciculus activation during therapeutic deep brain stimulation. *J Neurophysiol* 96:1569–1580.

Moran, A., Bergman, H., Israel, Z., & Bar-Gad, I. (2008). Subthalamic nucleus functional organization revealed by parkinsonian neuronal oscillations and synchrony. *Brain* 131:3395–3409.

Ogura, M., & Kita, H. (2000). Dynorphin exerts both postsynaptic and presynaptic effects in the Globus pallidus of the rat. *J Neurophysiol* 83:3366–3376.

Pare, D., Curro'Dossi, R., & Steriade, M. (1990). Neuronal basis of the parkinsonian resting tremor: a hypothesis and its implications for treatment. *Neuroscience* 35:217–226.

Park, C., Worth, R. M., & Rubchinsky, L. L. (2011). Neural dynamics in parkinsonian brain: the boundary between synchronized and nonsynchronized dynamics. *Physical Review E* 83, 042901.

Plenz, D., & Kitai, S. T. (1999). A basal ganglia pacemaker formed by the subthalamic nucleus and external globus pallidus. *Nature* 400:677–682.

Pollock, L. J., & Davis, L. (1930). Muscle tone in parkinsonian states. *Arch Neurol Psychiatry* 23:303–319.

Rack, P. M., & Ross, H. F. (1986). The role of reflexes in the resting tremor of Parkinson's disease. *Brain* 109:115–141.

Raethjen, J., & Deuschl, G. (2009). Tremor. *Curr Opin Neurol* 22:400–405.

Raethjen, J., Govindan, R. B., Muthuraman, M., Kopper, F., Volkmann, J., & Deuschl, G. (2009). Cortical correlates of the basic and first harmonic frequency of Parkinsonian tremor. *Clin Neurophysiol* 120:1866–1872.

Ramanathan, S., Tkatch, T., Atherton, J. F., Wilson, C. J., & Bevan, M. D. (2008). D2-like dopamine receptors modulate SKCa channel function in subthalamic nucleus neurons through inhibition of Cav2.2 channels. *J Neurophysiol* 99:442–459.

Rivlin-Etzion, M., Marmor, O., Heimer, G., Raz, A., Nini, A., & Bergman, H. (2006). Basal ganglia oscillations and pathophysiology of movement disorders. *Curr Opin Neurobiol* 16:629–637.

Romo, R., & Schultz, W. (1992). Role of primate basal ganglia and frontal cortex in the internal generation of movements. III Neuronal activity in the supplementary motor area. *Exp Brain Res* 91:396–407.

Rubchinsky, L. L., Kopell, N., & Sigvardt, K. A. (2003). Modeling facilitation and inhibition of competing motor programs in basal ganglia subthalamic nucleus - pallidal circuits. *Proc Nat Acad Sci USA* 100:14427–14432.

Rubchinsky, L. L., Kuznetsov, A. S., Wheelock, V. L., & Sigvardt, K. A. (2007). Tremor. Scholarpedia 2(10):1379. http://www.scholarpedia.org/article/Tremor

Rubin, J. E., & Terman, D. (2004). High frequency stimulation of the subthalamic nucleus eliminates pathological thalamic rhythmicity in a computational model. *J Comput Neurosci* 16:211–235.

Shen, K. Z., & Johnson, S. W. (2000). Presynaptic dopamine D2 and muscarine M3 receptors inhibit excitatory and inhibitory transmission to rat subthalamic neurones in vitro. *J Physiol* 525(Pt 2):331–41.

Shen, K. Z., & Johnson, S. W. (2005). Dopamine depletion alters responses to glutamate and GABA in the rat subthalamic nucleus. *Neuroreport* 16:171–174.

Shen, K. Z., Zhu, Z. T., Munhall, A., & Johnson, S. W. (2003). Dopamine receptor supersensitivity in rat subthalamus after 6-hydroxydopamine lesions. *Eur J Neurosci* 18:2967–2974.

Smith, Y., Raju, D. V., Pare, J. F., & Sidibe, M. (2004). The thalamostriatal system: a highly specific network of the basal ganglia circuitry. *Trends Neurosci* 27:520–527.

Speelman, J. D., Schuurman, R., de Bie, R. M., Esselink, R. A., & Bosch, D. A. (2002). Stereotactic neurosurgery for tremor. *Mov Disord* 17 (Suppl 3):S84–S88.

Surmeier, D. J., Mercer, J. N., & Chan, C. S. (2005). Autonomous pacemakers in the basal ganglia: who needs excitatory synapses anyway? *Curr Opin Neurobiol* 15:312–318.

Tarsy, D., Vitek, J. L., & Lozano, A. M. (2003). *Surgical Treatment of Parkinson's Disease and Other Movement Disorders*. Totowa, NJ: Humana Press.

Terman, D., Rubin, J. E., Yew, A. C., & Wilson, C. J. (2002). Activity patterns in a model for subthalamopallidal network of basal ganglia. *J Neurosci* 22:2963–2976.

Timmermann, L., Gross, J., Dirks, M., Volkmann, J., Freund, H. J., & Schnitzler, A. (2003). The cerebral oscillatory network of parkinsonian resting tremor. *Brain* 126:199–212.

Volkmann, J., Joliot, M., Mogilner, A., Ioannides, A. A., Lado, F., Fazzini, E., Ribary, U., & Llinas, R. (1996). Central motor loop oscillations in parkinsonian resting tremor revealed by magnetoencephalography. *Neurology* 46:1359–1370.

Weinberger, M., Hutchison, W. D., Lozano, A. M., Hodaie, M., & Dostrovsky, J. O. (2009). Increased gamma oscillatory activity in the subthalamic nucleus during tremor in Parkinson's disease patients. *J Neurophysiol* 101:789–802.

Wichmann, T., & DeLong, M. R. (1999). Oscillations in the basal ganglia. *Nature* 400:621–622.

Wilms, H., Sievers, J., & Deuschl, G. (1999). Animal models of tremor. *Mov Disord* 14:557–571.

Wilson, C. J. (2004). Basal Ganglia. In G. M. Shepherd (Ed.), *The Synaptic Organization of the Brain* (pp. 361–413). New York: Oxford University Press.

Zirh, T. A., Lenz, F. A., Reich, S. G., & Dougherty, P. M. (1998). Patterns of bursting occurring in thalamic cells during parkinsonian tremor. *Neuroscience* 83:107–121.

3. DELAYED FEEDBACK DEEP BRAIN STIMULATION FAILURE IN PARTIALLY SYNCHRONOUS PARKINSONIAN BASAL GANGLIA

3.1 Introduction

Deep brain stimulation (DBS) entails the delivery of a stimulation signal to subcortical structures via implanted electrodes. DBS has received a lot of attention as a therapeutic procedure in various neurological and neuropsychiatric disorders (Wichmann and DeLong, 2006). DBS of different targets in the basal ganglia-thalamocortical loop is used to treat motor symptoms of Parkinson's disease (PD) as well as other motor disorders (Kringelbach et al., 2007). Standard surgical targets for DBS in Parkinson's disease are subthalamic nucleus (STN) and internal Globus Pallidus (GPi), and the ventral intermediate (Vim) nucleus of the thalamus may be used in tremor-dominant Parkinson's disease.

Hypokinetic symptoms of Parkinson's disease have been related to excessive beta-band oscillations and synchrony in the basal ganglia and other structures (Hammond et al., 2007; Brown, 2007; Eusibio and Brown, 2009; Kuhn et al., 2009). Thus DBS effectiveness has been linked to the destruction of this pathological rhythmicity (Lozano et al., 2002; Grill et al., 2004; McIntyre et al., 2004) by reducing the bursting and increasing regularity and synchrony in the high-frequency band. The standard DBS paradigm utilizes strong high-frequency stimuli. Apparently these stimuli are sufficiently

strong to override pathological firing patterns and induce a more regular and less bursty signal, which is not necessarily identical to the normal one but is superior to pathological patterns. These considerations are supported by experimental studies in humans with PD, in healthy rodents and primates, and in primate and rodent models of Parkinson's disease (Hashimoto et al., 2003; Meissner et al., 2005; Hahn et al., 2008; Dorval et al., 2008). Computational studies provide an additional explanation of the way in which DBS may act at a cellular level to reduce pathological oscillations (Miocinovich et al., 2006). The standard DBS probably induces more synchronized firing in the high-frequency band and reduces pathologically synchronous oscillatory activity in the beta band, as supported by experimental observations (Wingeier et al., 2006; Kuhn et al., 2008; McCairn and Turner, 2009; Eusibio et al., 2011).

However, standard DBS has substantial side effects, which may be related to its strong stimuli and "one size fits all" approach. In particular, standard DBS is associated with a variety of adverse effects such as dyskinesia, paraesthesia, dysarthria and gait disturbances (Umemura et al., 2003), and motor performance during DBS may not be completely identical to normal performance. In addition, non-motor adverse effects such as mania, impulsivity, depression, various cognitive alterations and suicidal behavior have been reported (Appleby et al., 2007). They can arise due to current spread to adjacent structures and due to the fact that associative, limbic and motor circuits, although traditionally viewed as largely parallel in the BG, are not completely independent (Pesseglione et al., 2005).

These considerations lead to a strong interest in new DBS algorithms. Ideally, stimulation waveforms should have small amplitudes and should be targeted specifically

to destruction of the pathological activity which results in the primary symptoms (demand-based or adaptive DBS). Low amplitudes of stimulation will also save battery life, reducing the need for battery-replacement surgeries.

One method which has received a lot of attention recently and has appeared to be very promising is nonlinear delayed feedback control. Pikovsky and Rosenblum (2004a, b) considered an elegant feedback control scheme, which rendered the synchronized state in an ensemble of all-to-all coupled abstract oscillators unstable. In the limit of the large number of oscillators, the amplitude of feedback signals vanishes, which makes it especially attractive for DBS applications. This control scheme was modified into a more realistic setting: Popovych et al. (2005, 2006) showed that a delayed feedback through a mean field (a proxy for easy-to-record local field potentials, LFP) may cancel the effect of coupling and desynchronize ensembles of coupled oscillators. Subsequent studies provided further computational evidence for the ability of nonlinear delayed feedback to destabilize a synchronized state and thus to desynchronize excessively synchronous dynamics (e.g., Tukhlina et al., 2007; Popovich et al., 2008; Popovich and Tass, 2010; Guo and Rubin, 2011).

Therefore, the delayed feedback desynchronization algorithm appears to be quite robust for experimental implementation *in vivo*. However, in spite of these advances and in spite of hardware availability (Hauptmann et al., 2009), we are not aware of any clinically successful implementation of this strategy. This is clearly a challenging task and there may be many reasons why the considered desynchronization technique has resisted effective realization. The goal of this paper is to explore the action of delayed feedback DBS on the dynamics of a realistically partially-synchronous network. We

conjecture that the complex origin of partially synchronous neural dynamics in parkinsonian brain may be a substantial obstacle to implementation of delayed feedback desynchronization.

To study this problem, we employ a computational model of the basal ganglia networks which successfully reproduces experimentally recorded neural activity (Park et al., 2011). The synchronous activity in the parkinsonian brain is very intermittent (Park et al., 2010; Rubchinsky et al., 2011). The model of (Park et al., 2011) is based on the membrane properties of the basal ganglia cells and is tuned in such a way as to reproduce not only the average synchrony levels, but also the temporal patterns of the synchronous dynamics seen in human experimental data. In the language of dynamical systems theory, that model realistically describes the dynamics not only in the vicinity of the synchronized state, but also in other parts of the phase space, ensuring more substantial similarity between the model and the experimental system (Ahn et al., 2011). In contrast, the models used in earlier studies use more generic oscillators, placed in a fully synchronized regime.

We study the effect of delayed feedback in numerical experiment. When the parameters of our model are such that the dynamics is strongly synchronous, the feedback, in line with earlier studies, exerts desynchronizing action. However, this strongly synchronous dynamics is not physiologically realistic. When the model is tuned to reproduce the highly variable temporal patterns observed experimentally, the same delayed feedback tends to increase the synchrony in the system. Hence, "desynchronizing" delayed feedback acting on realistic partially synchronous dynamics may boost rather than suppress synchronization. It suggests that delayed feedback DBS is

unlikely to be successful in Parkinson's disease. It also indicates that this desynchronization strategy is not guaranteed to work if the original dynamics is not fully synchronous to begin with.

3.2 Methods

3.2.1 Model Network

We use the model of the basal ganglia studied in (Park et al., 2011). This model network is based on the developments in (Terman et al., 2002), but its dopamine-modulated parameters are tuned in such a way as to reproduce experimentally recorded data. The model consists of two arrays of neurons: an array of 10 GPe model neurons and array of 10 STN model neurons; each array has a circular structure. Neurons are connected as in (Park et al., 2011): each GPe neuron receives synaptic input from one STN neuron, while each STN neuron receives inputs from the same neuron it transmits to as well as from two of its neighbors (Fig. 3.1). While the model is clearly limited in many ways and does not incorporate other brain structures beyond STN and GPe, the model is based on experimental anatomical and physiological data and captures the rich repertoire of parkinsonian rhythmicity, recorded in these circuits in parkinsonian patients and animals (Park et al., 2011). In addition, it appears to adequately reproduce the experimentally studied mechanisms of this rhythmicity resulting from sequences of recurrent excitation and inhibition in subthalamo-pallidal networks (Bevan et al., 2002; Mallet et al., 2008).

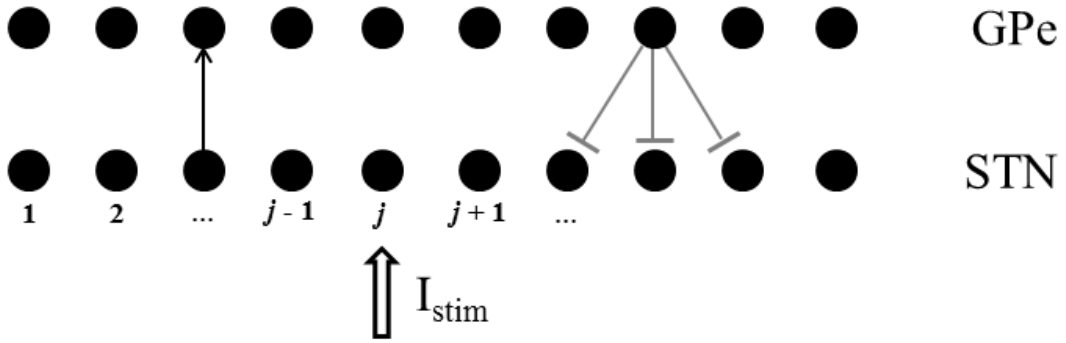

Figure 3.1. The schematics of the model network with examples of synaptic connections between neurons. Bars represent inhibitory synapses and arrows represent excitatory synapses. Delayed feedback stimulation I_{stim} is modeled as an applied current to specified STN neurons.

Both STN and GPe neuron models are described by conductance-based (Hodgkin-Huxley like) formalism, with channel properties recovered from experiment (Terman et al., 2002). The model includes leak current, fast spike-producing potassium and sodium currents, low threshold T-type and high-threshold Ca^{2+}-currents and Ca^{2+}-activated voltage-independent afterhyperpolarization (AHP) K^{+}-current in the current balance equation:

$$C\frac{dV}{dt} = -I_L - I_K - I_{Na} - I_T - I_{Ca} - I_{AHP} - I_{syn} + I_{app}$$

where $I_L = g_L(V - V_L)$, $I_K = g_K n^4 (V - V_K)$, $I_{Na} = g_{Na} m_\infty^3(V) h(V - V_{Na})$,

$I_T = g_T a_\infty^3(V) b_\infty^2(r)(V - V_{Ca})$, $I_{Ca} = g_{Ca} s_\infty^2(V)(V - V_{Ca})$, $I_{AHP} = g_{AHP}([Ca]/([Ca] + k_1))(V - V_K)$.

The intracellular concentration of calcium is described by the differential equation

$$d[Ca]/dt = \varepsilon(-I_{Ca} - I_T - k_{Ca}[Ca]).$$

The gating variables *n*, *h* and *r* obey first-order kinetic equation in the form:

$$dx/dt = \left(x_\infty(V) - x\right)/\tau_x(V).$$

Fast activation variables *m*, *a* and *s* are assumed to be instantaneous with voltage-dependent activation functions $m_\infty(V)$, $a_\infty(V)$ and $s_\infty(V)$, correspondingly. Synaptic current is given by

$$I_{syn} = g_{syn}\left(V - V_{syn}\right)\sum_j s_j,$$

where the sum is taken over the presynaptic neurons from which there are incoming connections to a given cell. The synaptic variable s_j satisfies

$$ds_j/dt = \alpha H_\infty\left(V_{presyn} - \theta_g\right)\left(1 - s_j\right) - \beta s_j.$$

While both STN and GPe neurons are described by the same kind of equations, the parameters of these equations are different, reflecting the difference in the biophysical properties of neuronal membranes. Parameters for GPe and STN neurons follow (Park et al., 2011).

3.2.2 Stimulation Setup

The scheme of the stimulation setup is given in Fig. 3.2. Time-delayed feedback is used for stimulation current following the ideas of (Rosenblum and Pikovsky, 2004a, b; Popovich et al., 2005, 2006). This type of feedback reliably disrupts correlated activity in a model of synaptically-coupled neuronal systems.

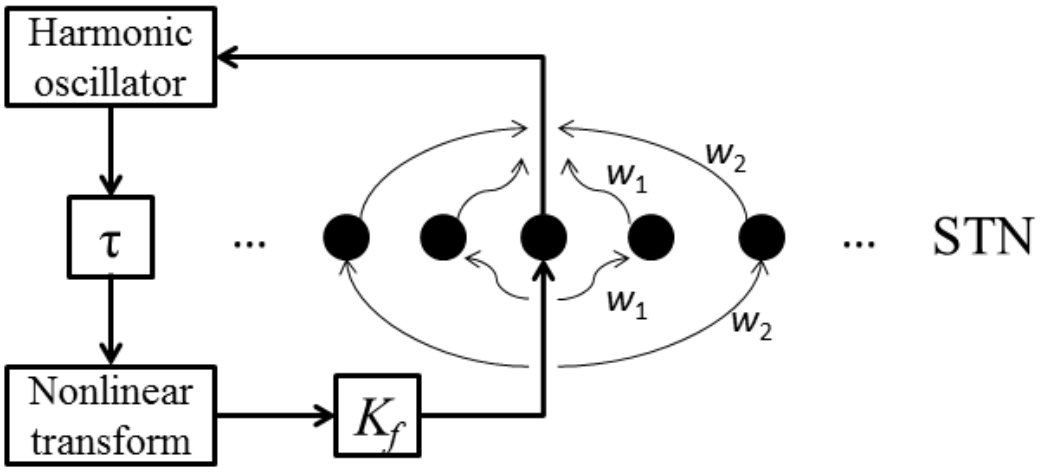

Figure 3.2. Stimulation setup for STN neurons. STN LFP is first computed from synaptic currents and then band-pass filtered using a damped harmonic oscillator. Differential delay signal is then constructed from the filtered signal, bounded by nonlinear transformation, amplified and injected into the same neurons.

The feedback signal is constructed by computing the local field potential (LFP). Following the rationale in (Park et al., 2011), STN LFP at the j^{th} neuron is computed as:

$$X_j(t) = -i_{syn,j} - w_1\left(i_{syn,j-1} + i_{syn,j+1}\right) - w_2\left(i_{syn,j-2} + i_{syn,j+2}\right) + I_{stim,j},$$

where $i_{syn,j}$ is the total synaptic current coming to the neuron j; w_1 and w_2 are weights representing the attenuation of the field with the distance. We set the weights w_1 and w_2 to several different values from the interval [0, 0.4]. We consider $w_1 > w_2$ to account for the attenuation of the signal by the tissue with $w_2 = 0.1$ or zero. However, for both choices of w_2 results were qualitatively similar.

The model LFP is measured at the same site at which stimulation is applied; therefore, the stimulation current $I_{stim,j}$ is added to $X_j(t)$. The resulting signal is then filtered using the damped harmonic oscillator as suggested in (Tukhlina et al., 2007)

$$\ddot{x}_j + \alpha_f \dot{x}_j + \omega^2 x_j = X_j(t),$$

where $\omega = 2\pi f$ and f is the bursting frequency of the model network without stimulation. Parameter $\alpha_f = \omega$ determines the band pass properties of the filter. To compensate for a phase shift introduced by filtering, the output of the harmonic oscillator is delayed by the value τ_s of the shift (Popovych et al., 2006): $\tilde{x}_j(t) = x_j\left(t - \tau_s\right)$. Time-delayed differential feedback is computed as $\tilde{x}_j(t-\tau) - \tilde{x}_j(t)$. Finally, the stimulation signal might become very strong and present danger to neuronal cells; thus it is reasonable to bound the stimulation signal. Here, we use a nonlinear transformation of the filtered signal that keeps the stimulation current strength below a maximum value K_f. The feedback stimulation current at the j^{th} STN neuron is then obtained as:

$$I_{stim,j} = 2K_f\left(1/\left(1+\exp\left(-C_1\left(\tilde{x}_j(t-\tau)-\tilde{x}_j(t)\right)/14\right)\right)-0.5\right)+w_1\left(I_{stim,j-1}+I_{stim,j+1}\right)+ w_2\left(I_{stim,j-2}+I_{stim,j+2}\right)$$

In our results in Section 3.3, we administer stimulation current to subsets of neurons in the STN array. In particular, up to three STN neurons are stimulated in every arrangement: a single neuron, two adjacent STN neurons, three adjacent neurons as well as two nonadjacent neurons (stimulation current is applied to STN neurons j and j+2) or three nonadjacent neurons (STN neurons j-2, j, and j+2 were stimulated). This gives a total of five different stimulation arrangements that we investigate in this study.

In numerical simulations, stimulation feedback was switched on 1 s after the start of simulations. A second later, the data was saved for 5 s and was subjected to the analysis (see Section 3.2.3). The model network equations were numerically solved with XPP software (Bard Ermentrout, University of Pittsburg, http://www.math.pitt.edu/~bard/xpp/xpp.html).

3.2.3 Network's Dynamics and Estimation of its Synchrony

The model network without stimulation was analyzed earlier in (Park et al., 2011) in the two-dimensional parameter space of (g_{syn}, I_{app}) – the strength of GPe to STN synaptic connections and the applied current to the GPe neurons (I_{app} represents synaptic input from striatum to pallidum). The choice of these parameters was grounded in the following considerations (Park et al., 2011; Rubchinsky et al., 2011). Both of these parameters (essentially, synaptic strengths) are affected by dopamine. In Parkinson's disease, dopaminergic cells of the substantia nigra pars compacta degenerate, thus depriving these synaptic connections of dopaminergic modulation. Larger values of g_{syn}

and smaller values of I_{app} would correspond to a parkinsonian-like state. In numerical experiments this would lead to more synchronous dynamics.

To quantitatively estimate the amount of synchrony among STN neurons principal component analysis (PCA) was used following (Park et al., 2011). The slow variable *r* from each of the STN neurons was used for the analysis (the choice of the slow variable is motivated by the fact that beta-band synchrony here is essentially a synchrony of bursting). We look at the number of principal components capturing 80% of the variation in PCA. The dynamics of the network without stimulation is presented in Fig. 3.3. The right lower corner of the network is a synchronized state, while the left upper corner is nonsynchronized state. The dashed contours in the figure indicate the parameter domain where the dynamics of the model network exhibits synchronous patterns similar to what is experimentally observed not only in average synchrony level, but also in the fine temporal structure of synchrony (Park et al., 2011). This area of parkinsonian dynamics is on the boundary between the (presumably healthy) nonsynchronous state (upper left corner) and an unrealistic strongly synchronous state (lower right corner). Given the location of the realistic firing patterns we confined our simulations to a smaller domain, which still captures the main types of dynamics (see dotted contour in Fig. 3.3). The effect of the delayed feedback stimulation on the degree of synchrony was measured by the change in the number of principal components in the model network with stimulation vs. without stimulation. This time-series analysis was done in MATLAB (Mathworks, Natick, MA).

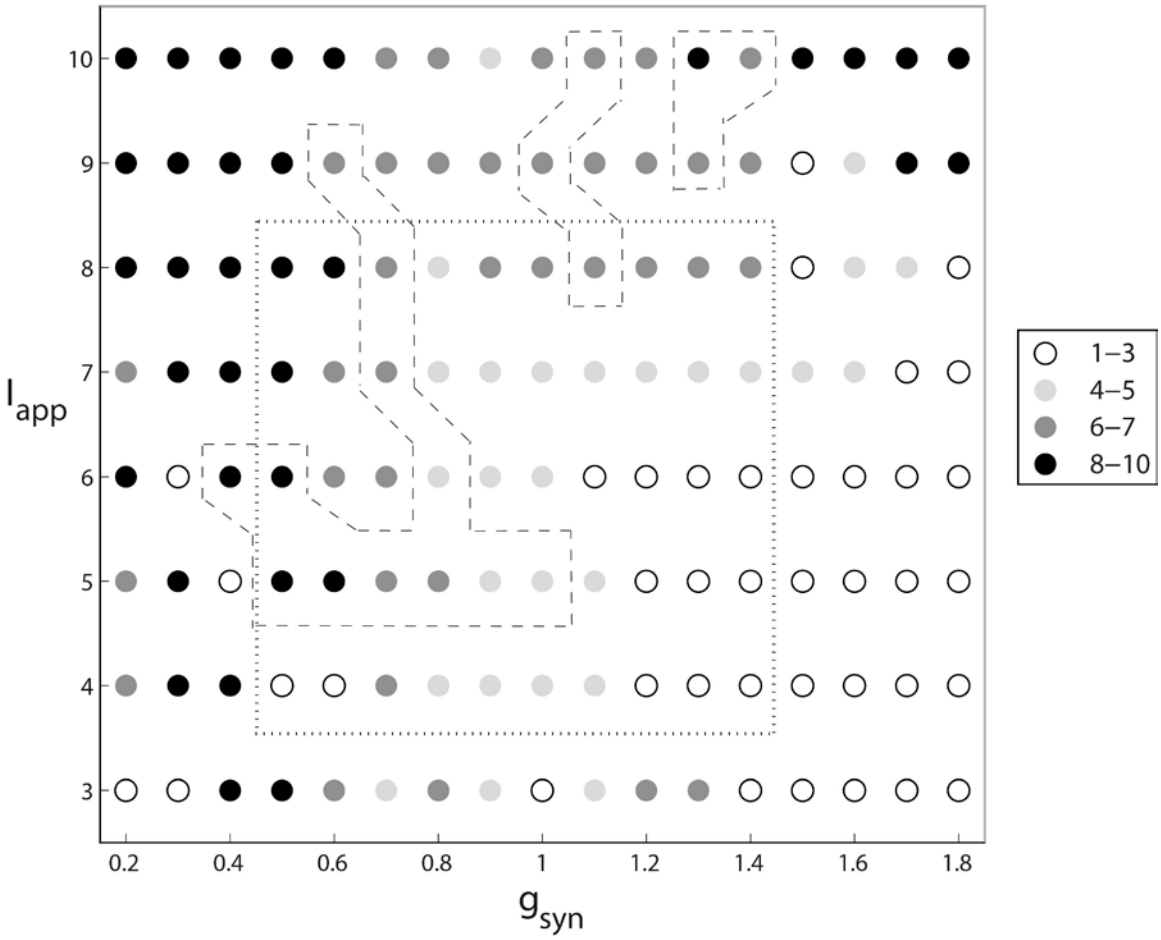

Figure 3.3. Parameter plane with the number of principal components in the network without stimulation. Points enclosed by dashed contours represent parameter values for which the model network synchronization dynamics is close to the experimental dynamics as analyzed in (Park et al., 2011) for the weight parameter $w_1 = 0.3$. Simulations with feedback stimulation were performed for the parameter values inside the dotted rectangle. The filling of the circles specifies the number of principle components; empty being synchronized dynamics and black being incoherent dynamics.

3.3 Results

Depending on the values of g_{syn} and I_{app} the STN-GPe model network may exhibit three characteristic types of collective behavior: irregular activity, strongly correlated spiking, or an intermittent synchrony regime on the boundary between the former two (Park et al., 2011). The intermittent activity in the model possesses the same temporal synchronization pattern as recorded from STN neurons in patients with Parkinson's disease (Park et al., 2010). Therefore, when measuring the effect of proposed feedback stimulation we were particularly interested in how delayed feedback stimulation acted on the realistically intermittent weak synchrony.

3.3.1 Examples of Synchronizing and Desynchronizing Action of Delayed Feedback Stimulation

An example of the action of feedback on strongly synchronous dynamics is given in Fig. 3.4a. It can be seen (Fig. 3.4a) that the stimulation leads to reduction in synchrony and more uncorrelated dynamics settles in, i.e. the phase locking between stimulated neurons is broken by the delayed feedback. Hence, feedback stimulation leads to decrease in synchronization of the whole STN network. On the contrary, in the intermittent regime (Fig. 3.4b) the same delayed feedback stimulation results in no apparent change in synchronization for moderate stimulation strengths, while stronger stimulation, in fact, leads to increased synchronization among STN neurons. While Fig. 3.4 illustrates the dynamics of only two neurons in the network, the synchronizing effect of the "desynchronizing" feedback stimulation is confirmed by the decrease in the number of principal components for the whole network as can be seen in Fig. 3.5.

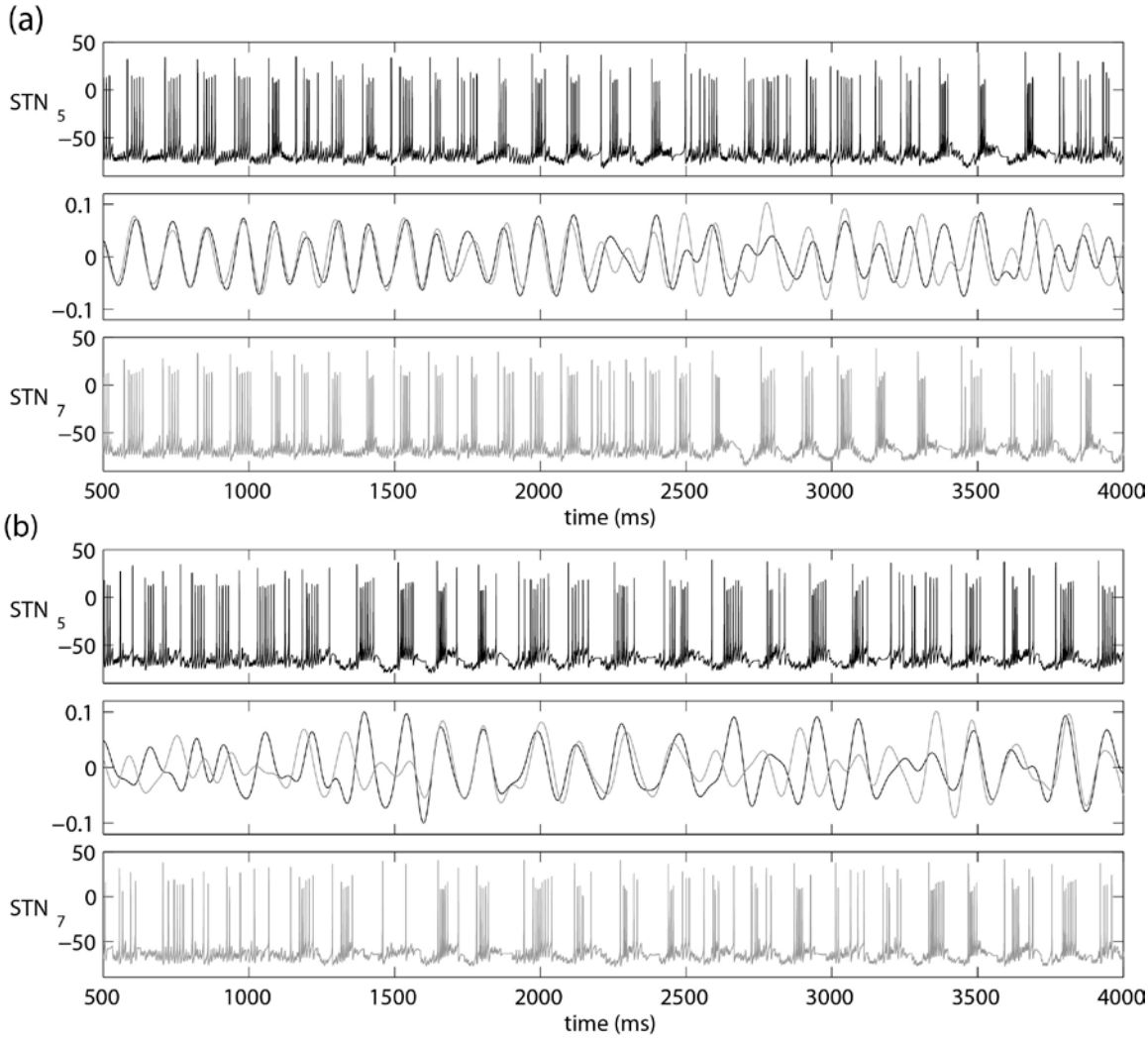

Figure 3.4. Nonlinear delayed feedback stimulation effect in the model network. a) Desynchronization of strongly synchronous STN neurons with delayed feedback stimulation. b) Feedback stimulation leads to increased synchrony in the model network in the physiological intermittent regime. The 5th and 7th STN neurons in the array are stimulated and their membrane potentials (in millivolts) are shown in the top and bottom time traces in a) and b). Middle boxes contain voltage for the 5th (black line) and 7th (gray line) STN neurons together filtered to the beta-band. Stimulation is switched on at 1000 ms. Parameters are: $w_1 = 0.3$, $w_2 = 0$, $I_{app} = 5$, a) $g_{syn} = 1.3$, $K_f = 40$. b) $g_{syn} = 0.9$, $K_f = 30$.

3.3.2 Delayed Feedback Effects on Networks with Different Synchrony Levels

To study these phenomena systematically, we consider the dynamics of the network in the two-dimensional space of parameters g_{syn} and I_{app} and vary strength of the feedback stimulation. We start by setting I_{app} at some intermediate value that, depending on the parameter g_{syn}, produces either intermittent synchrony or strongly correlated activity. Fig. 3.5 depicts the change in the number of principal components in the network stimulated with nonlinear delayed feedback compared to the network without stimulation. Here, the increase in stimulation strength leads to decrease in synchrony in the network (indicated by the increase in the number of principal components) when the synaptic parameter g_{syn} corresponds to the strongly correlated activity without stimulation (see Fig. 3.3). However, the model network which is in an intermittent synchronization regime before stimulation (see Fig. 3.3) shows no positive change in the number of principal components and eventually becomes more synchronous with stronger stimulation current. This is highlighted by the decrease in the number of principal components with higher values of K_f. Thus there is a marked difference in a trend: as g_{syn} decreases to produce less coherent pre-stimulation dynamics, the increase in the stimulation strength leads to more rather than less synchronized dynamics.

The results for several other types of spatial arrangement of stimulation electrodes are presented in Fig. 3.6. One can see that some stimulation set-ups may lead to desynchronizing effect even for moderate values of g_{syn}, however, there are nearby values of g_{syn} which yield no improvement in desynchronization.

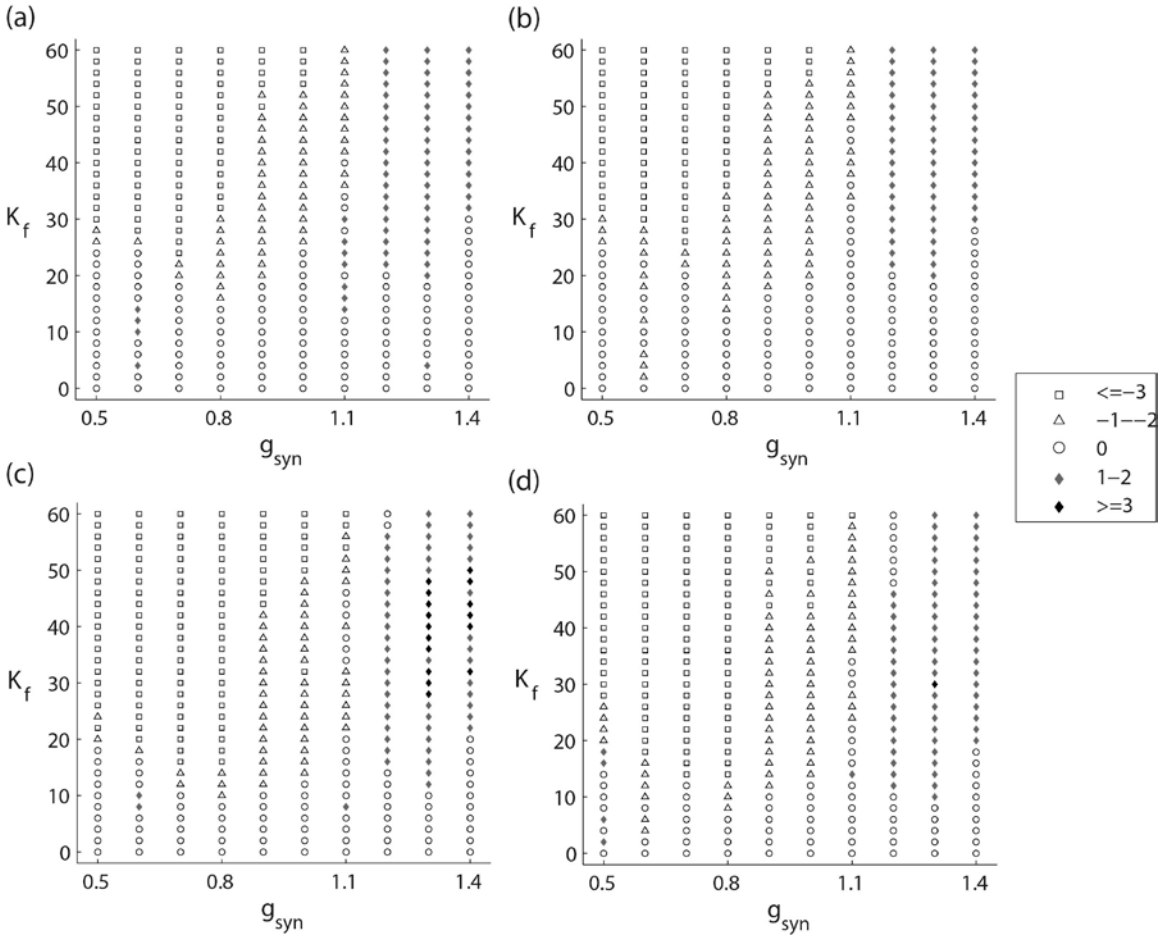

Figure 3.5. Change in the number of PCA components in the network with feedback stimulation set-ups. Positive change indicates dynamics less synchronous than pre-stimulation dynamics, negative change indicates more coherent dynamics. Two different spatial stimulation set-ups are presented and two different weights are presented. a, b) The 5th and 7th STN neurons in the array are stimulated. c, d) The 5th, 6th and 7th STN neurons are stimulated. Weight parameters are $w_1 = 0.3$, a, c) $w_2 = 0$; b, d) $w_2 = 0.1$. $I_{app} = 5$ in all simulations.

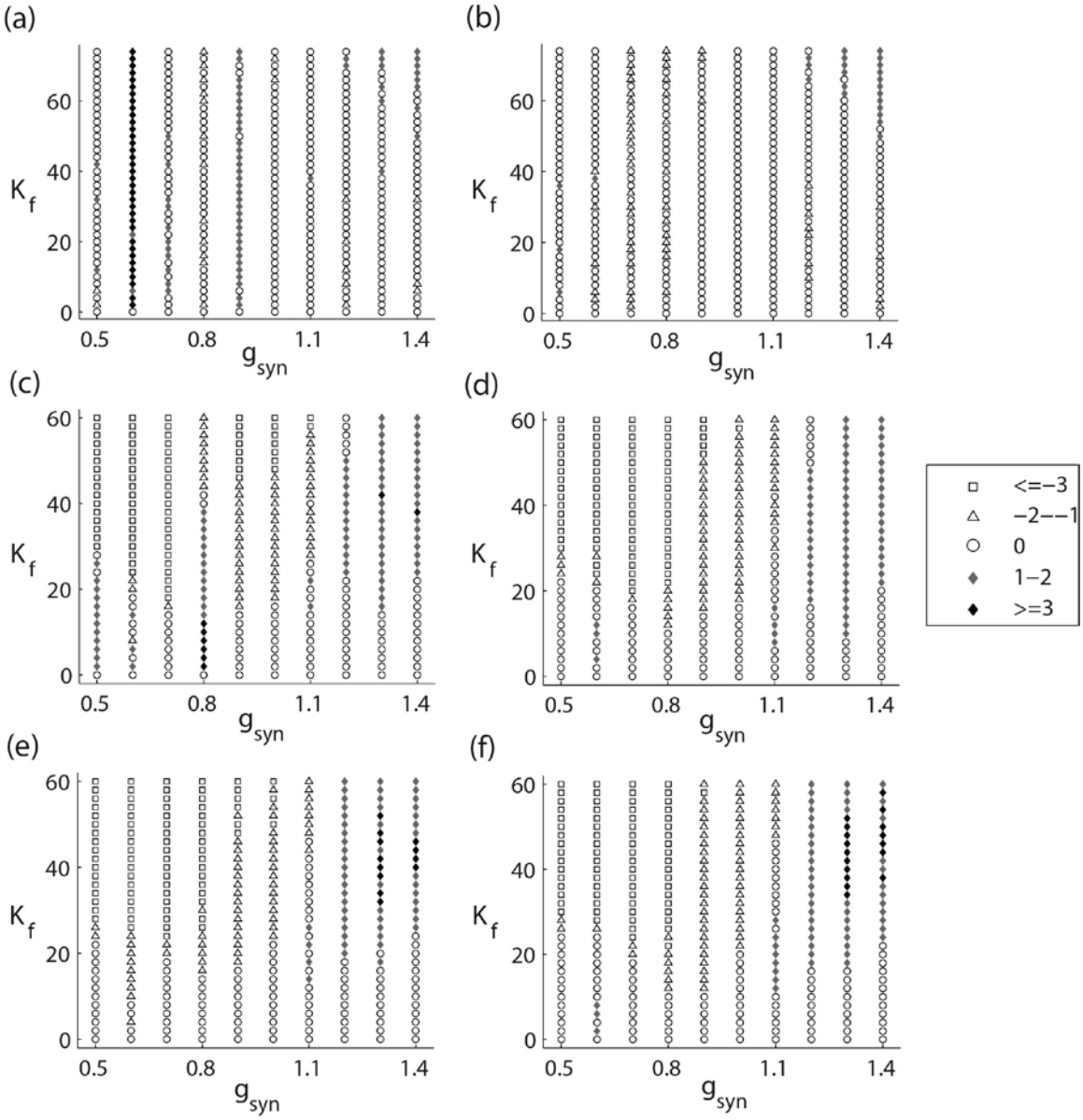

Figure 3.6. Change in the number of PCA components in a network with feedback stimulation, the spatial set-up of stimulation is different from that in figure 5. a, b) The 5th STN neuron in the array is stimulated. c, d) The 5th and 6th STN neurons are stimulated. e, f) The 5th, 7th and 9th STN neurons are stimulated. Weight parameters are $w_1 = 0.3$, a, c, e) $w_2 = 0$; b, d, f) $w_2 = 0.1$. $I_{app} = 5$ in all simulations.

Similar phenomena were observed by us for other values of I_{app}. Therefore, for a systematic study of these phenomena we will vary both control parameters (g_{syn} and I_{app}) in the model network to span a large repertoire of synchronized behavior and to include synchrony patterns similar to experimentally observed ones. To find the largest possible desynchronizing effect of the delayed feedback, we consider the maximum increase in the number of principal components, that is, the maximum desynchronization effect, in the two-parameter plane g_{syn}-I_{app} obtained over the full range of tested stimulation strengths (Fig. 3.7). The only consistent improvement in desynchronization was made in the region of strongly correlated activity (see Fig. 3.3). For the parameter values corresponding to uncorrelated activity and intermittent synchrony the desynchronization of the network was not usually achieved. On the contrary, as Fig. 3.5 shows, stronger delayed feedback stimulation at these parameter values frequently leads to stronger correlation and overall more synchronous dynamics in the network. Similar to Fig. 3.7, the effect of spatial electrode arrangements considered in Fig. 3.6 is summarized in Fig. 3.8.

Therefore, while the delayed feedback stimulation produces reliable synchrony suppression in the case of strongly correlated activity, it frequently fails to destroy synchronized activity in the network with intermittent synchrony regime that was shown to be similar to the pattern of synchrony observed in parkinsonian patients.

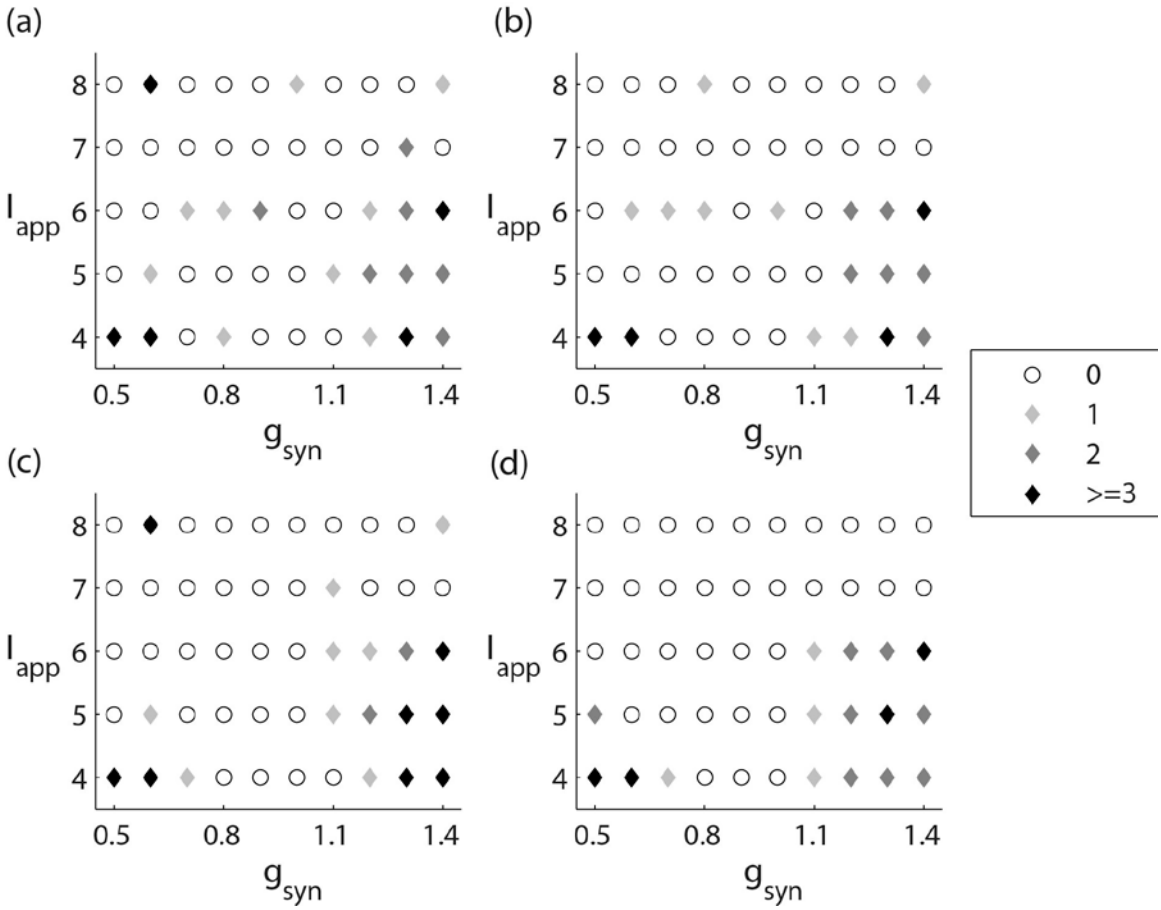

Figure 3.7. Maximum improvement in the number of principal components with the spatial electrode setups from Fig. 3.5. While the desynchronizing action (dark symbols) is consistent for the lower right corner (strongly correlated dynamics), it is very rare outside of that corner, for moderately synchronous (and more realistic) dynamics. Diamonds indicate desynchronizing action of stimulation of various efficiency (indicated by the darkness of the filling). Circles indicate no desynchronization. Note that unlike Fig. 3.5, here we consider the maximum improvement; so that it cannot be negative (it is always zero for zero stimulation strength). a, b) The 5^{th} and 7^{th} STN neurons in the array are stimulated. c, d) The 5^{th}, 6^{th} and 7^{th} STN neurons are stimulated. Weight parameters are $w_1 = 0.3$, a, c) $w_2 = 0$; b, d) $w_2 = 0.1$.

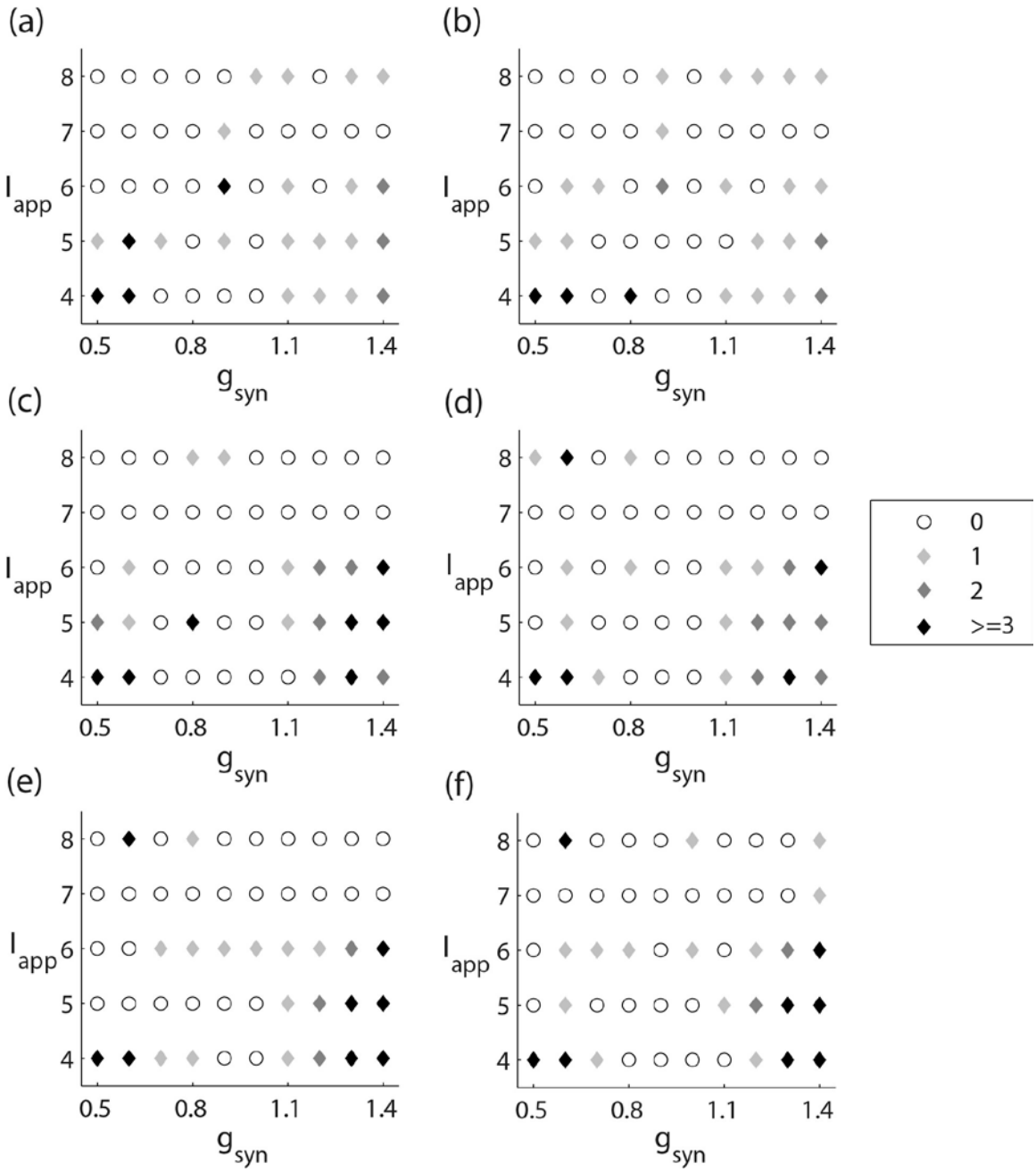

Figure 3.8. Maximum improvement in the number of principal components with the spatial electrode setups from Fig. 3.6. These results are overall similar to those in Fig. 3.7. a, b) The 5th STN neuron in the array is stimulated. c, d) The 5th and 6th STN neurons are stimulated. e, f) The 5th, 7th and 9th STN neurons are stimulated. Weight parameters are $w_1 = 0.3$, a, c, e) $w_2 = 0$; b, d, f) $w_2 = 0.1$.

3.4 Discussion

3.4.1 Potential Limitations of the Modeling

The modeling approach used here obviously does not include many factors which may be crucial for the physiology of parkinsonian basal ganglia. For example, the basal ganglia model is imperfect in that the real mechanisms of the generation of the synchronized beta-band oscillations may be much more complicated. However, the model does a good job at reproducing the experimentally observed synchrony patterns (Park et al., 2011). Therefore even though the model may have some mechanistic deficiencies, it appears to be dynamically adequate for studying the real basal ganglia circuits in Parkinson's disease. In the terms of the phase space, there is an equivalence of the phase spaces of the model and of the real dynamics not only in a vicinity of the synchronization manifold, but in other areas of the space. This is important because the overall synchrony level is not very strong and the system spends a substantial fraction of time in those areas of the phase space.

The computation of LFPs, stimulation field and its effect on the cells is relatively simplistic, however a more precise account of the field distribution (similar to is likely to make desynchronization even more challenging. The number of neurons in the model is relatively small. So that really vanishing stimulation desynchronization (where control term is zero in the desynchronized state) is not possible. However, this should not negate the observations of this study. We follow the change in the degree of synchrony in the

network, whether the stimulation truly vanishes or not. What is important is that if the stimulation is applied for a partially synchronous regime, desynchronization is not achieved.

Modeling studies suggest that the structure and parameters of the feedback stimulation affect the efficiency of desynchronization. For example, computing the mean field from a group of elements, not completely coincident with the group of stimulated elements, made the domain of existence of desynchronization smaller (Rosenblum et al., 2006). This may be of potential relevance to the subthalamic nucleus, because the mean filed is likely to be generated by pallidal synaptic activity and is represented in such a way in the model utilized here. Also, for moderate strengths of the feedback loop, the delayed feedback stimulation may exert a synchronizing effect; however the desynchronizing effect occurs for larger values of the strength of the feedback loop (Popovich et al., 2008). But these issues are unlikely to vitiate the major result of our study. We had no problem in obtaining desynchronization in a network which is fully synchronous to begin with. However as parameters of the network are gradually changed in such a way as to obtain experimentally realistic, partially synchronous firing patterns the “desynchronizing” feedback gradually loses the ability to decrease synchrony strength in the system and, in fact, eventually increases the synchrony level. We varied the strength of the feedback for each of the parameter sets of the model network to find the optimal stimulation characteristics, but it did not affected the general outcome. We do not completely exclude the possibility that *some* feedback control may potentially decrease synchrony of a partially synchronized dynamics in parkinsonian basal ganglia. However,

our results indicate that *the same* delayed feedback stimulation that desynchronizes complete synchrony may actually increase synchrony strength in a partially synchronized regime.

3.4.2 Conclusions

In the context of Parkinson's disease the results indicate that delayed nonlinear feedback is likely to increase synchrony in the basal ganglia of parkinsonian patients rather than suppress it. This suggests a need for further attention to other DBS techniques. For example, coordinated resetting (e.g., Hauptmann and Tass, 2010) may be efficient in desynchronizing (it is also may be beneficial due to the improvement in thalamocortical relay function, Guo and Rubin, 2011). However, unlike the delayed feedback stimulation it does not vanish in the limit of a large number of oscillators. Another non-vanishing, but potentially efficient technique is based on the optimization of the stimulation waveforms (Feng et al., 2007a,b; Wongsarnpigoon and Grill, 2010), where the stimulation signals are drawn from a broad class of waveforms and optimized by genetic search algorithms. An emerging model-based approach based on Kalman filtering may be promising too (Schiff, 2010).

The other important implication of the present study extends beyond the context of DBS in Parkinson's disease. Our results indicate that even if a control strategy destabilizes a fully synchronized state, its action on weakly synchronous dynamics may be quite opposite. This, perhaps, should not be very surprising. The major idea behind desynchronizing algorithms like desynchronizing nonlinear delayed feedback is that they are set up in such a way as to make the synchronous state unstable. However the neural

synchrony, especially in human brain is far from being stable even in pathological conditions; rather it varies in time and has a moderate overall strength. Thus what defines synchrony strength in the system is not only the stability/instability properties of the synchronized state, but also the mechanisms pushing the system back to a synchronous state. The desynchronizing strategies such as delayed nonlinear feedback are mostly concerned with destabilizing synchronous state and do not address these other issues.

A number of neurological and psychiatric conditions have being associated with elevated levels of synchrony of neural oscillations (Schnitzler and Gross, 2005; Uhlhaas and Singer, 2006). Desynchronizing deep brain stimulation may have therapeutic potential for treatment of any conditions where excessive synchrony leads to pathological symptoms. However, as the current study suggests, to identify a viable desynchronization algorithm, one needs to test it in models with reasonably accurate reproduction of the clinically relevant features of synchronized oscillatory activity.

Bibliography

Ahn, S., Park, C., & Rubchinsky, L. L. (2011). Detecting the temporal structure of intermittent phase locking. *Physical Review E* 84:016201.

Appleby, B. S., Duggan, P. S., Regenberg, A., & Rabins, P. V. (2007). Psychiatric and neuropsychiatric adverse events associated with deep brain stimulation: A meta-analysis of ten years' experience. *Mov Disord* 22:1722–28.

Bevan, M. D., Magill, P. J., Terman, D., Bolam, J. P., & Wilson, C. J. (2002). Move to the rhythm: oscillations in the subthalamic nucleus-external globus pallidus network. *Trends Neurosci* 25:525–31.

Brown, P. (2007). Abnormal oscillatory synchronisation in the motor system leads to impaired movement. *Curr Opin Neurobio.* 17:656–64.

Dorval, A. D., Russo, G. S., Hashimoto, T., Xu, W., Grill, W. M., & Vitek, J. L. (2008). Deep brain stimulation reduces neuronal entropy in the MPTP-primate model of Parkinson's disease. *J Neurophysiol* 100:2807–18.

Eusebio, A., & Brown, P. (2009). Synchronisation in the beta frequency-band – the bad boy of parkinsonism or an innocent bystander? *Exp Neuro* 217:1–3.

Eusebio, A., Thevathasan, W., Doyle Gaynor, L., Pogosyan, A., Bye, E., Foltynie, T., Zrinzo, L., Ashkan, K., Aziz, T., & Brown, P. (2011). Deep brain stimulation can suppress pathological synchronisation in parkinsonian patients. *J Neurol Neurosurg Psychiatry* 82:569–73.

Feng, X. J., Greenwald, B., Rabitz, H., Shea-Brown, E. & Kosut, R. (2007). Toward closed-loop optimization of deep brain stimulation for Parkinson's disease: concepts and lessons from a computational model. *J Neural Eng* 4:L14–21.

Grill, W. M., Snyder, A. N., & Miocinovic, S. (2004). Deep brain stimulation creates an informational lesion of the stimulated nucleus. *Neuroreport* 15:1137–40.

Guo, Y., & Rubin, J. E. (2011). Multi-site stimulation of subthalamic nucleus diminishes thalamocortical relay errors in a biophysical network model. *Neural Netw* 24:602–16.

Hahn, P. J., Russo, G. S., Hashimoto, T., Miocinovic, S., Xu, W., McIntyre, C. C., & Vitek, J. L. (2008). Pallidal burst activity during therapeutic deep brain stimulation. *Exp Neuro.* 211:243–351.

Hammond, C., Bergman, H., & Brown, P. (2007). Pathological synchronization in Parkinson's disease: networks, models and treatments. *Trends Neurosci* 30:357–64.

Hashimoto, T., Elder, C. M., Okun, M. S., Patrick, S. K., & Vitek, J. L. (2003). Stimulation of the subthalamic nucleus changes the firing pattern of pallidal neurons. *J Neurosci* 23:1916–23.

Hauptmann, C., Roulet, J. C., Niederhauser, J. J., Döll, W., Kirlangic, M. E., Lysyansky, B., Krachkovskyi, V., Bhatti, M. A., Barnikol, U. B., Sasse, L., Bührle, C. P., Speckmann, E. J., Götz, M., Sturm, V., Freund, H. J., Schnell, U., & Tass, P. A. (2009). External trial deep brain stimulation device for the application of desynchronizing stimulation techniques. *J Neural Eng* 6:066003.

Hauptmann, C., & Tass, P. A. (2010). Restoration of segregated, physiological neuronal connectivity by desynchronizing stimulation. *J Neural Eng* 7:056008.

Hurtado, J. M., Rubchinsky, L. L., Sigvardt, K. A., Wheelock, V. L., & Pappas, C. T. E. (2005). Temporal evolution of oscillations and synchrony in GPi/muscle pairs in Parkinson's disease. *J Neurophysio.* 93:1569–84.

Kringelbach, M. L., Jenkinson, N., Owen, S. L., & Aziz, T. Z. (2007). Translational principles of deep brain stimulation. *Nat Rev Neurosci* 8:623–35.

Kühn, A. A., Hauptmann, C., Roulet, J. C., Niederhauser, J. J., Döll, W., Kirlangic, M. E., Lysyansky, B., Krachkovskyi, V., Bhatti, M. A., Barnikol, U. B., Sasse, L., Bührle, C. P., Speckmann, E. J., Götz, M., Sturm, V., Freund, H. J., Schnell, U., & Tass, P. A. (2008). High-frequency stimulation of the subthalamic nucleus suppresses oscillatory beta activity in patients with Parkinson's disease in parallel with improvement in motor performance. *J Neurosci* 28:6165–73.

Lozano, A. M., Dostrovsky, J., Chen, R., & Ashby, P. (2002). Deep brain stimulation for Parkinson's disease: disrupting the disruption. *Lancet Neurol* 1:225–31.

Mallet, N., Pogosyan, A., Marton, L. F., Bolam, J. P., Brown, P., & Magill, P. J. (2008). Parkinsonian beta oscillations in the external globus pallidus and their relationship with subthalamic nucleus activity. *J Neurosci* 28:14245–58.

McCairn, K. W., & Turner, R. S. (2009). Deep brain stimulation of the globus pallidus internus in the parkinsonian primate: local entrainment and suppression of low-frequency oscillations. *J Neurophysiol* 101:1941–60.

McIntyre, C. C., Mori, S., Sherman, D. L., Thakor, N. V., & Vitek, J. L. (2004). Electric field and stimulating influence generated by deep brain stimulation of the subthalamic nucleus. *Clin Neurophysiol* 115:589–95.

Meissner, W., Leblois, A., Hansel, D., Bioulac, B., Gross, C. E., Benazzouz, A., & Boraud, T. (2005). Subthalamic high frequency stimulation resets subthalamic firing and reduces abnormal oscillations. *Brain* 128:2372–82.

Miocinovic, S., Parent, M., Butson, C. R., Hahn, P. J., Russo, G. S., Vitek, J. L., & McIntyre, C. C. (2006). Computational analysis of subthalamic nucleus and lenticular fasciculus activation during therapeutic deep brain stimulation. *J Neurophysiol* 96:1569–80.

Park, C., Worth, R. M., & Rubchinsky, L. L. (2010). Fine temporal structure of beta oscillations synchronization in subthalamic nucleus in Parkinson's disease. *J Neurophysiol* 103:2707–16.

Park, C., Worth, R., & Rubchinsky, L. L. (2011). Neural Dynamics in Parkinsonian Brain: The Boundary Between Synchronized and Nonsynchronized Dynamics. *Physical Review E* 83:042901.

Pessiglione, M., Guehl, D., Rolland, A. S., Francois, C., Hirsch, E. C., Feger, J., & Tremblay, L. (2005). Thalamic neuronal activity in dopamine-depleted primates: evidence for a loss of functional segregation within basal ganglia circuits. *J Neurosci* 25:1523–31.

Popovych, O. V., Hauptmann, C., & Tass, P. A. (2005). Effective desynchronization by nonlinear delayed feedback. *Phys Rev Lett* 94:164102.

Popovych, O. V., Hauptmann, C., & Tass, P. A. (2006). Control of neuronal synchrony by nonlinear delayed feedback. *Biol Cybern* 95:69–85.

Popovych, O. V., Hauptmann, C., & Tass, P. A. (2008). Impact of nonlinear delayed feedback on synchronized oscillators. *J Biol Phys* 34:267–79.

Popovych, O. V., & Tass, P. A. (2010). Synchronization control of interacting oscillatory ensembles by mixed nonlinear delayed feedback. *Phys Rev E Stat Nonlin Soft Matter Phys* 82:026204.

Rosenblum, M. G., & Pikovsky, A. S. (2004a). Controlling synchronization in an ensemble of globally coupled oscillators. *Phys Rev Lett* 92:114102.

Rosenblum, M., & Pikovsky, A. (2004b). Delayed feedback control of collective synchrony: an approach to suppression of pathological brain rhythms. *Phys Rev E Stat Nonlin Soft Matter Phys* 70:041904.

Rosenblum, M., Tukhlina, N., Pikovsky, A., & Cimponeriu, L. (2006). Delayed Feedback Suppression of Collective Rhythmic Activity in a Neuronal Ensemble. *Int J Bifurcation and Chaos* 16:1989–99.

Rubchinsky, L. L., Park, C., & Worth, R. M. (2011). Intermittent neural synchronization in Parkinson's disease. To appear in *Nonlinear Dynamics* (DOI: 10.1007/s11071-011-0223-z).

Schiff, S. J. (2010). Towards model-based control of Parkinson's disease. *Philos Transact A Math Phys Eng Sci* 368:2269–308.

Schnitzler, A., & Gross, J. (2005). Normal and pathological oscillatory communication in the brain. *Nat Rev Neurosci* 6:285–96.

Terman, D., Rubin, J. E., Yew, A. C., & Wilson, C. J. (2002). Activity patterns in a model for subthalamopallidal network of basal ganglia. *J Neurosci* 22:2963–76.

Tukhlina, N., Rosenblum, M., Pikovsky, A., & Kurth, J. (2007). Feedback suppression of neural synchrony by vanishing stimulation. *Phys Rev E Stat Phys Plasmas Fluids Relat Interdiscip Topics* 75:011918.

Tukhlina, N., & Rosenblum, M. (2008). Feedback suppression of neural synchrony in two interacting populations by vanishing stimulation. *J Biol Phys* 34:301–14.

Uhlhaas, P. J., & Singer, W. (2006). Neural synchrony in brain disorders: relevance for cognitive dysfunctions and pathophysiology. *Neuron* 52:155–68.

Umemura, A., Jaggi, J. L., Hurtig, H. I., Siderowf, A. D., Colcher, A., Stern, M. B., & Baltuch, G. H. (2003). Deep brain stimulation for movement disorders: morbidity and mortality in 109 patients. *J Neurosurg* 98:779–84.

Wichmann, T., & Delong, M. R. (2006). Deep brain stimulation for neurologic and neuropsychiatric disorders. *Neuron* 52:197–204.

Wingeier. B., Tcheng, T., Koop, M. M., Hill, B. C., Heit, G., & Bronte-Stewart, H. M. (2006). Intra-operative STN DBS attenuates the prominent beta rhythm in the STN in Parkinson's disease. *Exp Neurol* 197:244–51.

Wongsarnpigoon, A., & Grill, W. (2010). Energy-efficient waveform shapes for neural stimulation revealed with a genetic algorithm. *J Neural Eng* 7:046009.

4. EXPLORING NEURONAL BISTABILITY AT THE DEPOLARIZATION BLOCK

4.1 Introduction

Bistability – coexistence of two firing modes in the same experimental conditions – has been documented in different types of neurons. Tonic spiking coexists with bursting (Shilnikov et al., 2005) or with a different spiking mode (Cymbalyuk and Shilnikov, 2005) in leach heart cells. Bistability of bursting and spiking was also discovered in neuron R15 of the marine mollusk *Aplysia* (Lechner et al., 1996). In this paper, we focus on the bistability between a resting and tonic spiking states. This type of bistability was observed in different motor neurons (Hounsgaard et al., 1984; Le et al., 2006; Lee and Heckman, 1996). The same type of bistability is hypothesized to be involved in short-term memory (discussed in Marder et al., 1996). In a bistable cell, a short signal triggers a long-lasting change in the firing, which encodes the last input. Altogether, bistability is common among neurons and endows them with richer forms of information processing.

In this study we focus on the bistability at the transition to the state called depolarization block – a silent state that occurs in every neuron when it receives excessive excitation. *In vitro*, a neuron enters depolarization block whenever the applied current exceeds a certain level. In a slightly different experiment, an iontophoresis current that supplies an excitatory neurotransmitter can also lead the neuron into depolarization block. Its minimal value that silences the neuron characterizes the neuron and the specific

receptor (e.g. NMDA). Furthermore, depolarization block was suggested to explain the therapeutic action of antipsychotic drugs (Grace et al., 1997). In schizophrenia and other diseases, the level of the neurotransmitter dopamine (DA) is abnormally high. Antipsychotics were shown to have a direct excitatory influence on the neurons releasing dopamine – dopaminergic neurons. This should further elevate the DA levels unless the DA neuron enters depolarization block and stops releasing dopamine. The effectiveness of the antipsychotics was linked to their ability to suppress DA neuron activity by depolarization block. DA neuron is one of two examples explored in this article.

Bistability at the transition to depolarization block has been observed in multiple neurons (Guttman et al., 1980; Hounsgaard et al., 1984; Lee and Heckman, 1996; Marder et al., 1996; Le et al., 2006). However, it was not studied in models (but see Rinzel, 1978) and, more importantly, most experimental studies pay no attention to bistability at this transition. The terminology itself is not ready to account for two separate transitions – the stabilization of the silent state and the cessation of spiking. Which of these transitions should be called depolarization block? Which one is observed in experiments? This depends on the experimental protocol. What does it say about the neuron when spiking and the silent state are both stable in a wide range of the applied current? We address these questions and prepare a theoretical basis for experimental studies of bistability. We investigate what factors contribute to bistability at the transition to depolarization block.

4.1.1 Definitions

We start by defining the notions of bistability and hysteresis in a dynamical system.

Definition 1. The lack of reversibility as a parameter is varied is called hysteresis (Strogatz, 1994).

Definition 2. A dynamical system having two coexisting attractors (stable solutions) is called bistable (Izhikevich, 2007). The solutions attract trajectories starting from different initial conditions and determine distinct long-term behavior.

Bistability is realized in a range of a parameter and is generally lost at bifurcations as a stable solution disappears or loses stability. Bistability for some range of the parameter is a necessary condition for hysteresis in any dynamical system.

The definition of depolarization block and the experimental protocols do not take into account bistability at a strong applied depolarization. The cessation of oscillations involves the loss of stability or the disappearance of the oscillatory solution and transition to the stable equilibrium state. This may occur by different scenarios.

Scenario 1: The oscillatory solution that corresponds to spiking decreases in amplitude to zero and merges with the equilibrium that corresponds to the silent state. The silent state becomes stable. This transition is a single supercritical Andronov-Hopf bifurcation, and it does not involve any hysteresis (see e.g. Fig. 4.3c).

Scenario 2: The equilibrium state becomes stable by giving birth to an unstable oscillatory solution. This is a subcritical Andronov-Hopf bifurcation. Further increase in the applied current causes the unstable oscillatory solution to merge with the stable one, which corresponds to spiking (see e.g. Fig. 4.3b). Both solutions disappear, and this

transition is a saddle-node bifurcation of oscillatory solutions (limit cycles). This transition involves bistability because between the Andronov-Hopf and the saddle-node bifurcations, the stable equilibrium and the stable oscillatory solution coexist.

To correctly describe the range of applied current where both solutions are stable - bistability range, we introduce the following definitions:

Definition 3. We call the range of the applied current where the equilibrium state is unstable the instability range.

Definition 4. We call the range of the applied current where a stable oscillatory solution exists the oscillatory range.

When there is no bistability in the model, these parameter ranges coincide. On the other hand, when the oscillatory solution disappears in a saddle-node bifurcation of limit cycles, the oscillatory range extends to higher applied currents than the instability range. The difference between these ranges is exactly the bistability range.

The main objective of the current study is to reveal mechanisms that cause bistability in the spiking subsystem of a neuron comprised of the fast sodium and the rectifying potassium currents. Virtually every neuron has these currents and their interaction results in very different transitions between tonic spiking and the silent state. One example we consider in this article is the giant squid axon modeled by Hodgkin and Huxley (1952). We call it the Hodgkin-Huxley (HH) neuron in the rest of the article. In the HH neuron, there is no bistability at the transition to depolarization block (Fig. 4.3c). The transition from spiking to silence occurs through the supercritical Andronov-Hopf bifurcation. The other example we consider is the spiking subsystem of the dopaminergic (DA) neuron (Kuznetsov et al., 2006). The DA neuron model displays strong bistability

over a large range of applied depolarization. The model includes several currents that work in the voltage range below the spike initiation threshold, but bistability remains strong even when the model is reduced to spiking currents only. We call this reduced model the DA neuron in the rest of the paper for simplicity. After the reduction, the model includes exactly the same set of spiking currents and has the same structure and dimension as the model in (Hodgkin and Huxley, 1952). Thus, it's not a different set of currents, but rather altered parameters of the same spike-producing currents that determine if the model displays bistability or not. In this paper, we identify particular parameters of the spiking currents that produce hysteresis and discuss physiological distinctions that characterize these currents in different neuron types.

4.2 Methods

4.2.1 Conductance-Based Model

Our DA and HH neurons are simply two different sets of parameters for the following conductance-based model. The model contains delayed rectifier potassium, fast sodium and leak currents and is given by the following system of differential equations:

$$C\frac{dv}{dt} = I_{app} - g_K n^4 (v - E_K) - g_{Na} m_\infty^3 (v) h (v - E_{Na}) - g_L (v - E_L)$$

$$\frac{dn}{dt} = \left(n_\infty (v) - n\right)/\tau_n (v)$$

$$\frac{dh}{dt} = \left(h_\infty (v) - h\right)/\tau_h (v)$$

where *v* is the membrane potential in mV, *n* and *h* are the activation gating variable for the K^+ current and the inactivation gating variable for the Na^+ current, correspondingly.

Thus the model is a 3-dimensional dynamical system with variables *v*, *n* and *h*. Gating variables have steady state voltage-dependent functions in the form

$$X_\infty(v) = 1/\left(1+\exp\left(-(v-v_{Xh})/S_X\right)\right)$$

(where *X* can be *m*, *n* or *h*) and voltage-dependent time constant functions given by

$$\tau_X(v) = \tau_X{}^0 + \tau_X{}^1 \exp\left(-(v-\theta_X)^2 / S_X{}^\tau\right)$$

(where X is *n* or *h*). The model parameter values for the HH neuron and the DA neuron are given in table 4.1. Computer simulations were performed in XPPAUT (Ermentrout, 2002) using the stiff method and a time step of 0.1 ms.

The comparison of the steady state functions of the DA neuron and the HH neuron shows that the half-activation/inactivation values for the DA neuron are about 20 mV above the corresponding values for the HH neuron (Figs. 4.1a-b, 4.2a). Also, the DA neuron steady state functions are steeper than those of the HH neuron. The timescales of all three variables change by an order of magnitude as the system evolves in the phase space. Thus, there is no permanent timescale separation among the variables, and we only compare the timescales of the corresponding variables in the two neurons. The time constants of the K^+ and the Na^+ currents display steeper voltage dependence in the DA neuron and are an order of magnitude greater. This makes the K^+ current activation and the Na^+ current inactivation effectively slower than in the HH neuron (Figs. 4.1c, 4.2b). The time constant τ_v of the membrane potential *v* depends on what currents are open. Its minimum is determined by the conductance of the sodium current $\tau_{v\min} = C/g_{Na}$, and has

Table 4.1. Parameter values for the DA neuron and the HH neuron.

Parameter	Value		Dimension
	DA neuron	HH neuron	
C	1	1	$\mu F/cm^2$
g_K	4	36	mS/cm^2
g_{Na}	150	120	mS/cm^2
g_L	0.05	0.3	mS/cm^2
E_K	-90	-77	mV
E_{Na}	55	55	mV
E_L	-34.4	-54.4	mV
Na^+ current activation constants			
v_{mh}	-18	-40	mV
S_m	8	9	
Na^+ current inactivation constants			
v_{hh}	-48	-62	mV
S_h	-4	-7	
τ_h^0	1	1.2	
τ_h^1	55	7.4	
θ_h	-53	-67	
S_h^τ	12	20	
DR current activation constants			
v_{nh}	-35	-53	mV
S_n	8	15	
τ_n^0	5	1.1	
τ_n^1	51	4.7	
θ_n	-79	-53	
S_n^τ	23	50	

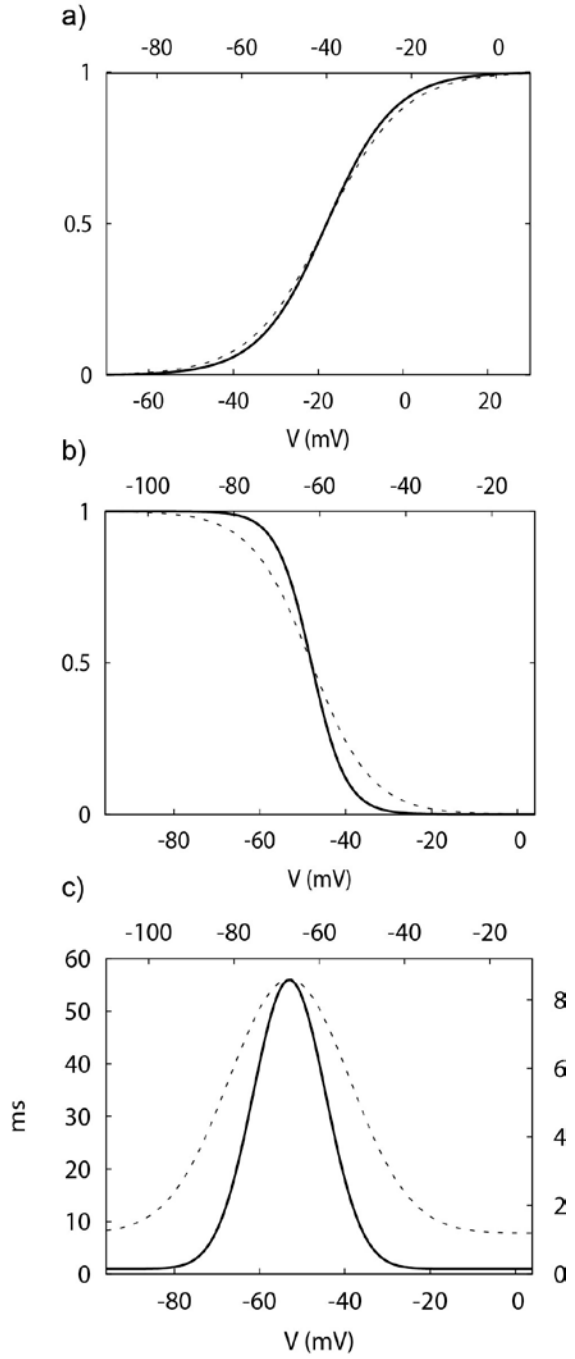

Figure 4.1. The activation a) and inactivation b) functions of the Na^+ current in the DA neuron (solid curve) and the HH neuron (dashed curve). c) The time constant function of the Na^+ current. Note that the functions are shifted by around 20 mV for a better comparison of the slopes. The ranges for the HH neuron are at the top and to the right.

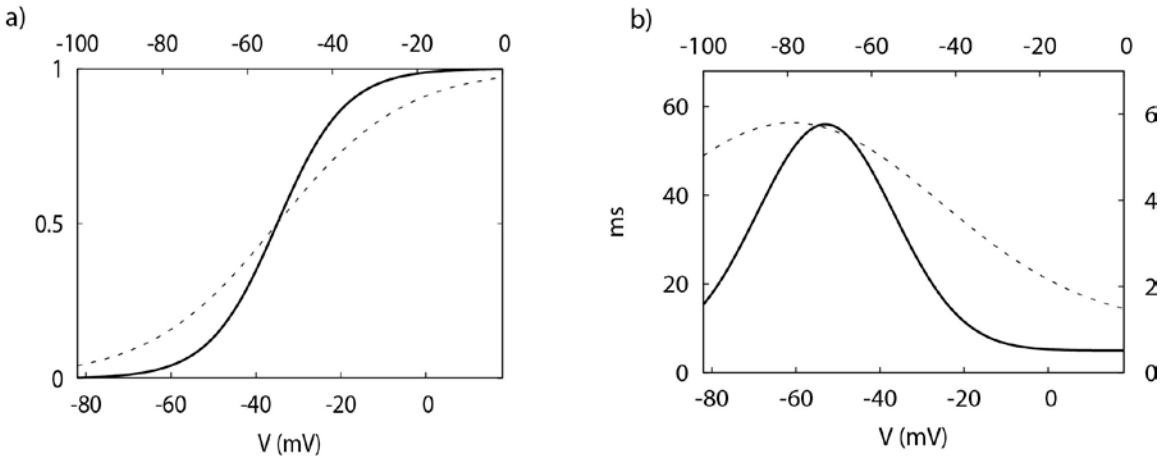

Figure 4.2. The activation a) and time constant b) functions of the K^+ current from the DA neuron (solid curve) and the HH neuron (dashed curve). The ranges for the HH neuron are at the top and to the right.

a similar value in both neurons. Its maximum is approximated by the leak conductance $\tau_{v\max} = C/g_L$, and has a much greater value in the DA neuron (τ_v = 20 ms) than in the HH neuron (τ_v = 3.3 ms).

Below we change half-(in)activation parameter values v_{nh} and v_{hh} simultaneously with θ_n and θ_h, respectively. These parameters are linked for all channels, and such manipulation is the most physiologically relevant.

4.3 Results

The DA neuron demonstrates Class 3 excitability (Izhikevich, 2007): The resting state remains stable for any value of the applied current. The oscillatory solution emerges from a saddle-node bifurcation of limit cycles, and stays completely isolated from the equilibrium state (Fig. 4.3a). When the half-activation of the K^+ current, v_{nh}, is increased

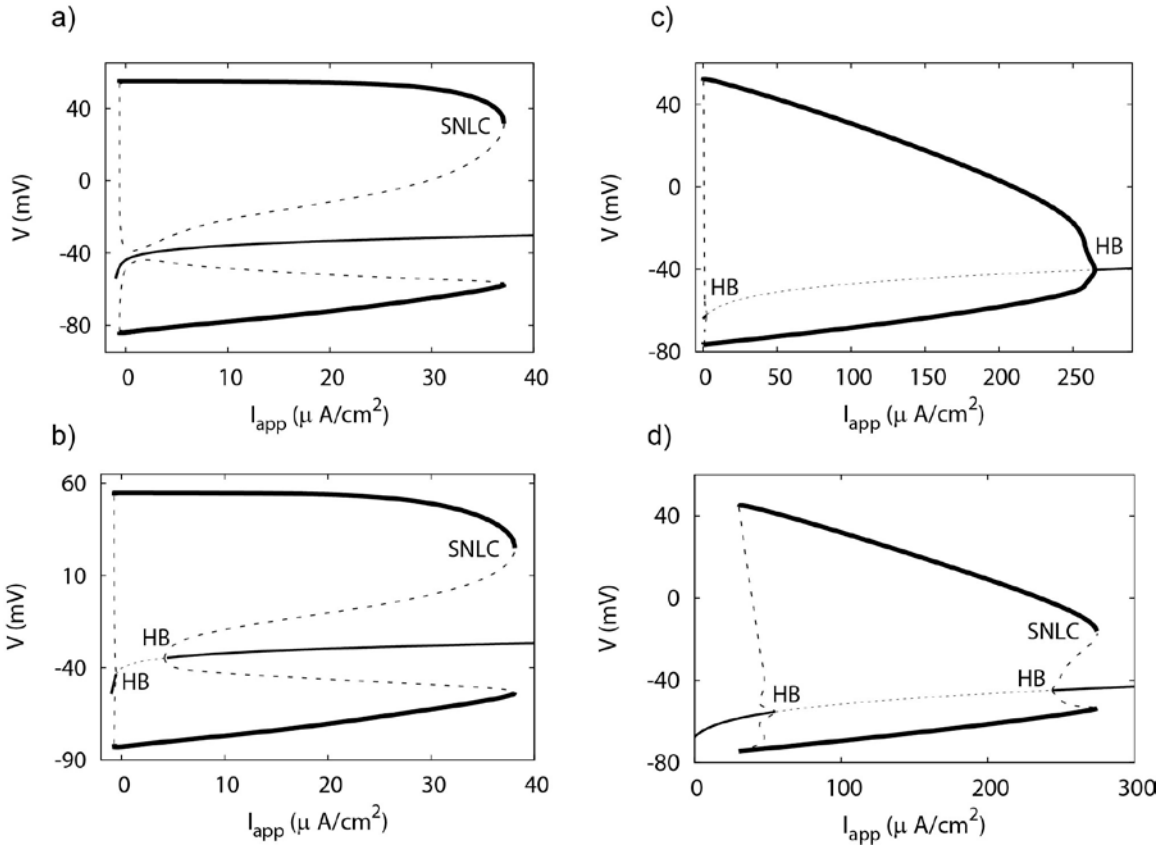

Figure 4.3. One-parameter bifurcation diagrams for the DA and HH neurons. a) Oscillatory solution stays isolated from the equilibrium state in the DA neuron. This is Class 3 excitability. Parameters for the DA neuron are from table 4.1. b) The oscillatory solution connects to the equilibrium state in an Andronov-Hopf bifurcation in the DA neuron. Parameters are from a), except that the K^+ current half-activation is increased by 5 mV (v_{nh} = -31 mV). c) Hysteresis is not present at the upper boundary of the oscillatory range in the HH neuron. Parameters for the HH neuron are from table 4.1. d) The oscillatory solution connects to the equilibrium state in an Andronov-Hopf bifurcation in the HH neuron. Parameters are from c), except that the K^+ current half-activation is decreased by 5 mV (v_{nh} = -58 mV). Thin curves represent equilibrium states, thick curves - limit cycles. Solid (dashed) curves represent stable (unstable) solutions. HB is the Andronov-Hopf bifurcation, SNLC is the saddle-node of limit cycles bifurcation.

to -31 mV (Fig. 4.3b), the class of excitability of the DA neuron changes to Class 2: The oscillatory solution emerges again from a saddle-node bifurcation of limit cycles, but in this case the equilibrium state becomes unstable via subcritical Andronov-Hopf bifurcations. We use the parameter set from Fig. 4.3b in all two-parameter bifurcation diagrams for the DA neuron given below.

The HH neuron possesses no hysteresis and has Class 2 excitability (Fig. 4.3c). However, relatively weak bistability and hysteresis compared to the DA neuron may be induced in the HH neuron with a decrease in the half-activation of the K^+ current v_{nh} (Fig. 4.3d). Similarly, we use the parameter set from Fig. 4.3d in all two-parameter bifurcation diagrams for the HH neuron that follow.

4.3.1 Half-Activation/Inactivation Parameters' Effect on Hysteresis

To investigate the effect of the half-(in)activation parameters on hysteresis in both neurons we consider the two-parameter bifurcation diagrams where the K^+ current half-activation v_{nh} or the Na^+ current half-inactivation v_{hh} are varied together with the applied current.

The two-parameter bifurcation diagram in v_{nh} and I_{app} for the DA neuron is shown in Fig. 4.4a. This diagram shows the location of the Andronov-Hopf and the saddle-node bifurcations marked in Fig. 4.3b for different values of the bifurcation parameters. Every horizontal cross section of this diagram at a particular value of v_{nh} defines the instability range and the oscillatory range which are bounded by these bifurcations. The ranges extend in the parameter v_{nh} and span two-dimensional regions. Likewise, the bistability range spans the shaded region in the bifurcation diagram. We characterize the strength of

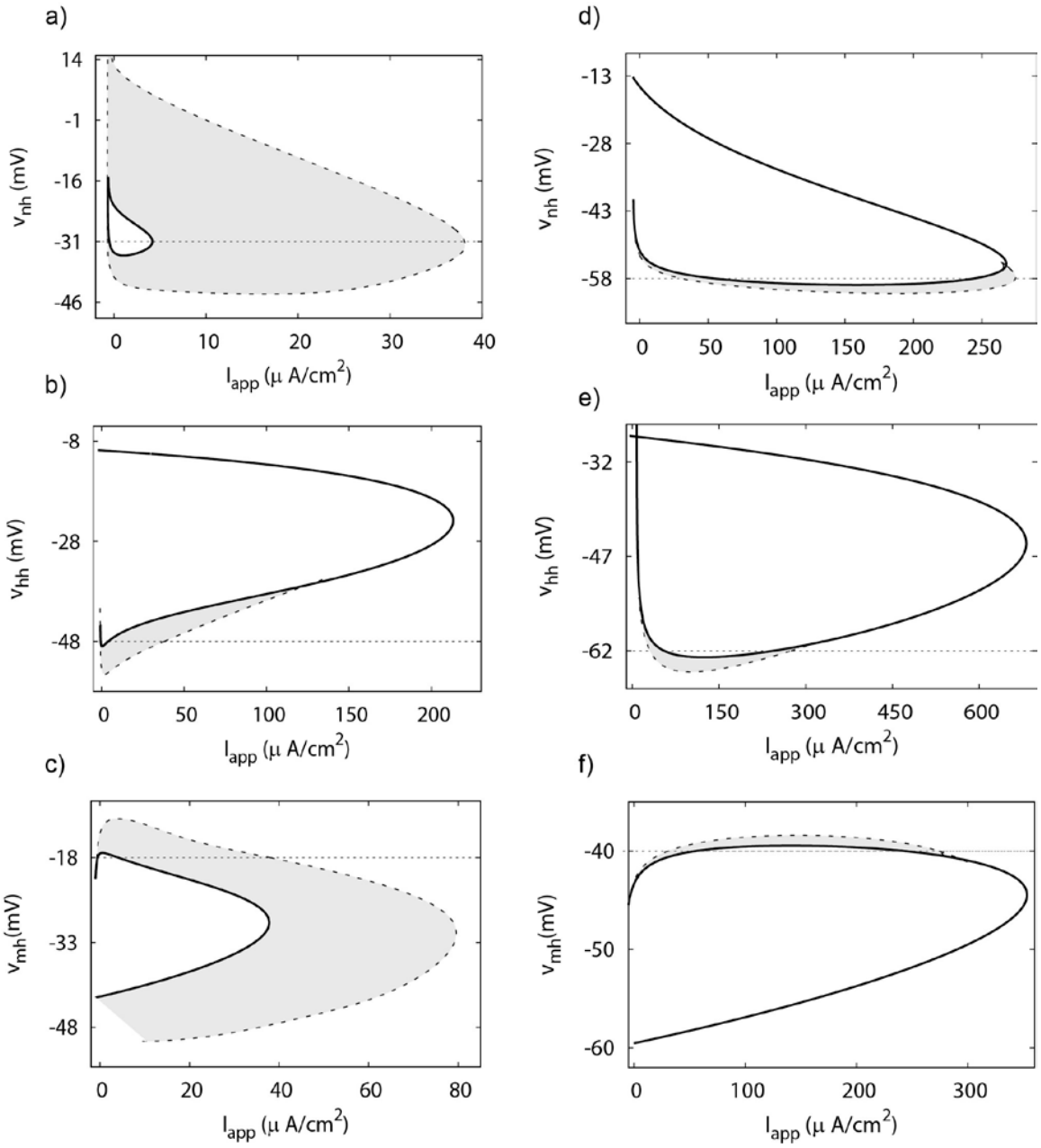
a)
14
-1
-16
-31
-46
v_{nh} (mV)
0
10
20
30
40
I_{app} (μ A/cm^2)
b)
-8
-28
-48
v_{hh} (mV)
0
50
100
150
200
I_{app} (μ A/cm^2)
c)
-18
-33
-48
v_{mh}(mV)
0
20
40
60
80
I_{app} (μ A/cm^2)
d)
-13
-28
-43
-58
v_{nh} (mV)
0
50
100
150
200
250
I_{app} (μ A/cm^2)
e)
-32
-47
-62
v_{hh} (mV)
0
150
300
450
600
I_{app} (μ A/cm^2)
f)
-40
-50
-60
v_{mh}(mV)
0
100
200
300
I_{app} (μ A/cm^2)

Figure 4.4

Figure 4.4. Two-parameter bifurcation diagrams of the DA neuron and the HH neuron in $v_{nh}/v_{hh}/v_{mh}$ and I_{app} planes. a) Hysteresis is strong in the DA neuron. Parameters are from table 4.1. b) Hysteresis is removed and oscillatory region expands in the DA neuron with the increase in the half-inactivation of the Na^+ current. Parameters are from Fig. 4.3b. c) Hysteresis is not reduced with the decrease in the half-activation of the Na^+ current. Parameters are from Fig. 4.3b. d) Hysteresis is weak in the HH neuron. Parameters are from table 4.1. e) Hysteresis is removed in the HH neuron with an increase of v_{hh}. Parameters are from Fig. 4.3d. f) Hysteresis is weak in the HH neuron with an increase of v_{mh}. Parameters are from Fig. 4.3d. A solid curve represents an Andronov-Hopf bifurcation, a dashed curve – a saddle-node bifurcation of limit cycles. Horizontal dotted lines in a) and d) represent the values of half-activation of the K^+ current taken in b, c) and e, f), correspondingly. Horizontal dotted lines in b, c) and e, f) represent the values of half-(in)activations from table 4.1 for the DA and HH neurons, correspondingly. Hysteresis regions are shaded gray.

hysteresis by the relative size of this shaded region compared to the instability region (bounded by solid curves in Fig. 4.4).

At intermediate values of the applied current, the depolarization block boundary consists of two transitions: First, the equilibrium state becomes stable in a subcritical Andronov-Hopf bifurcation; second, the stable oscillatory solution disappears in a saddle-node bifurcation of limit cycles (see e.g. Fig. 4.3b). In the range between the two bifurcations, the system is bistable and may show oscillations or a steady voltage depending on the initial conditions. At higher values of v_{nh}, the two bifurcation curves stay at a nearly constant distance (Fig. 4.4a) and hysteresis remains strong. Instability range shortens and disappears at v_{nh} = -15 mV and oscillatory range follows at v_{nh} = 14 mV, at which point all oscillations cease in the DA neuron.

Fig. 4.4d shows the same bifurcation diagram for the HH neuron. The area between the bifurcation curves is small. The model can show a significant bistability in response to variations in the applied current, but only with a very precise tuning of v_{nh} to values right above -60 mV (see e.g. Fig. 4.3d). The comparison of the areas of the bistability regions in the two neurons allows us to say that bistability is much stronger in the DA neuron.

An increase in the Na^+ current half-inactivation reduces and then completely abolishes hysteresis in both neurons (Fig. 4.4b, e). In Fig. 4.4b we fix the half-activation of the K^+ current at the level indicated in Fig. 4.4a. Thus, Fig. 4.4a and Fig. 4.4b are perpendicular sections of the parameter space that intersect along the indicated levels.

The influence of the Na^+ current half-inactivation is remarkably similar in the two neurons. Along with removing bistability, increasing half-inactivation expands the

oscillatory range very much, so that it becomes similar in the two neurons (Fig. 4.4b, e). This parameter change makes the inactivation effectively weaker, and the Na^+ window current greater. Therefore, a weaker Na^+ current inactivation promotes oscillations at a higher applied depolarization. However, a further elevation of the half-inactivation blocks oscillations completely. Thus, inactivation is necessary for generating oscillations in both neurons. Altogether, there is an optimal value of the half-inactivation of the Na^+ current that maximizes the oscillatory range and abolishes hysteresis in the model.

The influence of the Na^+ current half-activation v_{mh} on the transition to the depolarization block in the DA and HH neurons is shown in Fig. 4.4c, f, respectively. In the DA neuron a decrease in the Na^+ current half-activation initially expands both oscillatory and instability regions and moderately increases hysteresis, but below v_{mh} =-31 mV, the dependence is reversed. Further decrease in v_{mh} results in simultaneous shrinking of oscillatory and instability regions, but their upper boundaries remain almost parallel and hysteresis remains strong. In the HH neuron (Fig. 4.4f), the oscillatory range also peaks at an intermediate level of v_{mh} around -45 mV. Both low and high values of the half-activation abolish oscillations. However, hysteresis exists only in a very narrow range of the Na^+ current half-activation and is substantially smaller than in the DA neuron (Fig. 4.4c).

4.3.2 Half-Activation/Inactivation Slope Parameters' Effect on Hysteresis

The slopes of the activation and inactivation functions differ substantially in the DA and HH neurons (Figs. 4.1a, b and 4.2a). Therefore, we also estimate the effect of the slope parameters on hysteresis in both neurons.

We change the slope of the Na^+ current inactivation function from steep ($|S_h| = 4$) as in the DA neuron to gradual ($|S_h| = 7$) as in the HH neuron (see Fig. 4.1b) in both neurons. The decrease in the slope (larger $|S_h|$) increased the instability range. However, it reduced and then completely abolished bistability in both neurons (Fig. 4.5a, d). This occurs because the instability range expands strongly and merges with the oscillatory range as S_h increases in both neurons. Interestingly, in the HH neuron instability region was not present until the value of the slope parameter was around $|S_h| = 6.5$, but then instability region quickly expanded removing hysteresis similarly to Fig. 4.4d. As for the variations in the half-inactivation above, the influence of S_h in the two neurons is remarkably similar. First, it removes the difference in the length of the instability region between the neurons. Second, its increase abolishes hysteresis. Therefore, the slope of the Na^+ current inactivation controls hysteresis and the length of the oscillatory and instability ranges in both neurons.

The Na^+ current activation function is steeper in the DA than in the HH neuron (Fig. 4.1a). A decrease in the slope of the function ($S_m \rightarrow 9$, Fig. 4.5b) leads to an almost linear expansion of the instability and oscillatory regions in the DA neuron. Hysteresis remains unchanged because the boundaries are parallel. In the HH neuron, both the instability and oscillatory regions shrink and shift into higher values of the applied current with a steeper activation of the Na^+ current ($S_m \rightarrow 8$). While hysteresis increases at the low applied currents (hyperpolarization block), at the depolarization block, hysteresis remains unchanged because upper boundaries of both the oscillatory and instability ranges expand almost equally. Altogether, changes in S_m only slightly shift the upper boundaries, and both the oscillatory and the instability ranges remain of different

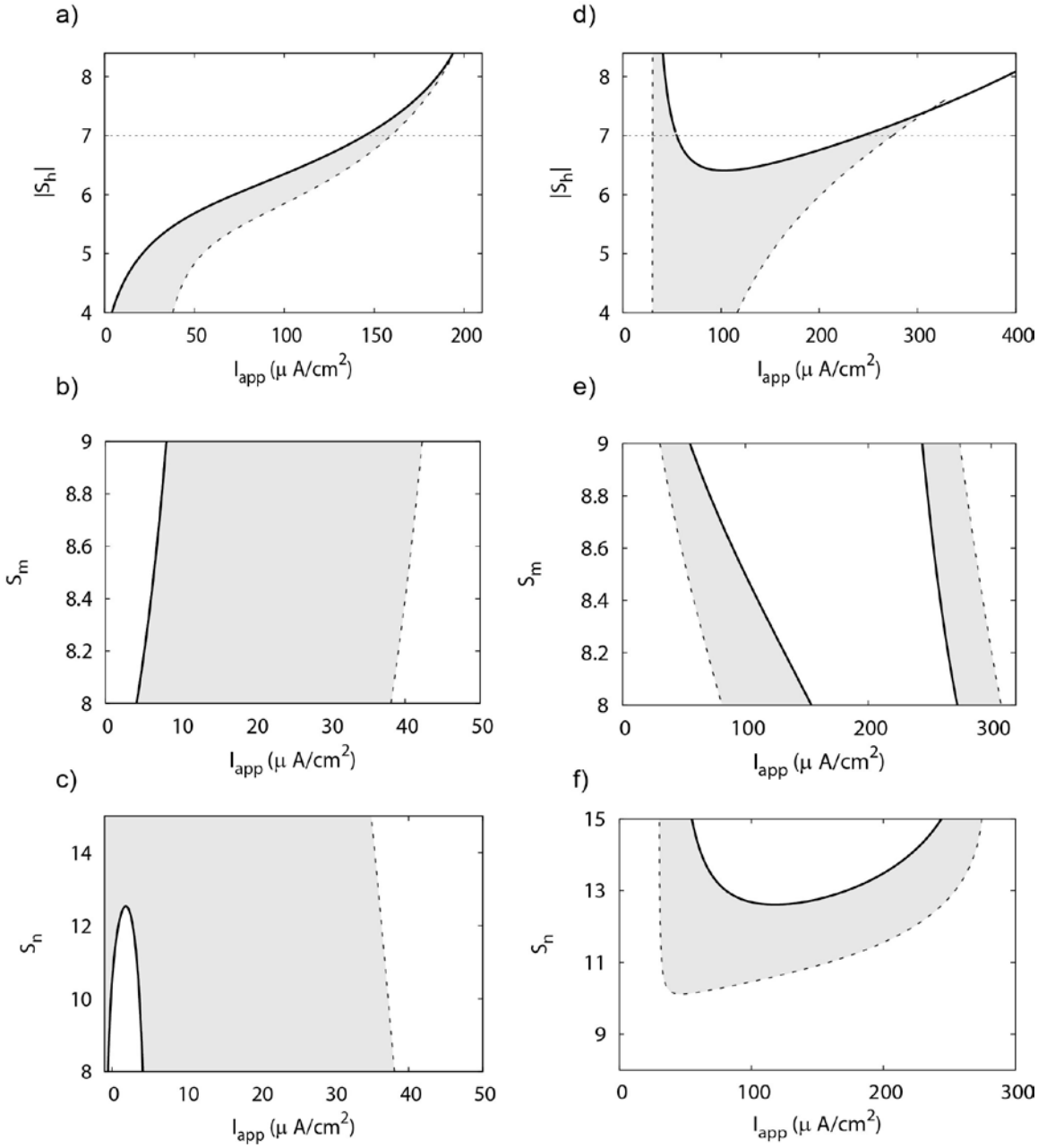

Figure 4.5

Figure 4.5. Two-parameter bifurcation diagrams of the DA and HH neuron for the change in slope of (in)activation functions. a) A gradual voltage dependence of the Na^+ current inactivation function removes hysteresis in the DA neuron. b) Steeper voltage dependence of the activation of the Na^+ current has no effect on hysteresis in the DA neuron. c) More gradual voltage dependence of the K^+ current has minimal effect on hysteresis in the DA neuron. Parameters are from Fig. 4.3b. d) Steeper voltage dependence of the Na^+ current leads to stronger hysteresis in the HH neuron. e) Gradual voltage dependence of the activation of the Na^+ current has no effect on hysteresis at the upper boundary of oscillatory region in the HH neuron. f) Gradual voltage dependence of the K^+ current increases hysteresis in the DA neuron. A solid curve represents an Andronov-Hopf bifurcation, a dashed curve – a saddle-node bifurcation of limit cycles. Parameters are from Fig. 4.3d. Horizontal dotted lines in (a) and (d) mark the value of slope parameter from table 4.1 for the HH neuron. Hysteresis regions are shaded gray.

orders of magnitude in the HH and DA neurons. Moreover, the boundaries shift in the opposite directions in the two neurons, which only emphasizes the difference between their parameter sets.

To test how steepness of the activation function for the K^+ current affects bistability we change the slope of the K^+ current activation in both neurons from steep (S_n = 8) as in the DA neuron to a more gradual (S_n = 15) as in the HH neuron (Fig. 4.2a). In the DA neuron (Fig. 4.5c), the upper boundaries of oscillatory and instability regions remain almost parallel until the instability region disappears at around S_n = 12. Even above that point, the slope parameter only weakly affects the boundary of the oscillatory region, and hysteresis remains almost unchanged. In contrast, in the HH neuron (Fig. 4.5f) the oscillations are not present for smaller values of S_n, i.e. for the steeper voltage dependence of the K^+ current. The oscillatory range emerges above S_n = 10 and quickly expands, whereas the equilibrium remains stable giving rise to strong hysteresis. The instability region appears above S_n = 13, rapidly expands and limits hysteresis to short ranges at both boundaries. Therefore, the decrease in the slope of the K^+ current activation function ($S_n \rightarrow 15$) has an opposite effect on the instability range in the two neurons. Extending the distinction, in the HH, but not in DA neuron, the parameter strongly affects the oscillatory and hysteresis regions.

4.3.3 Gating Variables' Kinetics Effect on Hysteresis

None of the variables in the model is uniformly slow or uniformly fast. The timescale of the voltage is minimal when the Na^+ current is open, and elevates to the maximum when the leak current works alone. Likewise, the timescales of the gating

variables depend on the voltage (Figs. 4.1c and 4.2b). Therefore, there is no permanent separation onto fast and slow variables in the model. On the other hand, comparing timescales of the corresponding variables in the two neurons is more straightforward and has a clear physiological meaning. By changing kinetics of the gating variables below, we study how the difference in the timescales affects the oscillatory and instability ranges.

The inactivation variable is much faster in the HH neuron compared to the DA neuron (Fig. 4.1c). Therefore, we now study how hysteresis is affected by accelerating the Na^+ current inactivation uniformly at all voltages ($f_h > 1$). Fig. 4.6a shows that accelerating the inactivation moderately reduces the distance between the Andronov-Hopf and the saddle-node of limit cycles bifurcations. Instability range shortens slower than the oscillatory range. After the instability range disappears, the oscillatory range continues to shrink until all oscillations cease in the DA neuron. In the HH neuron, the transition should be made in the opposite direction because inactivation is initially much faster compared to the DA neuron; therefore we reduce its rate of change ($f_h < 1$). In contrast to the DA neuron, the instability range does not depend on the inactivation timescale (Fig. 4.6d). The oscillatory range shortens with slower Na^+ current inactivation because the hysteresis ranges at both boundaries of the instability range disappear (Fig. 4.6d).

Similar results hold when the K^+ current activation variable *n* is accelerated ($f_n > 1$) in both the DA neuron and the HH neuron (Fig. 4.6b, e). In the DA neuron, instability range shortens and disappears at around four times faster activation ($f_n = 4$) of the K^+ current. The oscillatory range, first, expands with a faster K^+ activation, but then starts to

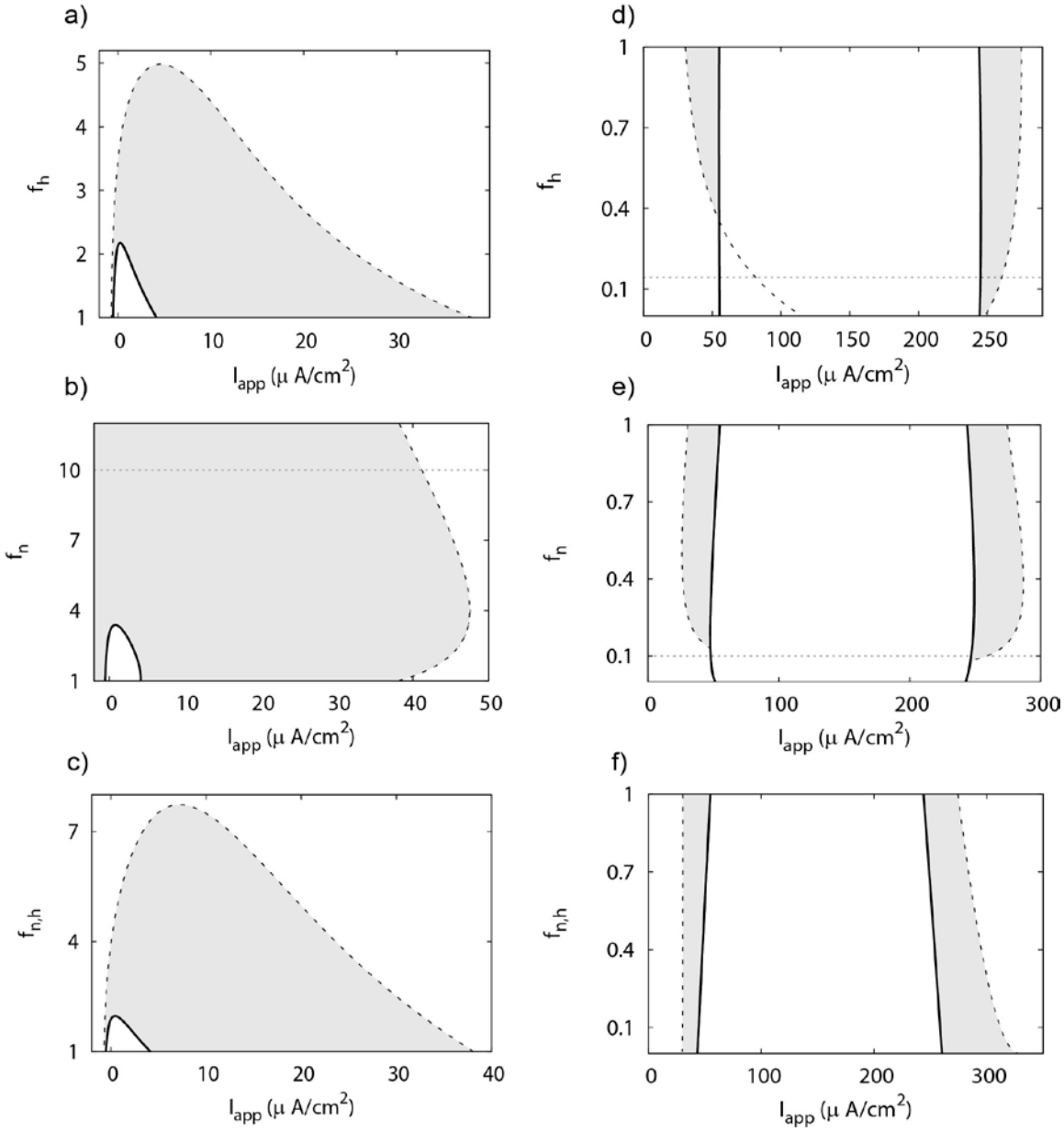

Figure 4.6

Figure 4.6. Changing kinetics of gating variables in the DA and HH neurons. a, b) Bistability region shortens with accelerating kinetics of the gating variables *h* ($f_h > 1$) and *n* ($f_n > 1$) in the DA neuron. $f_h = 1$ and $f_n = 1$ correspond to parameter set from Fig. 4.3b. c) Simultaneous acceleration of both *n* and *h* variables ($f_{n,h} > 1$) decreases the size of bistability range. $f_{n,h} = 1$ corresponds to parameter set from Fig. 4.3b. d, e) Hysteresis is reduced (d) or eliminated (e) in the HH neuron with slowing the individual current kinetics ($f_h < 1$ or $f_n < 1$). $f_h = 1$ and $f_n = 1$ correspond to parameter set from Fig. 4.3d. f) Hysteresis is increased with simultaneous slowing of gating variables *n* and *h* ($f_{n,h} < 1$). $f_{n,h} = 1$ corresponds to parameter set from Fig. 4.3d. A solid curve represents an Andronov-Hopf bifurcation, a dashed curve – a saddle-node bifurcation of limit cycles. Horizontal dotted lines (where shown) give the values of f_h and f_n for which the maximum value of the corresponding time constant function for the DA (HH) neuron matches the maximum value of the time constant for the HH (DA) neuron. Hysteresis regions are shaded gray.

decrease in size. This decrease is more gradual than in Fig. 4.6a for the Na^+ current inactivation, and bistability remains in the neuron when the Na^+ current becomes as fast as in the HH neuron ($f_n = 10$). In the HH neuron, the instability range weakly depends on the timescale of the K^+ current activation variable *n.* When the variable becomes slower ($f_n < 1$), the oscillatory range shortens, and hysteresis disappears ($f_n = 0.1$).

Finally, we change both the Na^+ current inactivation and the K^+ current activation timescales simultaneously in both neurons. The diagram for the DA neuron (Fig. 4.6c) is very similar to Fig. 4.6a. This suggests that the changes in the dynamics are not due to the introduced mismatch between the timescales of the two gating variables, but mostly due to the mismatch between the timescales of the voltage and the gating variables. Furthermore, as follows from the similarity of Fig 4.6a, c, the accelerated Na^+ current inactivation contributes the most to the loss of oscillations. When K^+ current activation is also accelerated, the gating variables remain at the same timescale, but this only moderately expands the oscillatory region.

In the HH neuron, when we make the kinetics of both variables slower ($f_{n/h} \rightarrow 0.1$), hysteresis at the upper boundary of the oscillatory range increases (Fig. 4.6f). This is opposite to the results for the differential changes in these two parameters above (Fig. 4.6d, e). This also contrasts the results for the DA neuron. Hence, the reduction in hysteresis was due to a mismatch between the timescales of the gating variables. By contrast, concurrent slowing of the gating variables, which creates a mismatch between the timescale of voltage and that of the two gating variables, expand the hysteresis range.

4.3.4 Contribution of Other Parameters to Hysteresis

The susceptibility of the DA neuron to depolarization block was attributed to the weakness of the delayed rectifier current long ago. The common sense explanation is that the voltage stays high near the state of depolarization block because the potassium current cannot lower it enough. The increase in the maximal conductance of the K^+ current g_K in the DA neuron leads to the monotone increase of the oscillatory range and the decrease and disappearance of the instability range (Fig. 4.7a). The growth of the oscillatory range is consistent with the logic outlined above, but stabilization of the equilibrium state that entail strong hysteresis is unexpected. In the HH neuron, the increase in g_K also leads, at first, to the expansion of the instability range without hysteresis. Then the instability range shortens abruptly, but the oscillatory range persists, and a significant hysteresis region emerges (Fig. 4.7d). Hence, the maximal conductance of the K^+ current g_K efficiently controls the length of the oscillatory range in both neurons. However, the strength of hysteresis is controlled by other parameters because it is drastically different in the two diagrams.

The reversal potential of the K^+ current is defined by the extracellular potassium concentration, can be controlled in experiments, and has been found to affect hysteresis in pre-Botzinger complex respiratory neurons (Y. Molkov, private communications). An increase in E_K monotonically reduces oscillatory and instability ranges in both the DA and the HH neurons (Fig. 4.7b, e). Furthermore, the upper boundaries of both oscillatory and instability regions in the HH neuron are very close to straight parallel lines (Fig. 4.7e). This suggests a passive contribution of the K^+ current at the transition to

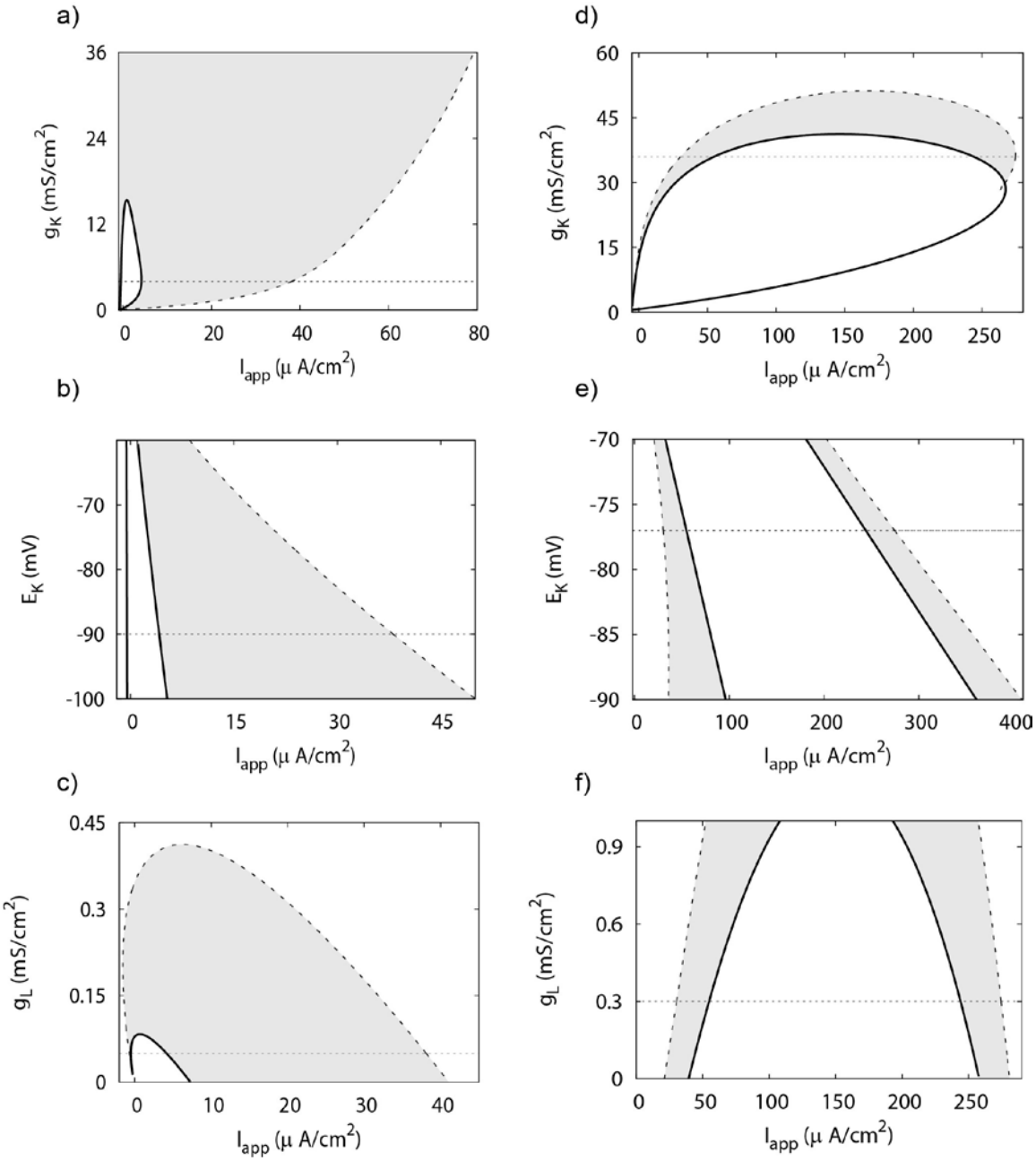
a)
36
24
12
0
g_K (mS/cm^2)
0
20
40
60
80
I_{app} (μ A/cm^2)
d)
60
45
30
15
0
g_K (mS/cm^2)
0
50
100
150
200
250
I_{app} (μ A/cm^2)
b)
-70
-80
-90
-100
E_K (mV)
0
15
30
45
I_{app} (μ A/cm^2)
e)
-70
-75
-80
-85
-90
E_K (mV)
0
100
200
300
400
I_{app} (μ A/cm^2)
c)
0.45
0.3
0.15
0
g_L (mS/cm^2)
0
10
20
30
40
I_{app} (μ A/cm^2)
f)
0.9
0.6
0.3
0
g_L (mS/cm^2)
0
50
100
150
200
250
I_{app} (μ A/cm^2)

Figure 4.7

Figure 4.7. Two-parameter bifurcation diagrams for the change in maximal conductances and equilibrium potential. a) Increase in g_K expands the oscillatory region, shortens the instability region and increases hysteresis in the DA neuron. b) Increase in K^+ current reversal potential shortens oscillatory region much faster than the instability region, reducing hysteresis in the DA neuron. c) Increase in the maximum conductance of the leak current shortens both instability and oscillatory regions and finally eliminates oscillations in the neuron in the DA neuron. d) Hysteresis exists in a narrow range of parameter g_K in the HH neuron. e) Hysteresis at the upper boundary of oscillatory region is not affected by the decrease in E_K in the HH neuron. f) Hysteresis is slightly reduced with the decrease in the maximum leak conductance in the HH neuron. a, b, c) Parameter values from Fig. 4.3b. d, e, f) Parameter values from Fig. 4.3d. A solid curve represents an Andronov-Hopf bifurcation, a dashed curve – a saddle-node bifurcation of limit cycles. Horizontal dotted lines mark parameter values from table 4.1 for the DA and the HH neurons, correspondingly. The hysteresis regions are shaded gray.

depolarization block and a linear compensation by I_{app}. In the DA neuron, this dependence is more nonlinear (Fig. 4.7b), and the reduction in hysteresis is much stronger.

The maximum conductance of the leak current is very different in the two neurons (see table 4.1), and determines the slowest timescale of voltage changes (see discussion in the Model subsection). The increase in g_L in the DA neuron shortens both instability and oscillatory ranges (Fig. 4.7c). Instability range disappears first and then the oscillatory range follows at $g_L = 0.4$. This influence of increasing g_L is very similar to the influence of accelerating both gating variables (compare Figs. 4.7c and 4.6c). This differentiates the oscillatory mechanism in the DA neuron from a relaxation oscillator. In a relaxation oscillator, oscillations disappear if the timescale separation is decreased or reversed. Therefore, accelerating a slow variable would abolish oscillations, whereas accelerating a fast variable would only promote them. The fact that accelerating any variable abolished oscillations in the DA neuron means that the oscillatory mechanism does not tolerate a significant mismatch in the timescales, distinguishing it from the relaxation oscillator.

In the HH neuron, increase in the maximum conductance of the leak current shortens both the oscillatory and instability ranges (Fig. 4.7f). This also tells against the relaxation oscillator mechanism and the role of the voltage as a fast variable in the HH neuron. The elevation in g_L significantly increases the hysteresis range. Increasing g_L makes the voltage, or more precisely its slowest timescale, faster. This introduces timescale separation similar to the one achieved by slowing the two gating variables (Fig. 4.6f). In both cases (Figs. 4.6f and 4.7f) this leads to the increase in hysteresis at the

depolarization block. However, slowing the gating variables hardly affects the instability region and only reduces hysteresis at the hyperpolarization block. Therefore, the slowest voltage changes determined by the leak conductance promote oscillations and the instability of the equilibrium state in both neurons.

4.3.5 Normalized Contributions of Parameters to Hysteresis

To compare the effect of different parameters on hysteresis we compute changes in the hysteresis range with changes in each parameter. The parameters were increased by 10%. The changes in the length of the hysteresis range were normalized by its initial length to obtain the relative contributions. The results are shown in table 4.2. For example, the increase in the maximal conductance of the K^+ current in the HH neuron from 36 mS/cm^2 to 39.6 mS/cm^2 (10% increase) leads to the increase in the length of hysteresis range from 30.5 to 67.8 (122% increase) (see Fig. 4.7d). The increase in the (in)activation parameters v_{hh} and v_{nh} in the HH neuron leads to the complete removal of hysteresis (Fig. 4.4c, d) and is reflected by the 100% decrease in hysteresis in table 4.2. Overall, normalized change in hysteresis in the HH neuron is an order of magnitude higher than in the DA neuron for most of the parameters. This provides another indication that hysteresis in the HH neuron exists in the narrow parameter ranges and is not as robust as in the DA neuron since small changes in parameter values lead to large changes in hysteresis.

Table 4.2. Normalized parameter contribution to hysteresis in the DA and HH neurons.

Model\parameters	g_K	g_{Na}	g_L	v_{hh}	v_{nh}	S_h	S_m	S_n
HH neuron, %	122	-56	3	-100	-100	426	-55	-21
DA neuron, %	4	6	0	5	0	1.5	-0.5	0

4.3.6 Summary of the Results

The parameters in the two model neurons can be separated into three groups. The first group of parameters consists of the half-inactivation of the Na^+ current v_{hh} and the slope of the inactivation function S_h. The two-parameter diagrams in v_{hh} and S_h are very similar for the HH and the DA neurons in spite of the differences in other parameters (Figs. 4.4b, e and 4.5a, d). First, the diagrams show the strongest expansion of the oscillatory and instability ranges. By changing these two parameters, we can remove the order of magnitude difference in the length of these ranges in the HH vs. DA neuron. Second, they control hysteresis in a very similar way in the two neurons. Therefore, these parameters contribute most to the difference between the neurons in both hysteresis and the length of the instability/oscillatory ranges.

The second group of parameters includes the half-activation of the K^+ and Na^+ currents v_{nh} and v_{mh}, reversal potential of the K^+ current E_K, leak conductance g_L and the slope of the activation function of the Na^+ current S_m. Variations in these parameters produce the diagrams that are quite distinct in the HH and DA neurons, i.e. cannot make the dynamics of the two neurons similar. This suggests that these parameters do not

contribute to the difference between the DA and the HH neurons. Nevertheless, they influence hysteresis and the length of the oscillatory and instability ranges similarly in both neurons.

Finally, the third group of parameters consists of the slope of the K^+ current activation function S_n and parameters that influence the kinetics of the gating variables, i.e. f_n, f_h and $f_{n,h}$. Variations in these parameters not only produce different diagrams, but also influence the neurons in the opposite ways.

4.4 Discussion

In this paper, we have analyzed bistability that distinguishes two types of neurons. We identified their spike-producing currents as responsible for bistability. The neurons were reduced to the same model and differed by the values of the parameters. We examined transitions between the two parameter sets and found that bistability is present in a wide region of the multidimensional parameter space. The values of the parameters in the bistability regions are physiologically plausible because transitions span the intervals between values corresponding to two types of neurons. This is consistent with bistability between tonic spiking and the silent state commonly observed in neurons. Our modeling suggests that this bistability arises from the interaction of the spiking currents.

Bistability is useful in qualitative classification of neurons based on the firing patterns. Electrophysiological and pharmacological characterization of neurons separates them into numerous types. The neurons differ by their neurotransmitters, the composition of currents, typical firing patterns, responses to pharmacological manipulations, etc. Managing the diversity of neurons is an enormously complex task. Thus, of critical

importance are criteria that can identify broad classes of neurons sharing some functional similarities. A great example is the neuron characterization by a phase response curve (Hansel et al., 1995) or classification of neurons into resonators and integrators; bistable and monostable dynamical systems (Izhikevich, 2007). These characteristics separate broad groups of neurons, and are very useful for predicting how neurons behave when they interact in a network. Another example is the separation of neurons into three classes of excitability (Hodgkin, 1948). The class of neuron excitability is determined in one of the simplest experiments – a negative current is applied into the soma through an electrode and then gradually removed. In response, the neuron first enters the silent state of hyperpolarization and then resumes firing as the hyperpolarizing applied current is removed. The transition from quiescence to firing determines the excitability class.

Bistability between tonic spiking and silence has been used in explaining the mechanisms of bursting (Izhikevich, 2007). In this case, an additional variable plays the role of a parameter that provides hysteresis and switches the system from spiking to silence and back. Only artificially treating this variable as a parameter in the model allows for observing bistability in simulations. We consider a true parameter, applied current, and bistability that occurs in experiments as the parameter is manipulated. Our model did not take into account the subthreshold currents. Their inclusion may suppress bistability in some cases. Our modeling of the DA neuron (Kuznetsov et al., 2006) shows that a model that includes subthreshold currents together with the spike-producing ones retains the same bistability. How bistability is affected by subthreshold currents in other neurons is a subject of future studies focused on particular neurons.

We have found that bistability is much stronger in the DA neuron than in the HH neuron. The major factors contributing to this difference are a low half-inactivation and a steep voltage dependence of the inactivation of the Na^+ current. Only the manipulations of these two parameters were able to abolish the order of magnitude difference in the length of the oscillatory region in the two neurons. They also control hysteresis in a very similar way in spite of the difference in other parameters. The rest of the parameters produce very different diagrams in the two neurons. Some of them have the opposite influence on the dynamics of the two neurons.

In order to interpret the result for the future experiments, we connect it to physiological characteristics. The window Na^+ current is its small steady state component that remains after a strong transient component as the current inactivates. Lowering half-inactivation parameter of the current decreases its window component. Increasing the slope of the inactivation voltage dependence reduces the window current as well. Our way of changing the slope excludes any shift in the half-inactivation. Thus, two manipulations that decrease the window current promote bistability. Altogether, our results suggest a connection between the characterization of the Na^+ window current in a neuron and strong bistability in response to changes in the applied current.

Bistability endows neurons with richer forms of information processing. A bistable cell encodes a brief signal by a long-lasting change in its firing. Hence, the bistability between resting and tonic spiking states studied in this article has been hypothesized to be involved in short-term memory (discussed in Marder et al., 1996). This type of bistability was also observed in different motor neurons (Hounsgaard et al.,

1984; Le et al., 2006; Lee and Heckman, 1996). Bistable motor neurons have been hypothesized to support prolonged low force tasks, like posture.

Hysteresis at the upper boundary of oscillatory range may be essential for pacemaker-type neurons as it may improve robustness of oscillations and lead to a more efficient control of the dynamics (Guttman et al., 1980). Efficiency and robustness follow from the inability of small perturbations (e.g. noise) in the control parameter to switch the neuronal activity from one mode to the other as soon as the bifurcation parameter (applied current) is perturbed. For this reason, many physical systems like heating thermostats utilize hysteresis to improve efficiency by reducing the frequency of on-off switching.

Bistability studied in this article is generally independent of the excitability class. In particular, Class 3 excitability is always accompanied by bistability simply because the equilibrium state remains stable for the whole parameter range where the oscillatory solutions exist. However, in other cases where the equilibrium loses stability, the excitability class is unrelated to the presence of bistability. In most cases we examined, strong bistability occurs at the upper boundary of the instability (oscillatory) range, i.e., at the depolarization block. The excitability class refers to the transition at the hyperpolarization block. These two transitions are independent. The saddle-node on invariant circle bifurcation, which is responsible for Class 1 excitability, never occurs at the upper boundary of the oscillatory range. The half-activation of the K^+ current was the most effective in spanning all three excitability classes, but did not abolish bistability completely. By contrast, changing the half-inactivation of the Na^+ current or kinetics of

the gating variables switches the excitability only between Class 2 and Class 3. Therefore, bistability can be used in conjunction with the excitability class in characterizing the neurons.

Our results show that the silent state of depolarization block may be stable together with the tonic spiking state. In DA neurons, progressive depolarization block was proposed as a mechanism for the maximal therapeutic action of antipsychotic drugs (Grace et al., 1997). Chronic administration of drugs used in treatment of schizophrenia results in silencing of the DA neurons due to depolarization block (Boye and Rompre, 2000; Valenti et al., 2011). Taken together with our results, the DA neurons may stay in the silent state after lowering the dose or complete cessation of the drug administration because of the possible bistability between the silent and active states.

Bibliography

Boye, S. M., & Rompre, P.-P. (2000) Behavioral evidence of depolarization block of dopamine neurons after chronic treatment with haloperidol and clozapine. *J Neurosci* 20(3):1229–1239.

Cymbalyuk, G., & Shilnikov, A. (2005). Coexistence of tonic spiking oscillations in a leech neuron model. *J Comput Neurosci* 18(3):255–63.

Ermentrout, B. (2002). *Simulating, Analyzing, and Animating Dynamical Systems: A Guide to XPPAUT for Researchers and Students*. Philadelphia, PA: Society for Industrial and Applied Mathematics.

Grace, A. A., Bunney, B. S., Moore, H., & Todd, C. L. (1997). Dopamine-cell depolarization block as a model for the therapeutic actions of antipsychotic drugs. *Trends Neurosci* 20(1):31–37.

Guttman, R., Lewis, S., & Rinzel, J. (1980). Control of repetitive firing in squid axon membrane as a model for a neuron oscillator. *J Physiol* 305:377–95.

Hansel, D., Mato, G., & Meunier, C. (1995). Synchrony in excitatory neural networks. *Neural Computation* 7:307–337.

Hodgkin, A. L. (1948). The local electric changes associated with repetitive action in a non-medullated axon. *J Physiol* 107(2):165–81.

Hodgkin, A. L., & Huxley, A. F. (1952). A quantitative description of membrane current and its application to conduction and excitation in nerve. *J Physiol* 117(4):500–44.

Hounsgaard, J., Hultborn, H., Jespersen, B., & Kiehn, O. (1984). Intrinsic membrane properties causing a bistable behavior of alpha-motoneurons. *Exp Brain Res* 55: 391–394.

Izhikevich, E. (2007). *Dynamical systems in neuroscience*. Cambridge, MA: The MIT Press.

Kiehn, O. (1991). Plateau potentials and active integration in the 'final common pathway' for motor behaviour. *Trends Neurosci* 14(2):68–73.

Kuznetsov, A., Kopell, N., & Wilson, C. (2006). Transient high-frequency firing in a coupled-oscillator model of the mesencephalic dopamine neuron. *J Neurophysiol* 95:932–47.

Le, T., Verley, D. R., Goaillard, J. M., Messinger, D. I., Christie, A. E., & Birmingham, J. T. (2006). Bistable behavior originating in the axon of a crustacean motor neuron. *J Neurophysiol* 95(3):1356–68.

Lechner, H. A., Baxter, D. A., Clark, J. W., & Byrne, J. H. (1996). Bistability and its regulation by serotonin in the endogenously bursting neuron R15 in aplysia. *J Neurophysiol* 75:957–62.

Lee, R. H., & Heckman, C. J. (1996). Influence of voltage-sensitive dendritic conductances on bistable firing and effective synaptic current in cat spinal motoneurons in vivo. *J Neurophysiol* 76 (3):2107–10.

Li, Y., & Bennett, D. J. (2003). Persistent sodium and calcium currents cause plateau potentials in motoneurons of chronic spinal rats. *J Neurophysiol* 90(2): 857–69.

Marder, E., Abbott, L. F., Turrigiano, G. G., Liu, Z., & Golowasch, J. (1996). Memory from the dynamics of intrinsic membrane currents. *Proc Natl Acad Sci USA* 93:13481–13486.

Morriset, V., & Nagy, F. (1999). Ionic basis for plateau potentials in deep dorsal horn neurons of the rat spinal cord. *J Neurosci* 19:7309–7316.

Powers, R. K., & Binder, M. D. (2003). Persistent sodium and calcium currents in rat hypoglossal motoneurons. *J Neurophysiol* 89(1):615–24.

Rinzel, J. (1978). On repetitive activity in nerve. *Fed Proc.* 37(14):2793–802.

Shilnikov, A., Calabrese, R. L., & Cymbalyuk, G. (2005). Mechanism of bistability: tonic spiking and bursting in a neuron model. *Phys Rev E Stat Nonlin Soft Matter Phys.* 71(5 Pt 2):056214.

Strogatz, S.H. (1994). *Nonlinear Dynamics and Chaos*, Reading, MA: Addison-Wesley.

Valenti, O., Cifelli, P., Gill, K. M., & Grace, A. A. (2011). Antipsychotic drugs rapidly induce dopaminergic neuron depolarization block in a developmental rat model of schizophrenia. *J Neurosci* 31(34):21330–338.

VITA

VITA

Andrey A. Dovzhenok

Education

Purdue University, West Lafayette, Indiana

Ph.D., Mathematics, May 2012

- Dissertation topic: Mathematical models of basal ganglia dynamics
- Advisor: Leonid Rubchinsky

Saratov State University, Saratov, Russia

B.S., Fluid Mechanics, June 2005

Papers

"On the origin of tremor in Parkinson's disease," with Leonid Rubchinsky. Under review

"Delayed feedback deep brain stimulation failure in partially synchronous parkinsonian basal ganglia," with Choongseok Park, Robert Worth and Leonid Rubchinsky. Under review

"Exploring neuronal bistability at the depolarization block," with Alexey Kuznetsov. Under review